# Development of an E85 Engine for the EcoCAR Challenge Hybrid Vehicle Competition

Undergraduate Honors Thesis

Presented in Partial Fulfillment of the Requirements for

Graduation with Distinction

at The Ohio State University

By

Jonathan M. Davis

* * * * *

The Ohio State University

2010

Defense Committee:

Shawn Midlam-Mohler, Advisor

Professor Yann Guezennec

# Abstract

The EcoCAR challenge is a three year competition amongst 16 universities in which teams are to re-engineer a 2009 General Motors crossover vehicle to reduce petroleum consumption, greenhouse gases and regulated emissions while increasing fuel economy. Ohio State's EcoCAR team is using a high compression ratio (12.5:1) 1.8L Honda engine designed for compressed natural gas (CNG). The engine has been converted to operate on cellulosic E85 (85% ethanol, 15% regular gasoline) which is a largely renewable fuel and reduces petroleum consumption significantly even when compared to corn-based E85. High compression ratios create thermal efficiency gains 10% higher than a conventional gasoline engine, resulting in higher fuel economy. However, in order to realize these benefits a new engine control algorithm must be developed. The purpose of this research is the development of two engine control maps to be used in the new engine controller. A spark timing map was created to optimize fuel economy. Secondly, a volumetric efficiency map was created to improve transient emissions. These maps are an integral part of the control system of an advanced alternative fuel engine. A new engine wiring harness design was completed to implement the new engine controller and fit with the EcoCAR vehicle design. The results were obtained through engine dynamometer tests consisting of a 189 point matrix of engine speed and manifold pressure (MAP) conditions. A maximum brake efficiency of 40.74% was obtained. Volumetric efficiency

maps used in engine controller mass air flow calculations presented good agreement with lab measurements. The creation of these two maps have allowed for the use of a high efficiency advanced alternative fuel engine in conjunction with the Ohio State EcoCAR team's advanced hybrid crossover vehicle.

## Acknowledgements

I would like to thank Dr. Shawn Midlam-Mohler for the opportunity to participate in this research project and all the guidance along the way. I would also like to thank Brad Cooley for help with the engine control code and general help setting up the engine. I would like to thank Josh Supplee for the help setting up the engine in order to obtain experimental data.

# Table of Contents

# List of Tables

Figure Page

# List of Figures

Figure Page

# Chapter 1

## 1.1 Introduction

This project assists the EcoCAR Challenge team by creating 2 different engine maps which will be used to create the engine controller code. The EcoCAR challenge is a competition amongst 16 North American Universities and is spread out through three years. The EcoCAR challenge competition goals are to re-engineer a 2009 General Motors crossover vehicle to enhance the fuel efficiency, minimize greenhouse gases and regulated exhaust emissions. While the vehicle must be fuel efficient, it must also retain the safety, performance and consumer appeal that will make it a marketable automobile.

Ohio State's EcoCAR team is using a high compression ratio (12.5:1) 1.8L Honda R18A3 engine designed for compressed natural gas (CNG). Instead of using this fuel the team has decided to use cellulosic E85 (85% ethanol, 15% regular gasoline) which is a largely renewable fuel. High compression ratios are synergetic with E85 due to the fuels high octane level (100-105). Normal gasoline cannot withstand these high compression ratios and will cause the engine to knock. High compression ratios create thermal efficiency gains that allow the engine to reach efficiencies 10% higher than a conventional gasoline engine.

In order to use this engine, an entirely new engine control unit has been developed with help from this research. This research project was conducted at the Center of Automotive Research (CAR) using their engine test labs. Data was collected from engine

tests in order to create two engine control maps. These include a volumetric efficiency and spark timing map. Volumetric efficiency is a measure of the effectiveness of the engines air induction process. It is at the heart of the speed density model, which is used in feed-forward air-fuel control. Precise air-fuel ratio control is necessary in order to meet increasingly stringent emissions standards. Catalyst efficiency is heavily dependent on the precise air-fuel control. The speed density model is important in limiting transient emissions by regulating the air-fuel ratio. Spark timing is critical to engine efficiency. Spark timing is the crank angle degree before top-dead-center at which combustion is initiated by the spark. The optimum spark timing advance is the degree which produces maximum brake torque (MBT). By maximizing torque output by changing spark, engine efficiency is positively impacted.

This research has provided the EcoCAR Challenge team with engine control maps that will optimize efficiency and improve transient exhaust emissions. As shown through data collected E85 fuel, in conjunction with a high compression engine, provide a significant advantage to using alternative fuels in automobiles. Every day the United States consumes a total of 20.6 million barrels of liquid fuels every day, over half of which is imported. E85 is a fuel that could help minimize the amount of liquid fuels the United States imports while decreasing emissions at the same time. This means that the research conducted in this project, such as creating engine control maps, provides valuable information as to the feasibility of using alternative fuels as an automobiles only fuel. Since the engine was designed for use with only E85, it can utilize the high

compression ratio unlike other current production vehicles which are Flex fuel, with the ability to switch between gasoline and E85.

## 1.2 Literature Review

### 1.2.1 Volumetric Efficiency and Spark Timing

Volumetric Efficiency and Spark Timing maps are not new. However, calibrating a multi-degree-of-freedom engine for the use of E85 as the engines only fuel takes these maps to a new level. Multi-degree-of-freedom engines are becoming increasing popular, adding variable valvetrain, variable compression ratio, variable length intake manifolds or stratified direct injection (Lumsden, Browett, Taylor, & Kennedy, 2004). These additions add complexity and increase engine calibration time. Model based calibration tools are increasingly being used to reduce calibration time (Lumsden, Browett, Taylor, & Kennedy, 2004). Models can be used in determining where multi-degree-of-freedom engines best operate. Suzuki, Nemoto and Machida were able to produce a multi-dimensional spark timing calibration for a variable valvetrain engine using engine models. These models were then fit using regression techniques to obtain polynomials for the MBT sweep. However, empirical parameters were needed in order to match the models with experimental data. This means that engine testing is still needed. On a smaller multi-degree-of-freedom engine, such as the Honda 1.8L used in this research which only has four operating modes, simulation maps are most likely too time consuming provide major benefits.

Referring to Equation (1), volumetric efficiency is defined by Heywood as the volume flow rate of air into the air intake system divided by the rate at which volume is displaced by the piston (Heywood, 1988). Volumetric efficiency is dependent on a number of phenomena that can either impede or assist in cylinder filling. Volumetric efficiency is dependent on engine speed which controls the time available to fill the cylinders during the intake event. Volumetric efficiency is also highly dependent on MAP since the throttle only impedes flow. Manifold geometry and intake tuning can also have a large influence. Valve timing can also be important. It is represented by the equation

$$VE = \frac{2\dot{m}_a}{\rho_{air} V_d N} \tag{1}$$

where 2 is the number of revolutions per cycle for a four-stroke engine, $\dot{m}_a$ is the mass flow rate of air into the engine, $\rho_{air}$ is the air density entering the engine, $V_d$ is the displacement volume and N is the engine speed. As mentioned in Heywood air density may be taken as either ambient or manifold. Ambient volumetric efficiency measures the induction effectiveness of the entire intake system, where manifold takes only into account the ports and valves. Either value can be used as long as it is consistent and clearly stated as to avoid confusion. Either ambient or manifold volumetric efficiency can be used to calculate mass air flow (Smith, Osborne, & Fickenscher, 1999).

There are many factors which influence volumetric efficiency, positively and negatively. This is shown graphically in Figure 1. Charge heating occurs when the air

temperature increases as it passes through the intake system. This is more important at low speeds because there is more time for heat transfer to occur. As the air raises the density increases which limits the amount of air that can flow through the intake system. Unlike charge heating flow friction is significantly greater at higher engine speeds. This is because higher engine speeds create greater larger flow velocities which results in more flow friction. This represents a major portion of the volumetric efficiency losses. Backflow occurs when there is exhaust that flows back into the cylinder. This hurts volumetric efficiency because the extra gas displaces potential fresh charge that could have entered the cylinders. Lastly choking occurs at high engine speeds, which is the point at which further increases in engine speed due not result in significant flow increases.

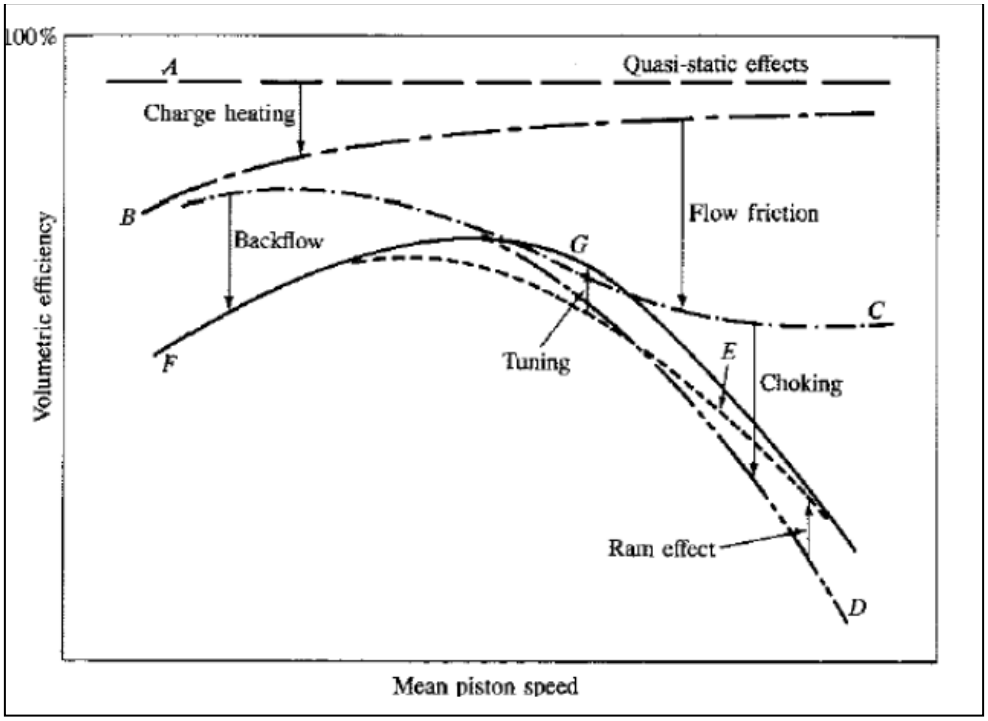


Figure 1: Factors affecting engine breathing (Heywood, 1988)

Ram effects and tuning can positively affect volumetric efficiency. Ram effects are taken advantage of by delaying the closure of the intake valve, which allows for more air to enter the cylinder even as the piston is in its compression stroke. This occurs due to the inertia of the air charge. When the intake valve begins to close the air slows down and the inertia creates a pressure rise which results in additional air entering the cylinder. This occurs at higher engine speeds due to greater air velocities leading to increased inertia.

An example of tuning is variable length intake runners as seen in Figure 2. A long runner increases the volumetric efficiency at low speeds and a short runner can increase volumetric efficiency at high speeds. This is due to wave dynamics and Helmholtz resonance.

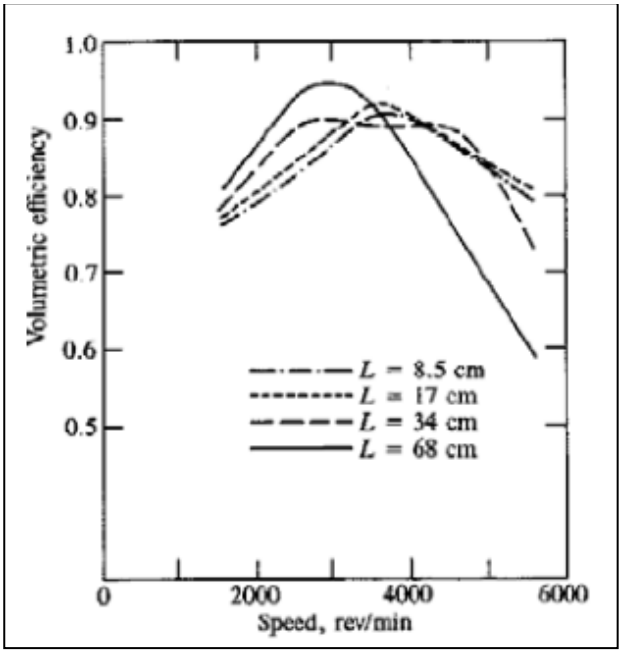


Figure 2: Effect of intake runner length on volumetric efficiency (Heywood, 1988)

Accurate Measurement of the values which make up the volumetric efficiency equation is necessary for using volumetric efficiency in feed forward air/fuel control. One important parameter is the mass flow of air into the cylinders. A key to accurate mass air flow measurements is a surge tank (Roussopoulos, 1990). This lessens flow pulsations and ensures that measurements are quasi-steady. Roussopoulos recommends measuring the flow into the surge tank volume. The size of the tank is debatable and limited by realistic size for low engine speeds, but SAE Recommended Practice J2444 offers Equation 2 (Roussopoulos, 1990).

$$\frac{9x10^4 xV_s}{min.rpm\ x\ \sqrt{no.intake\ strokes\ per\ rev}} \qquad (2)$$

Volumetric Efficiency is widely used in air/fuel control in modern engines. One of the major tasks of a modern ECU is to control fueling requirements to meet air-to-fuel ratio targets (Smith, Osborne, & Fickenscher, 1999). There are three methods generally used to account for mass air flow into the engine, which includes direct MAF measurements, volume flow rate measurements and theoretical predictions using volumetric efficiency. Mass air flow rate (MAF) measurements output a signal directly proportional to the mass flow rate of air entering the engine. An example of a MAF sensor is a hot-wire or hot-film sensor. Advantages of MAF sensors are low cost, little impediment to flow and direct relation to mass air flow (no other sensors needed). Volume flow rate sensors output a signal directly proportional to the volume flow rate of air entering the engine. This sensor must then be coupled with other sensors to measure

air density. Theoretical mass air flow predictions from volumetric efficiency can also be used. Theoretical mass air flow predictions can take the form of either Equation (1) or Equation (3).

Volumetric Efficiency is used to scale the theoretical airflow calculation since the engine is not a perfect pump. Volumetric Efficiency can be found under steady state engine operation. This requires extensive 'mapping' of a predefined matrix of engine speed and load. The ECU then stores tables of volumetric efficiency as functions of engine speed and MAP or engine speed and throttle position (Smith, Osborne, & Fickenscher, 1999). The ECU then uses the volumetric efficiency table to calculate mass air flow by rearranging Equation (1). Although mapping an engine is an extensive process, the addition of volumetric efficiency to the recorded data does not add a significant amount of time to the process. This is because calibrating an engine using the mapping process is currently a standard procedure and most of the data needed in order to calculate volumetric efficiency is already being recorded (Smith, Osborne, & Fickenscher, 1999). The use of volumetric efficiency in the speed density model means that volumetric efficiency is critical for controlling transient emissions. Precise air-fuel ratio control is necessary in order to maximize catalyst conversion efficiency. Conversion efficiencies must be maximized in order to meet increasingly strict emissions standards (Okazaki, Kato, Kako, & Ohata, 2009). Volumetric efficiency is also an important parameter in the filling and emptying models that will be used for feed forward fuel prediction. In filling and emptying maps the intake manifold is taken as a finite control

volume, with a uniform pressure. Air mass can then increase or decrease with time in this map (Heywood, 1988). From Heywood the filling and emptying map can be written as:

$$\frac{dp_m}{dt} + \frac{\eta_v V_d N}{2V_m} p_m = \dot{m}_{a,th} \frac{RT_m}{V_m} \tag{3}$$

Where $p_m$ is the intake manifold pressure, $\eta_v$ is the volumetric efficiency, $V_d$ is the displacement volume, N is the engine speed, $V_m$ is the volume of the manifold, $\dot{m}_{a,th}$ is the mass air flow entering the intake manifold, R is the gas constant and $T_m$ is the manifold air temperature. Due to manifold dynamics this equation is important in order to be able to predict intake manifold variations with respect to load changes. By solving this equation mass air flow out of the manifold can be predicted at some point in the future. This allows for fuel injection predictions as well.

When using volumetric efficiency for feed forward air predictions steady-state error will be present. There are two sources of this error. The first is the calibration error. Both engine variability and measurement error make up the calibration error. From previous work it is approximated that volumetric efficiency calculated from a LFE is 2% accurate. The second component of error is the finite spacing of the volumetric efficiency map. In between data points the engine controller must interpolate to find the value of volumetric efficiency for a given speed and load. The addition of error from interpolation is approximately 4%. Finally the MAF sensor also has error. When this and the other sources of error are taken into account the error from feed forward mass air flow predictions using a volumetric efficiency map should be within 5% accuracy.

For a given condition, with air mass, fuel mass, EGR and engine speed being the most important, there is an optimal spark timing which produces the maximum torque, which is termed maximum brake torque (MBT). Advancing the timing past this point will result combustion starting too early, which results in losses due to the extra work needed to compress the gases. Retarding the timing past this point will result in combustion starting too late which will lead to peak cylinder pressures to decrease and to occur later in the cycle, reducing the potential work output (Heywood, 1988). The spark timing degree location on a MBT curve is relatively flat (Heywood, 1988). Maximizing brake torque favorably impacts engine efficiency. Spark timing dependents on both speed and load. As the engine speed increases the crank angle degrees in which combustion occurs generally increases, which means that spark must be further advanced. Spark timing is not solely dependent on brake torque because $NO_x$ emissions can have an impact on the timing (Suzuki, Nemoto, & Machida, 2006). In practice, spark is retarded to lower torque 1 to 2 percent from MBT if active knock control is not implemented (Heywood, 1988). Spark retard can be used to lower in-cylinder temperatures (which benefits $NO_x$ emissions) and also to increase exhaust temperature, which lowers CO and HC emissions (Heywood, 1988). Retarding Spark is also used in knock control. Knock is defined as the noise that is heard when a portion of the air-fuel mixture spontaneously ignites ahead of the propagating flame. Surface ignition can also occur, where the air-fuel mixture is ignited from a hot-spot somewhere inside the cylinder. Only spark knock is controlled by spark timing. By advancing the spark, the knock intensity will increase and by retarding spark, the knock intensity will diminish. Knock also occurs mainly under high loading

conditions. Besides retarding spark, knock can also be controlled by the properties of the fuel used. The octane rating of a fuel is a measure of the fuels resistance to knock. In the test cell it is important to have some measure of engine knock. The human ear is routinely used in determining knock (Heywood, 1988). Knock sensors are also used that detect knock based on the acceleration caused by vibrations. Once a spark timing calibration has been performed, the engine controller must be able to easily obtain the necessary spark timing value. Spark timing maps are multi-dimensional which depend on the engines degree of freedom in important control parameters. At a minimum the map must reference both engine speed and manifold pressure (MAP). They can consist of a look-up table inside the ECU. This limits the computing power necessary to obtain the necessary values (as opposed to an empirical formula).

### 1.2.2 Engine Electrical

In order to utilize the Honda 1.8L engine and convert it from CNG to E85 a new ECU was used. Determining which sensors to pair to which hardware components of the ECU is not trivial. One of the more common engine sensors are variable resistor analog sensors. Temperature sensors and potentiometers are common variable resistors. A pull-up resistor is often used, such as the one shown in Figure 3.

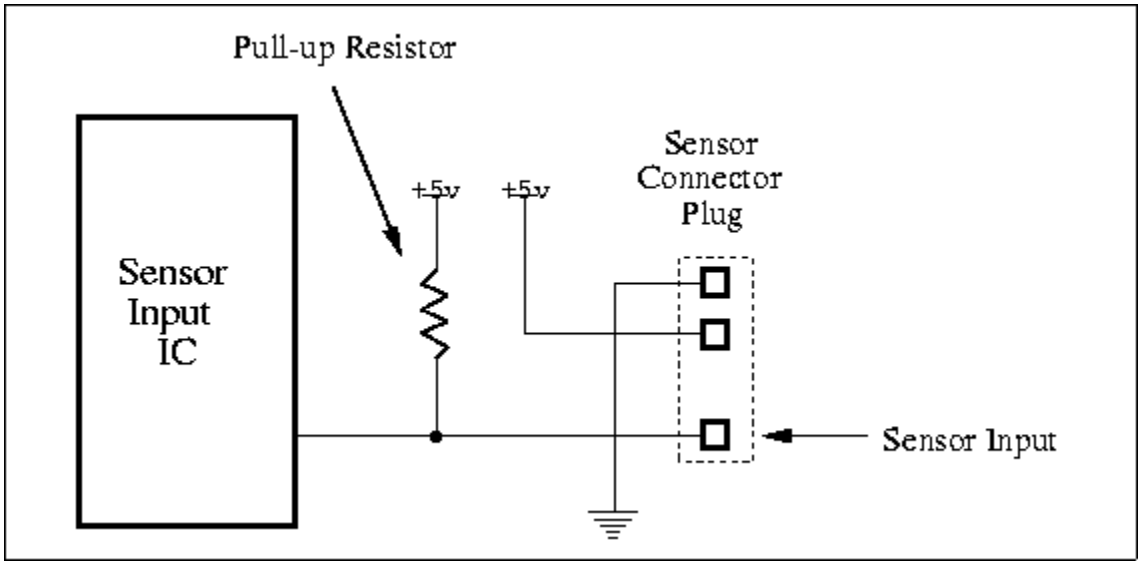


Figure 3: Pull-up resistor

There are two things to consider when selecting a pull-up resistor. First if the sensor is not connected the sensor input defaults to 5V. This can be good for error detection in a car, where an unrealistic high temperature is recorded at 5V, which could trigger a check engine light. Second is the type of sensor. Variable resistor sensors such as RTDs generally use a pull-up resistor. This is because a pull-up resistor is used to create a voltage divider circuit (Martin, 1992). This is seen in Figure 4. Pull-up resistors eliminate the need for external sensor power allowing sensors to only have a signal and ground wire.

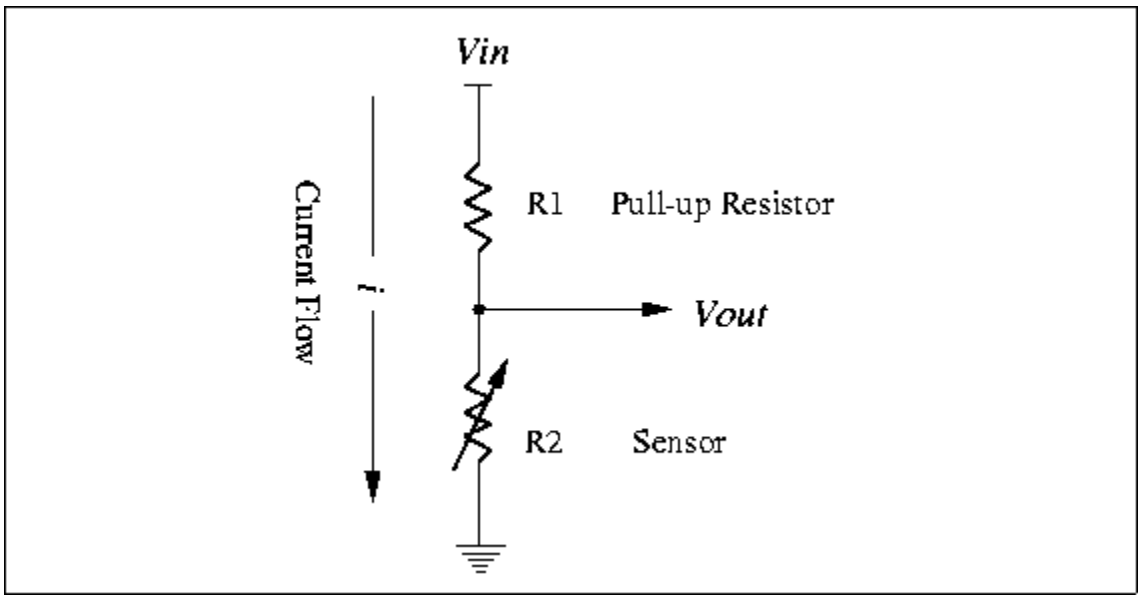


Figure 4: Variable resistor (R2) coupled with a pull-up resistor

A pull-down resistor is similar to a pull-up resistor except that it pulls down the voltage to 0. Again like the pull-up resistor there are two things to consider with pull-down resistors. First is when the sensor is disconnected the signal is pulled low to 0. This can be very beneficial with pressure sensors where a low pressure could be detected with error detection. If a pull-up resistor was used with a MAP sensor and the connection was lost, a high reading would result. The ECU would then inject more fuel than necessary which could flood the engine. A pull-down resistor would have the opposite effect, stalling the engine from the lack of fuel injection. The later is seen as the less harmful.

### 1.2.3 Honda R18A3 Engine

The Honda 1.8L R18A3 that is used in this research is a multi-degree-of-freedom engine. The engine is equipped with a variable length intake manifold as seen in Figure 5.

The valve is closed at lower speeds, allowing for a longer intake manifold. The valve is opened at high speeds. Figure 6 shows that the valve was intended to be opened around 5000 RPM. This gives a larger torque output due to wave dynamics.

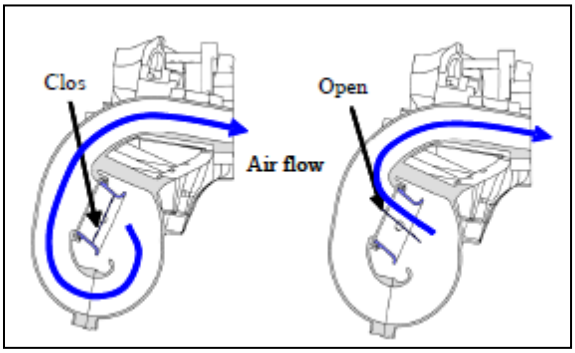


Figure 5: Honda R18A3 variable length intake runner

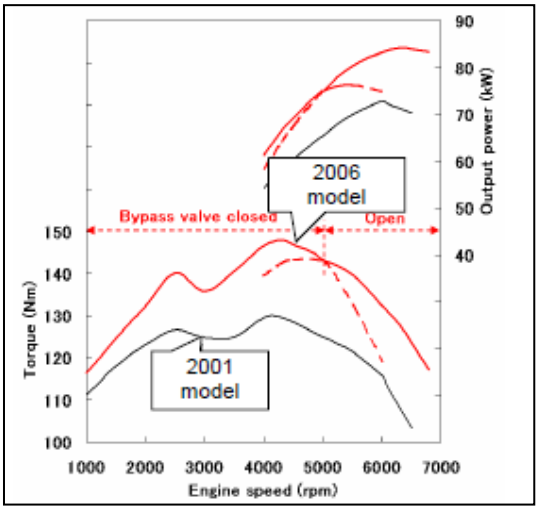


Figure 6: Honda R18A3 variable length runner torque curve

The engine is also equipped with variable valve lift which allows for greater efficiency gains. The variable valve lift consists of a high-output cam which is used to produce more power. When lower power levels are necessary for operation a delayed

closure cam is used. One of the two intake valves delays its closure after the intake stroke which allows for fresh charge to be pushed out of the cylinder. The delayed closure cam improves fuel efficiency by reducing the engines pumping losses since the throttle must be opened more to compensate for the fresh charge being pushed back into the intake manifold. These results can be seen in Figure 7, which displays a comparison between the gasoline engine and the CNG engine for the two different cam configurations.

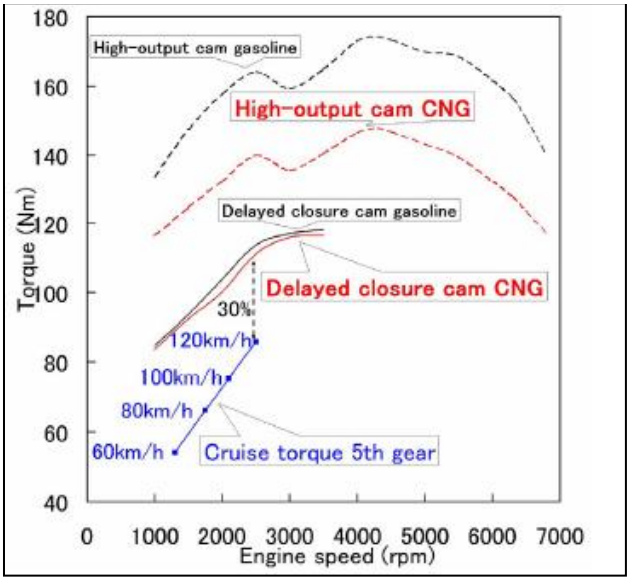


Figure 7: CNG engine vs. gasoline engine with cam configurations

## 1.3 **Motivation**

E85 was selected as the fuel of choice for the EcoCAR team due to its largely renewable nature as a fuel. E85 also has a high octane rating (~100-105) which can be beneficial. When coupled with a high compression ratio engine, higher thermal efficiencies result. The development of a new engine controller was necessary because the high compression ratio engine that was available was for CNG. Therefore new engine

calibrations had to be performed. Part of these engine calibrations were volumetric efficiency and spark timing maps, which are discussed in the subsequent sections.

## 1.4 **Project Objective**

The goal of this project was to create a volumetric efficiency map and a spark timing map that is used by Ohio State's EcoCAR challenge team in order to develop a new engine controller. By creating a volumetric efficiency map a feed forward based control can be used to predict the air entering the engine. This will allow for more precise control of the air to fuel ratio during engine transients, which will help lower transient emissions. The spark timing map will be used in order to optimize engine efficiency and limit engine knock. Feed Forward torque control maps were also created, which allows the supervisory controller for the vehicle to interact with the engine by requesting a desired torque the vehicle requires.

# Chapter 2 : Experimental Setup

The research described was performed at The Center for Automotive Research at The Ohio State University. A engine test cell was used which was equipped with a four-quadrant 200 hp DC dynamometer which was used to control engine speed. The test cell is also equipped with a mobile laminar flow element which is used for precise engine air flow measurements. The laminar flow element is attached to a 55 gallon drum, which serves as an accumulator to dampen out high frequency oscillations. The test cell is also equipped with emissions analyzer equipment. This consists of a Horiba emission analyzer (Horiba MEXA 7500) with the capability to measure dry CO, NOx, $O_2$, wet THC and $CO_2$. The Horiba also has two individual analyzers, both having the ability to measure with 2 sample lines.

## 2.1 Engine Instrumentation

The engine is equipped with many sensors. As seen from Table 1 some are attached to the Woodward ECU and others attached to other data acquisition systems, such as ETAS and National Instruments. The engine is equipped with a water cooled cooling tower with a built in thermostat to regulate coolant temperature. An external electric water pump is used in place of the stock belt driven engine water pump. The engine also has 4 in-cylinder pressure sensors which are a combination of a spark plug and pressure transducer.

Table 1: Engine sensors

| Woodward ECU sensors | | | ETAS/other sensors |
|---|---|---|---|
| 1 | CMP (Camshaft position) sensor | 18 | Barometric pressure |
| 2 | CKP (Crankshaft position) Sensor | 19 | Catalyst thermocouples |
| 3 | ECT (Engine coolant temperature) sensor | 20 | Crank encoder |
| 4 | EOP (Engine oil pressure) sensor | 21 | Engine coolant flow rate sensor |
| 5 | EGR (Exhaust gas recirculation) valve | 22 | Exhaust manifold pressure sensor |
| 6 | Ethanol concentration sensor | 23 | In-cylinder pressure transducers |
| 7 | Exhaust RTD | 24 | Individual intake port thermocouples |
| 8 | FTP (Fuel tank pressure) sensor | 25 | Intake manifold thermocouple |
| 9 | Fuel level sensor | 26 | LFE thermocouples |
| 10 | Fuel rail pressure sensor | 27 | LFE differential pressure sensor |
| 11 | IAT (Intake air temperature) sensor | 28 | |
| 12 | MAF (Mass air flow) Sensor | | |
| 13 | MAP (Manifold air pressure) sensor | | |
| 14 | Oil Pressure Switch | | |
| 15 | Post CAT EGO sensor | | |
| 16 | TP (throttle position) Sensor | | |
| 17 | UEGO sensor | | |

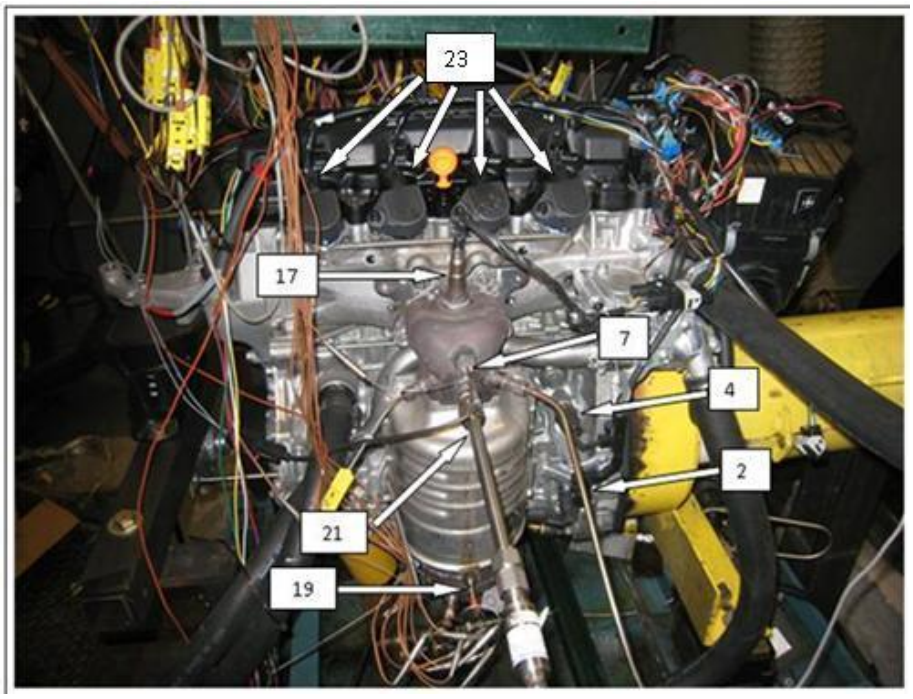


Figure 8: Engine Sensor Locations

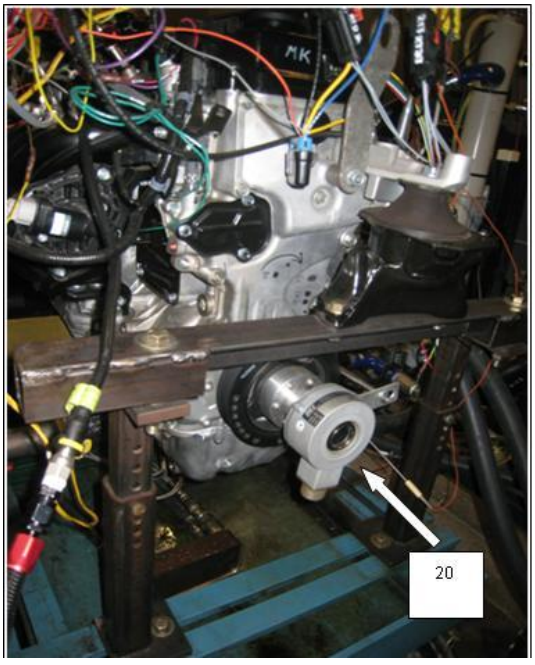


Figure 9: Crank encoder location

Figure 8 and Figure 9 correlate to Table 1 and show some of the sensors used during engine testing. Figure 10 shows many of the stock engine sensors as well as some of the new sensors used during engine testing.

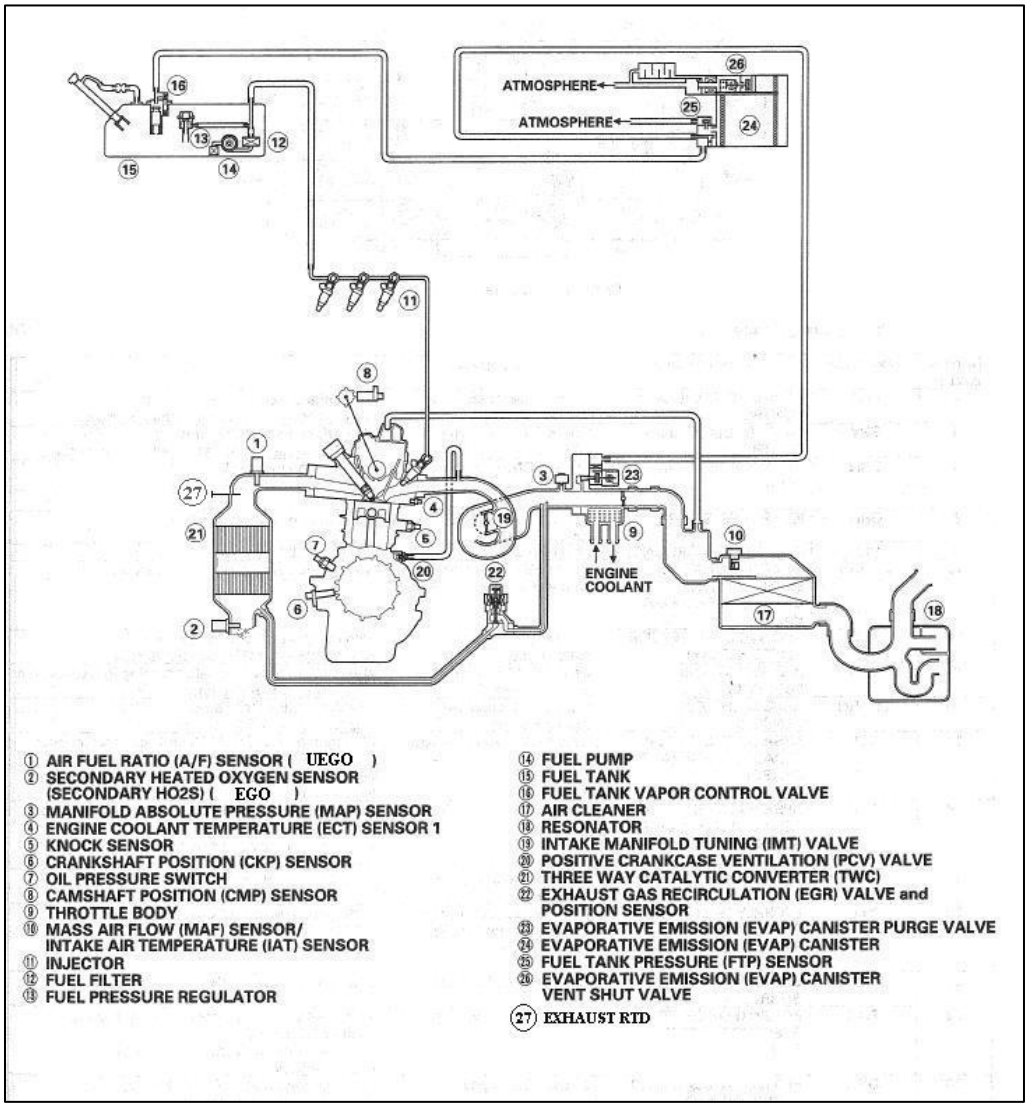


Figure 10: Engine sensor location diagram

In order to record engine knock during the spark sweeps a listening device was used. This device was made of copper tubing and was attached to the engine block. The

device was attached where the original Honda piezoelectric knock sensor was located. This system was patterned after what is used in industry for routine engine testing. It produced good results in the ability to hear when the engine was knocking.

Volumetric efficiency calculations require a number of necessary sensors. These include the MAP sensor, intake air temperature (IAT) sensor, MAF sensor and engine speed. The MAP sensor is located right after the throttle plate. The IAT sensor is located with the MAF sensor in the air cleaner box. Since volumetric efficiency can be referenced to any location, the location of these sensors can vary. Engine speed was recorded using the engines speed sensor.

A 360 degree crank encoder was attached to the crank shaft to be used in conjunction with in-cylinder pressure measurements. Using this encoder in-cylinder pressure was referenced to every crank-angle degree. The encoder also emits a top-dead-center (TDC) pulse which allows for references where the cylinders are with respect to crank angle. This encoder ties into a National Instruments card, which is then connected to a computer to be used in conjunction with LabVIEW.

## 2.2 **Data Acquisition System**

Data is recorded using multiple data acquisition devices. The first are several ETAS modules that allow for BNC and thermocouple connections. A ETAS ES410, 8 channel analog module, ETAS ES411, 4 channel analog with sensor supply voltage and ETAS ES420, 8 Channel Thermocouple modules were used. Each of these modules were used for sensors that were not in the wiring harness design. Examples of devices that

were coupled with these modules is the laminar flow element (LFE), which had thermocouples attached to the thermocouple module and pressure sensors attached to the analog module. Each of these modules are connected to one another and then connected to INCA via an Ethernet connection.

The rest of the sensors that are included in the engine wiring harness are attached to the Woodward 128 pin ECU. The Woodward ECU uses Matlab SIMULINK to program the engine control code. A Motohawk development library is used in conjunction with SIMULINK which allows for the interfacing with the Woodward ECU. Mototune is then used to flash the ECU. Mototune also is used for indexing and updating calibration files for new engine controller code builds.

INCA is primarily used as an experimental tool, although calibrations can also be modified in INCA. INCA communicates with the ECU via CAN Calibration Protocol (CCP). INCA is then used by the user on a laptop which is connects with the CCP network via a PCMCIA card. INCA is also the user interface used when running engine tests. INCA allows for the control of all parameters inside the ECU. This means that the user can control parameters such as throttle position and spark timing. INCA is also used to record data that was used in this research. This can be done since it is interfaced with the ECU. The advantage of using INCA is that it easily works with the ETAS modules allowing for seamless acquisition of almost all data needed.

In-cylinder pressure data was also recorded. In-cylinder pressure was used for basic monitoring and diagnostics during engine testing. In-cylinder pressure was

referenced to a one degree of crank angle resolve encoder. In-cylinder pressure was recorded using piezoelectric pressure sensors which were integrated into the engines spark plugs. This eliminated the need for any engine head or block modifications. The pressure sensors output a 16 pico coulomb per bar of pressure. This signal is then routed into a charge amp. The charge amp converts the 16 pico coulomb per bar of pressure signal into a voltage signal. This voltage is then fed into a National Instruments data acquisition system which is equipped with BNC cable inputs. The National Instruments system is connected to a computer card where LabVIEW is used to record the data. The crank encoder is also tied into the computer, which allows for referencing of the in-cylinder pressure data.

# Chapter 3 : Engine Harness Development

In order to convert the Honda 1.8L CNG engine to E85, a new Woodward programmable ECU was used. This is due a few reasons. First the stock ECU was not available for our use. Second it would not have been useful since the calibrations such as spark timing were for CNG, not E85. The use of the programmable ECU with the stock Honda wiring harness required a significant amount of design and modification of the stock harness. In addition to coupling the stock Honda harness with the new ECU, quite a bit of the harness was not needed. Some of the harness was a coupling to the cabin of the car; other parts were for redundant components such as the battery or alternator. Significant time was taken to decide which components of the wiring harness were unnecessary for use with EcoCAR's vehicle and carefully remove them. Before connections between the stock Honda harness and the new ECU could be made the inputs into the ECU for each sensor needed to be decided.

First a careful review of all sensors and inputs into the stock ECU was made. The Honda harness was designed to work in conjunction with a vehicle that the EcoCAR team was not using and thus many parts of the harness were eliminated. The remaining sensors were paired with compatible inputs into the Woodward ECU. This design can be viewed in Appendix A. Once the design of which sensors were to be paired with what inputs on

the Woodward ECU the wiring harness was built. Some of the considerations necessary for the design are described in the following sections.

Another important section of the harness design was providing adequate power and ground. The original Honda harness used the fuse/relay panels that would be located in a stock vehicle. This needed to be a complete redesign for several reasons. The main reason was that the Honda fuses/relay panel was not available. Also the original Honda fuse/relay panel would not be able to be utilized due to different needs for the EcoCAR vehicle. A new relay/fuse box was designed. This utilized a Bussman 15303-5-6-4 fuse/relay panel. The design can be viewed in Appendix A. The design consisted of distributing power through 5 different relays which would be controlled by the Woodward ECU. Care was taken to divide the sensors into groups to be controlled by a single relay then branched off power to multiple sensors. This is seen in Table 2.

Table 2: Relay and fuse design

| Relays | | | | |
|---|---|---|---|---|
| | | | | |
| **Relay** | **Location** | **Relay controlled by** | **Relay supplies power to** | **Fuse** |
| | | | | |
| Main relay | Bussmann # 1 | MRLY PWM (J2-B15) | DRVP J2-A18 | 15A |
| | | | DRVP J2-A19 | |
| | | | | |
| Fuel system relay | Bussmann # 2 | PWM (J2-B17) | Fuel Pump | 15A |
| | | | EVAP canister vent shut valve | |
| | | | EVAP canister purge valve | |
| | | | Ethanol Concentration sensor | |
| | | | Fuel Injectors | |
| | | | | |
| Ignition coil relay | Bussmann # 3 | PWM (J2-B12) | Ignition coils | 15A |
| | | | | |
| Cooling relay | Bussmann # 4 | PWM (J2-B19) | Variable speed radiator fan | 20A |
| | | | Electric water pump | |
| | | | | |
| Sensor power relay | Bussmann # 5 | PWM (J2-B20) | UEGO sensor 1 power | 15A |
| | | | Post CAT EGO sensor heater | |
| | | | MAF sensor | |
| | | | 24-pin connection pin 12 for CMP and CKP sensors | |
| | | | | |
| Power Relay | Electronics mounting board | Main Power Switch | Fuse and Relay box | 80A |

Once the design was completed the wiring harness was built. Each sensor was verified using the new wiring harness. New calibrations were created for each sensor as well. The ECU reads a voltage signal for each sensor. Therefore the conversion from what the sensor is measuring (ex. Pressure, temperature) to voltage must be known. Pressure was calibrated using a gas cylinder and a 0-30 psia Omega pressure transducer. A simple x-y graph was created to compare the ADC count read from the ECU for the pressure transducer to the pressure reading from the Omega sensor at various pressures. Temperature sensors were calibrated using a thermal chamber, which regulates the temperature in order to create a resistance versus temperature graph. The resistance value is then converted to a voltage using the ECU.

The wiring harness can be broken down into 3 sections. This includes analog and digital sensors and special circuitry.

## 3.1 Analog Sensors

Analog sensors are the most common sensor used on the engine wiring harness. The analog sensors can be divided into 3 sections for use with the Woodward controller. These are pull-up and pull-down resistors and then a combination known as a high impedance input.

### 3.1.1 Pull-up Resistors

Pull-up resistors are generally used in conjunction with variable resistor sensors. This is used to implement a simple voltage divider circuit. Each sensor that has been paired with a pull-up resistor in the wiring harness is a variable resistor. Three of these

are temperature sensors which include an engine coolant temperature sensor, intake air temperature sensor and exhaust RTD sensor. The other two sensors are two wire potentiometers (signal and ground). These include an intake manifold tuning valve position sensor and a fuel level sensor. The intake manifold tuning valve controls the variable length manifold. While the valve only operates in an open or closed position, the ability to know if the valve is stuck in between is an important error detection measure.

### 3.1.2 Pull-Down Resistors

Pull-down resistors are used in order to pull the signal down to zero if the signal is disconnected. The engine harnesses pressure sensors include a fuel rail pressure sensor, fuel tank pressure sensor, manifold air pressure (MAP) sensor and an engine oil pressure sensor. The engine oil pressure sensor is only activated when the variable valve timing is in operation. The powered potentiometers include the throttle position sensor and EGR position sensor. The throttle position sensor utilizes two different position sensors which monitors the differential between each other to eliminate drift. Finally the MAF sensor uses a pull-down resistor to read the sensors voltage output. It is essential to use a pull-down resistor in this circumstance because if the sensor fails it will bring the voltage to zero. This means that the engine controller will stop injecting fuel. On the contrary if a pull-up resistor was utilized and the sensor failed a high voltage would be read signaling a large amount of air entering the engine which could result in a rich stall due to too much fuel injection. The pull-down resistor could also cause the engine to stall, but it is better than flooding the engine with fuel.

### 3.1.3 High Impedance

The last type of analog sensor is a high impedance input. This incorporates both a pull-up and pull-down resistor, both which are in the mega ohm range. This type of sensor is used to eliminate noise. This is why the engines post-catalyst EGO sensor uses the high impedance input.

### 3.1.4 Hardware filters

Hardware filters inside the Woodward ECU created another option when choosing which ECU input to use. After hardware such as pull-up or pull-down resistors an R-C circuit is used to filter noise. In some cases different filters could be selected, which had different time constants. Faster responding signals utilized the low time constant filters. This is because lower time constants have higher cutoff frequencies, allowing the hardware to accept higher frequency signals. Slower moving signals such as throttle position use higher time constants in order to filter out higher frequencies.

One example of this is the use of two different possible pull-down resistor inputs to the Woodward ECU, which are shown in Figure 11 and Figure 12. The capacitor is altered in order to change the time constant value.

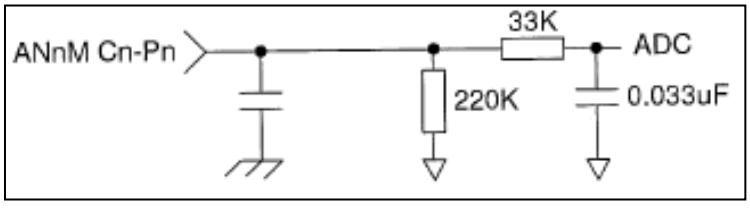


Figure 11: Woodward pull-down resistor input with 1ms time constant

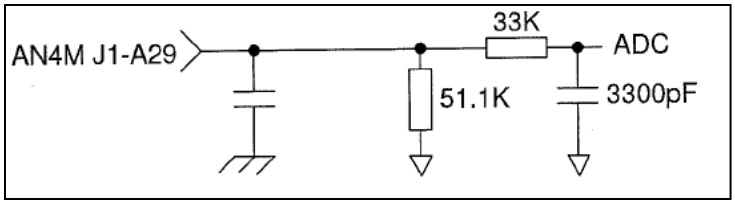


Figure 12: Woodward pull-down resistor input with 100 µs time constant

The input shown in Figure 11 was used with throttle position A and B signals. Figure 12 however was used with the MAP sensor. The same filter considerations were made when the choice of time constant was available.

## 3.2 **Digital Sensors**

Two digital sensors are used in the engines wiring harness. The first is an ethanol sensor. The ethanol sensor is used to determine the percentage of ethanol in the fuel and also the temperature of the fuel. The sensor outputs a square waveform in which both pulse width and frequency are used to interpret the temperature and ethanol percentage. If by chance the user accidently puts regular gasoline in the vehicle it would be very important to determine this. If a gasoline calibration is available on the engine controller, the controller would need to switch to gasoline mode. If no calibration is available engine damage could result if the engine was run. Regular gasoline cannot withstand the high compression rations of the engine. The second digital input is the oil pressure switch. This switch simply tells if the engine has built an acceptable amount of oil pressure. Without this pressure severe engine damage will result.

## 3.3 Special Circuitry

The engine has a variety of different special circuitry components.

### 3.3.1 Crank and Cam Sensor

The crank and cam sensors are used in order for the engine controller to determine the engines crankshaft speed and cam shaft speed. The camshaft originally consisted of a 4 tooth wheel. However the Woodward ECU camshaft encoder input could not interpret this setup. Therefore three of the teeth were ground off to make a 1 tooth wheel. Another addition to the camshaft encoder was a pull-up resistor circuit. This was an external circuit that was used in order to amplify the encoders signal. Without it the engine controller could not detect the signal.

### 3.3.2 Low and High-Side Driver

Many of the engine actuators utilize low and high-side drivers. These can be used in conjunction with pulse width modulation (PWM) which allows for the use of cheap digital circuits to implement variable current control. The evaporative emissions system which includes an EVAP canister shut valve and an EVAP canister purge valve. The canister shut valve is used for leak detection within the fuel tank, while the purge valve is used to take the evaporated gasoline in the fuel tank and put it in the engines intake stream to be combusted and therefore eliminated. Both of these use a low-side driver, which is used to ground the circuit. A MOSFET or BJT is used to perform this operation. The load is connected directly to the power and the NPN collector connects to the load. The emitter is grounded and the base is supplied with a positive current to turn on the

NPN transistor. This allows for the flow of current to ground. This operation is shown in Figure 13.

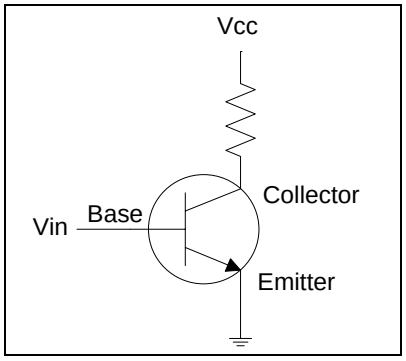


Figure 13: NPN transistor (low-side driver)

Low-side drivers are also used to open and close all of the engines relays. When the low-side drive closes a magnetic field closes the relays switch. The relay design can be viewed in Table 2.

A low-side driver is also used for the UEGO and EGO heaters. The only high-side driver that is used is with the engine's EGR valve.

In order to drive high power components that include the fuel pump and electric water pump an Infineon BTS555 high-side switch was used. The high-side switch is a MOSFET that has additional circuitry built-in to protect the MOSFET. The high-side switch is used to control power send to the component thus the term high-side. A low side lamp driver is used to control the switch. Figure 14 and Table 3 show the setup of the high-side switches. Figure 15 shows the incorporated into a circuit board for the fuel pump.

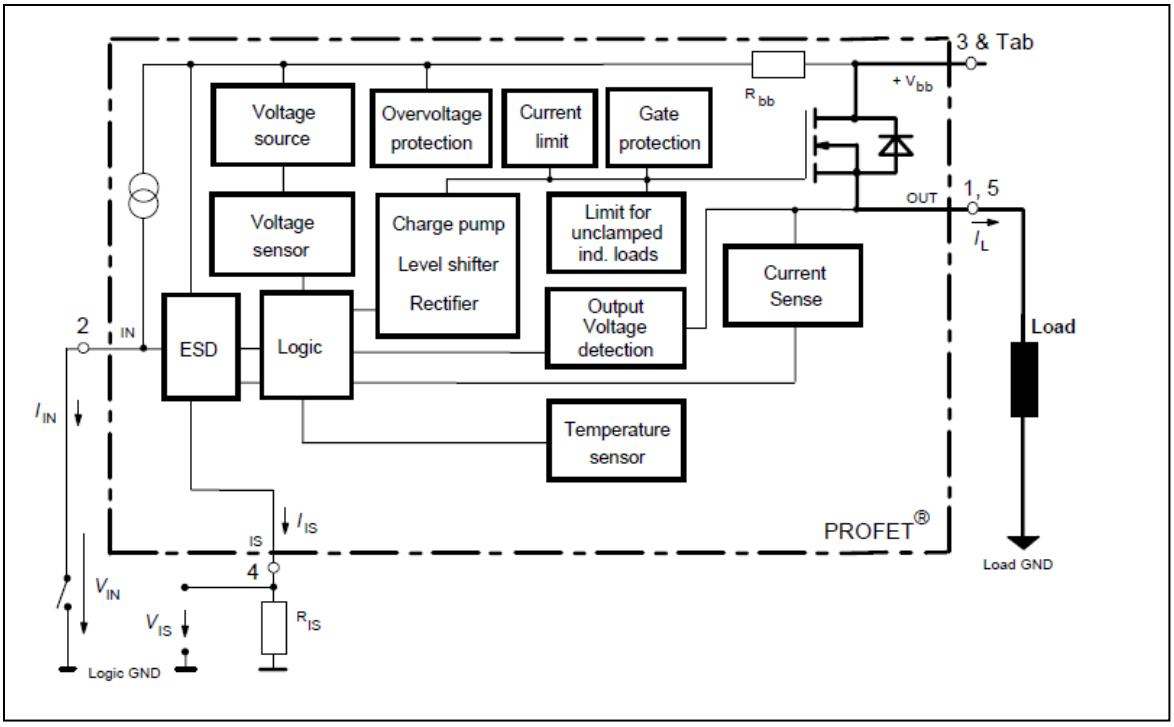


Figure 14: Infineon BTS555 high-side switch circuitry (Infineon, 2008)

Table 3: Infineon BTS555 high-side switch pins (Infineon, 2008)

| Pin | Symbol | Function |
|---|---|---|
| 1 | OUT | Output to the load. Pins 1 and 5 are shorted together in high current applications |
| 2 | IN | Input, activates the power switch in case of short to ground |
| 3 | Vbb | Positive power supply voltage. The tab is electrically connected to this pin. In high current applications the tab should be used for the Vbb connection instead of this pin |
| 4 | IS | Diagnostic feedback. Feedback proportional to current. |
| 5 | OUT | Output to load. Pins 1 and 5 must be shorted with each other especially in high current applications |

Figure 15: High-side switch for fuel pump

### 3.3.3 Fuel Injectors

The 4 fuel injectors use special circuitry to control their opening and closing. The fuel injector driver circuitry use a peak and hold method, which gives a high 3A current initially to open the injector and then holds at 1A, which saves power. Since the wiring harness was originally designed for use with CNG, it had larger injectors for the gaseous fuel. The wiring harness was modified to accommodate injectors designed for E85. This can be seen in Figure 16. A custom stainless steel fuel rail was made and fitted with a fuel pressure sensor. The fuel system is a returnless fuel injection system, so fuel pressure is regulated at 350 kPa using a feedback control loop.

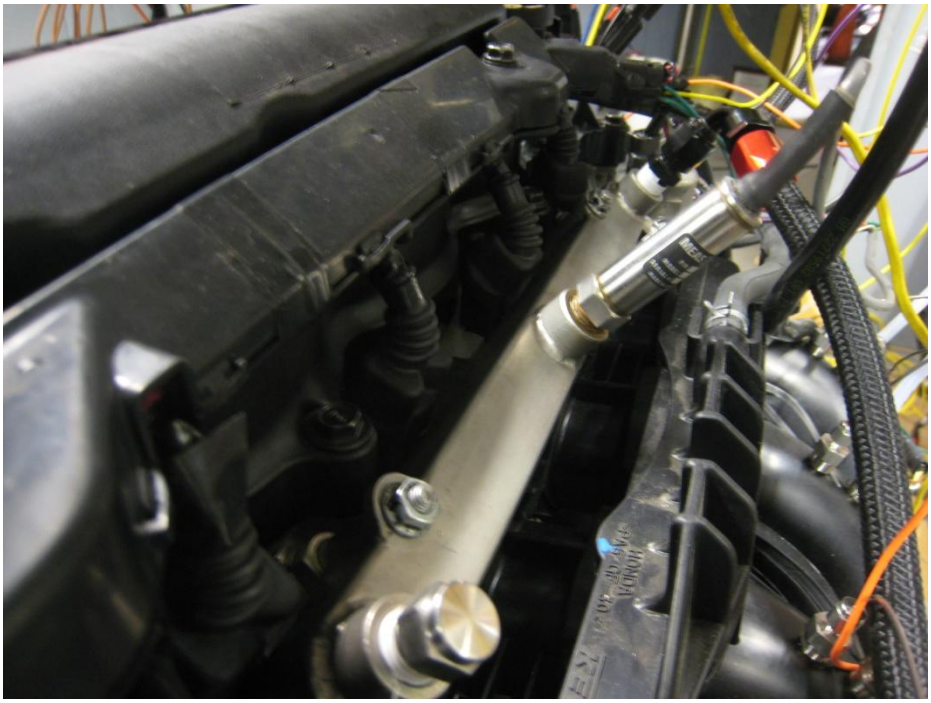

Figure 16: Fuel injectors, custom fuel rail and fuel pressure sensor

### 3.3.4 Spark Control

The electronic spark control circuitry is also specially incorporated in the engine controller. The engine uses a coil on plug system, which means that all spark timing components are controlled by the engine controller independently via digital outputs. This allows for spark timing controls such as the map created for this research project.

### 3.3.5 H-Bridge

An H-bridge utilizes a PWM to apply current bi-directionally through a load. The term H-bridge comes from the circuit shape as seen in Figure 17. The circuit is built using 4 switches which are opened or closed depending on the desired direction of current through the load.

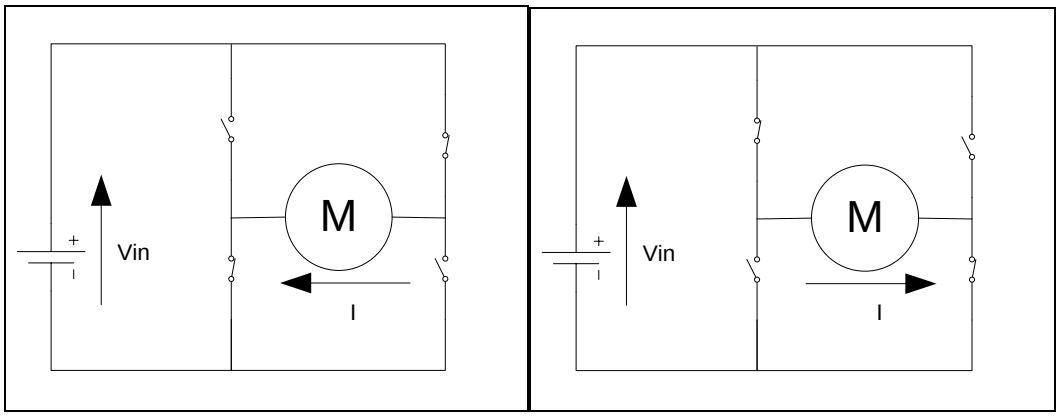


Figure 17: H bridge operation modes

Three different H-bridges are utilized in the wiring harness. The first is the intake manifold tuning valve. This must be able to open and then close, both which require electrical power. The throttle also uses an H-bridge to control the opening and closing. The rocker-arm control solenoid also uses an H-bridge, but only uses the positive side, since it will close on its own once power is not applied.

### 3.3.6 UEGO Circuitry

A complex circuit is involved in conditioning a UEGO sensor. The engine control has the ability to use 2 different UEGO sensors. Only one is utilized in the engine control design and is located before the catalyst. The UEGO sensor uses 6 wires, one for ground and one for heater power. The other 4 use the special circuitry from the engine controller. This contains a feedback control loop which is designed to regulate the gas current pump in order to keep the output of the electrochemical cell constant. The pump current is then the indicator of the oxygen content of the exhaust gas stream. The UEGO sensor can be

viewed in Figure 18 and Figure 19. It is placed before the catalyst and the EGO is placed after the catalyst.

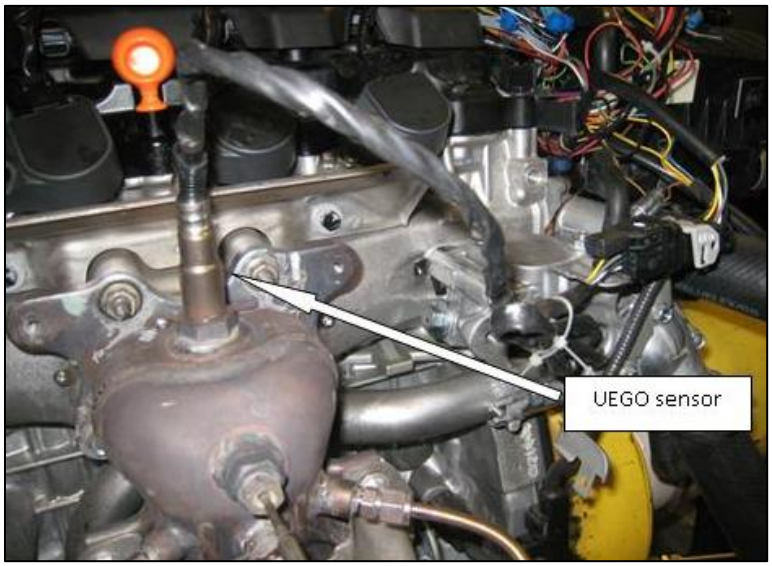


Figure 18: UEGO sensor

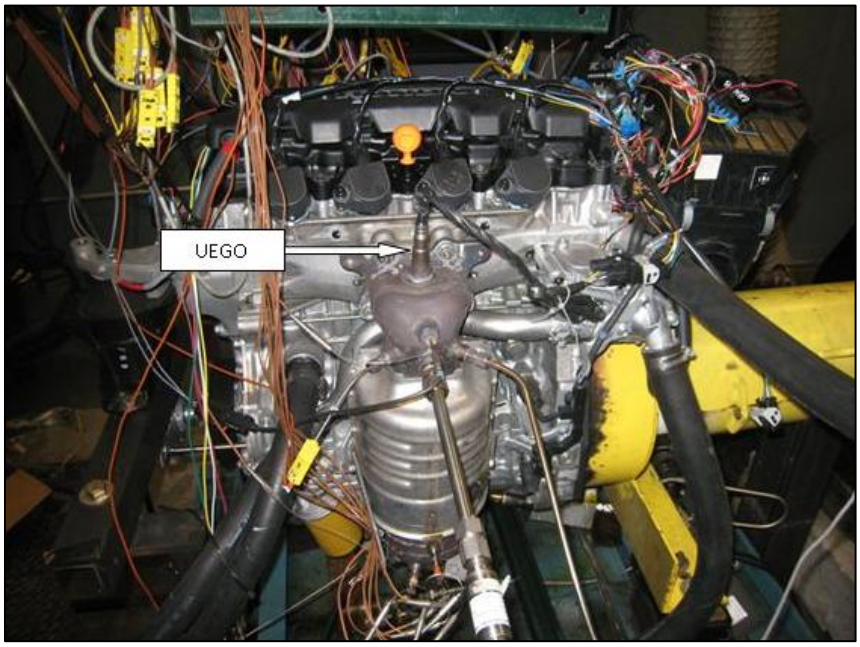


Figure 19: UEGO sensor location full view

# Chapter 4 : Engine Control Maps

Once the wiring harness was fabricated and tested, the engine control code finalized, and the engine was running smoothly engine testing could begin. Two engine control maps were developed using extensive testing of a large matrix of different operating conditions. The Honda engine used has four operating modes as seen in Table 4, which consists of variable valve timing and a variable length manifold.

Table 4: Honda engine operating modes

| Configuration Sequence | Variable Valve Timing | Variable Length Manifold |
|---|---|---|
| 1 | Delayed Closure Cam | Bypass Valve Closed |
| 2 | Delayed Closure Cam | Bypass Valve Open |
| 3 | High Output Cam | Bypass Valve Open |
| 4 | High Output Cam | Bypass Valve Closed |

To complete the full operating range all four operating modes would need to be calibrated. In an effort to save time in a project with a very short development cycle two of the configurations can easily be eliminated. Referring to Figure 6 the bypass valve on the variable length manifold is best opened around 5000 RPM. Since this engine is used in conjunction with an advanced hybrid powertrain for the EcoCAR vehicle, speeds exceeding 5000 RPM will not be used. This eliminates configurations 2 and 3 from Table

4. The remaining configurations (1 and 4) were examined using a coarse mapping process.

## 4.1 Coarse Mapping

The purpose of the coarse mapping process was to determine which valve timing to use. If a valve timing configuration could be eliminated from the engine testing matrix considerable time would be saved. Both the delayed closure cam (Configuration 1) and the high output cam (Configuration 4) were tested. Another reason for the initial coarse mapping was to determine approximant locations of MBT. This decreases the amount of time needed when doing spark sweeps. This is because when doing the fine mapping the spark sweep can be located around the MBT location which was found during the coarse mapping, which eliminates the need to do a full range spark sweep.

In order to create both a volumetric efficiency and spark timing map an extensive matrix of data points was be tested. The first testing matrix was a coarse mapping process whose design of experiment can be seen in Table 5.

Table 5: Design of experiment-Coarse

| **Stage** | |
|---|---|
| 1 | Engine speed set: 500 RPM intervals, 1000 RPM to 5000 RPM |
| 2 | Manifold pressure (MAP): 10 kPa intervals, 40 kPa to wide open throttle |

Engine speed and manifold pressure were selected as the two parameters to set during the testing matrix because they are two key parameters to engine operation. Both speed and manifold pressure are needed to determine the full matrix of engine operating points. Engine speed is a necessity to parameters such as volumetric efficiency and spark timing. Manifold pressure is more convenient than mass air flow, since the same range is present at each engine speed. Throttle angle is not an acceptable parameter to use because it is not always consistent.

The dynamometer controlled engine speed. Once this was set manifold pressure was changed by using INCA to change the throttle position. Throttle position was then varied until the desired MAP was set. It was important to be as close to the desired MAP value as possible. While not a major issue for spark sweeps, with volumetric efficiency, the table look up is based on an interpolation from the irregular spaced MAP and speed values to a regularly spaced values. Therefore the closer the actual MAP is to the desired value the less interpolation error will be present and a more accurate map will result.

Once a speed and manifold pressure was set, a spark sweep was performed. Initially for the coarse mapping process spark was started at 0 degrees before top-dead-center (BTDC) and advanced in 5 degree increments until MBT was reached. At each increase in spark advance the engine torque was observed. Spark advance was increased until the torque maximized and then started to decrease. Once the MBT spark advance point was set, the exhaust manifold temperature was observed. Only when the exhaust manifold temperature was constant was INCA then used to record data. This was to

ensure equilibrium after changing the spark advance. Thirty seconds of data was recorded for each load and speed configuration in order to average the data.

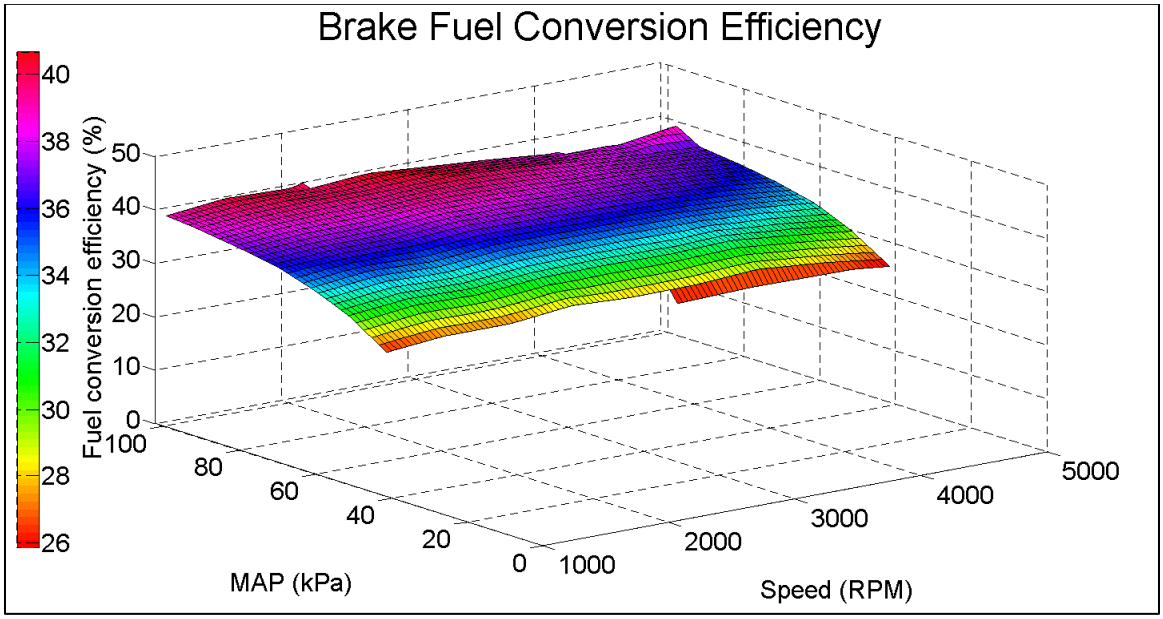


Figure 21: Coarse map surface brake efficiency with high output cam, long runner

Figure 20, Figure 21, Figure 22 and Figure 23 show the results of the coarse mapping process. Overall it was found that the high-output cam had higher or about the same efficiencies as the delayed closure cam when comparing against manifold pressure and engine speed. Both cams had similar peak brake fuel conversion efficiencies at WOT. This is because the main effect of the delayed closure cam is the opportunity to reduce pumping losses by opening the throttle more. The location of this peak was near the same engine speed with both cams. Brake efficiency varied mainly with manifold pressure for both cams. The high output cam overall had an average brake efficiency difference of 1.20% compared to the delayed closure cam, which represents a 3.94%

increase in brake efficiency. Figure 24 summarizes the results through the subtraction of the high output and delayed closure cam maps.

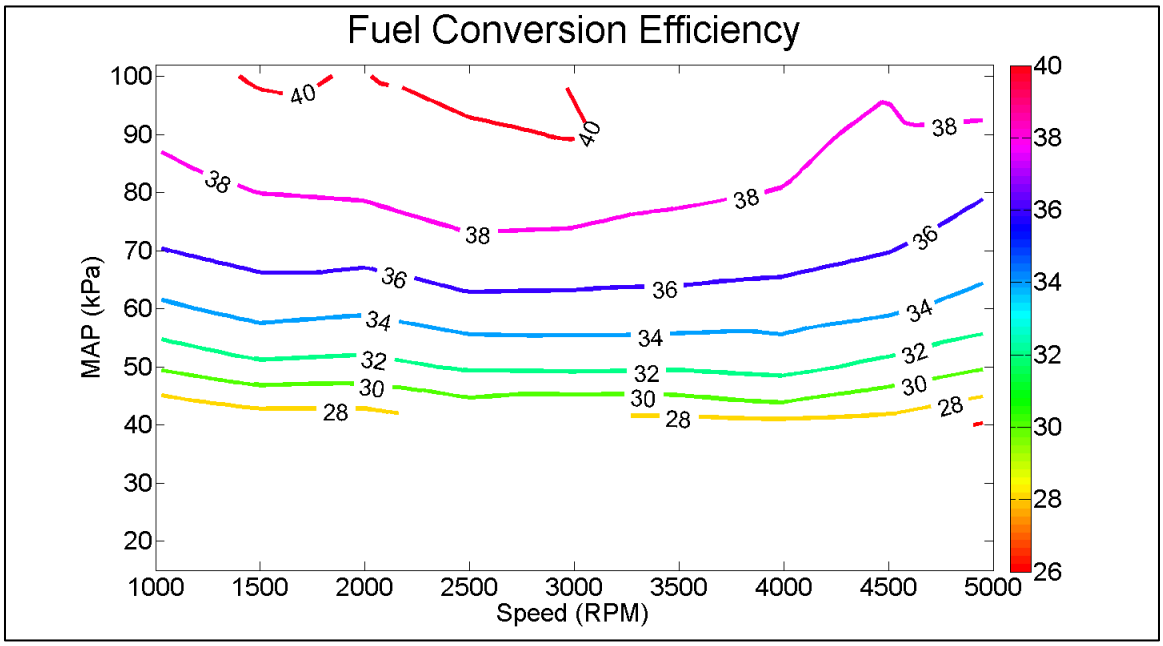


Figure 20: Coarse map contour brake efficiency with high output cam, long runner

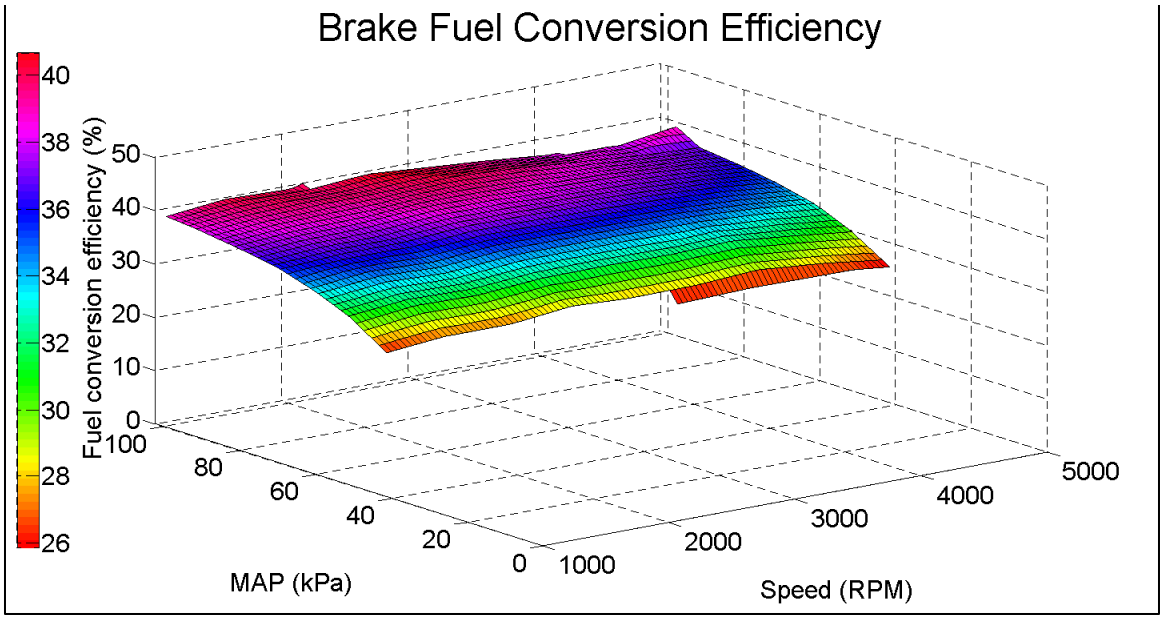


Figure 21: Coarse map surface brake efficiency with high output cam, long runner

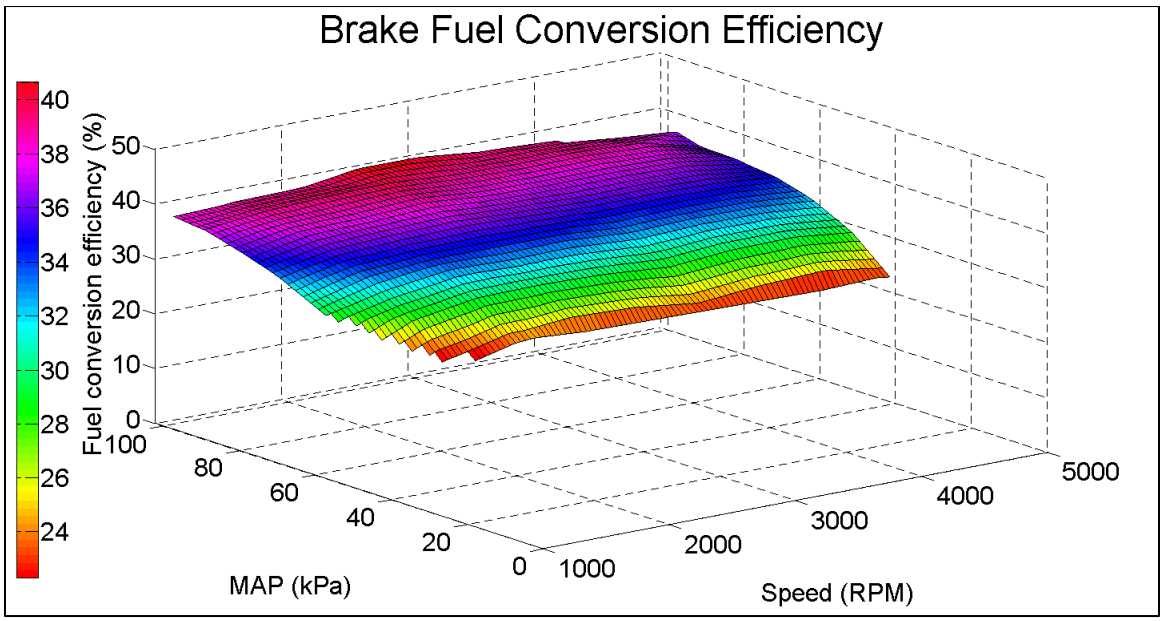


Figure 22: Coarse map surface brake efficiency with delayed closure cam, long runner

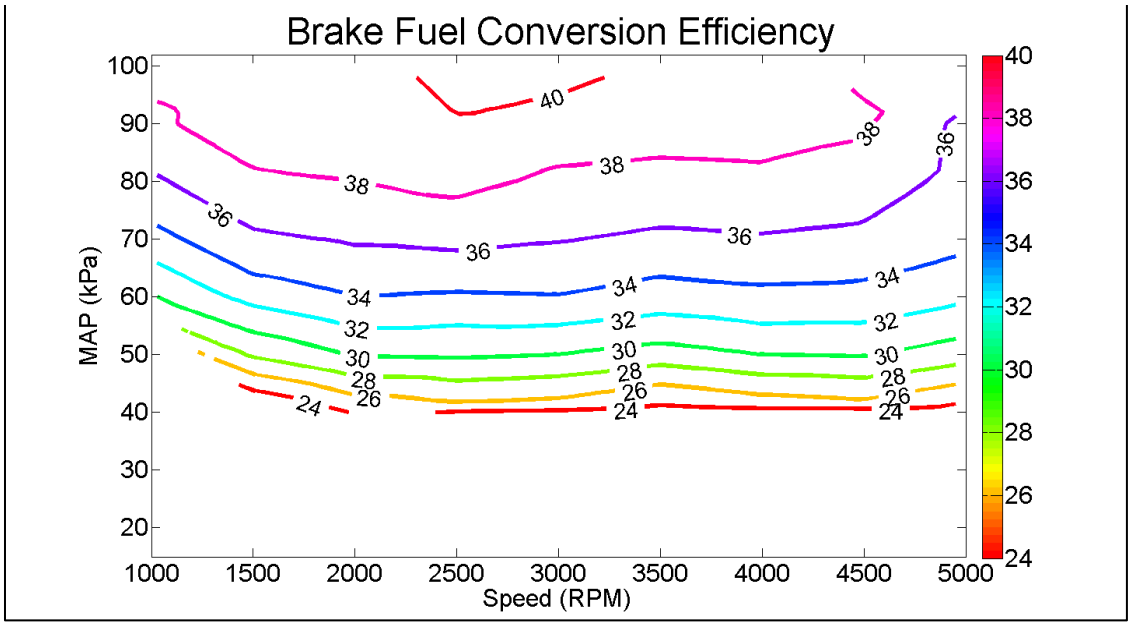


Figure 23: Coarse map contour brake efficiency with delayed closure cam, long runner

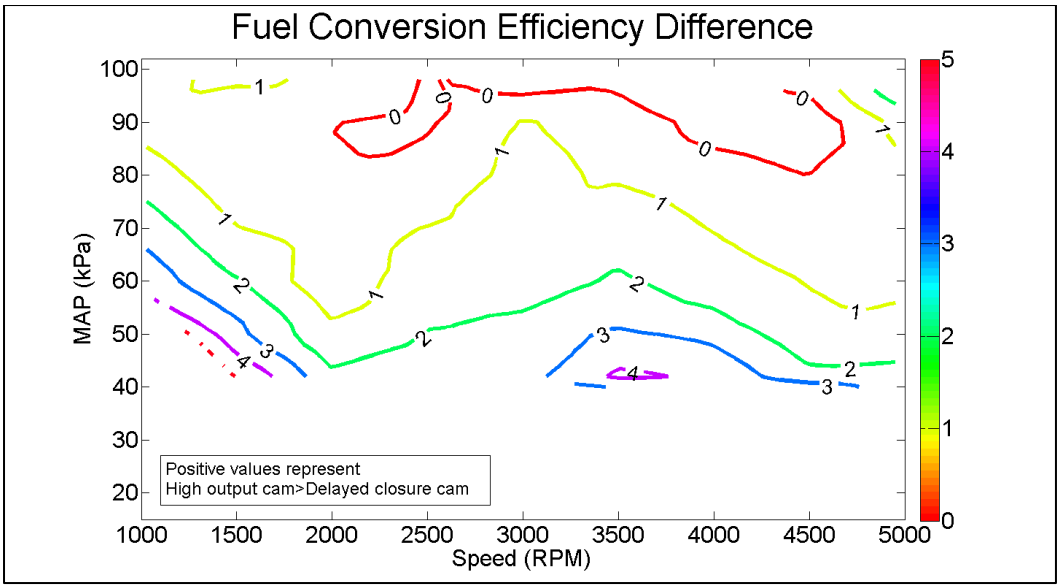


Figure 24: Subtraction of efficiency (%) high output and delayed closure cam maps

Brake torque differences between the high output cam and the delayed closure cam can be seen in Figure 25, Figure 26, Figure 27 and Figure 28. There is a notable difference in torque output between the two cam configurations. The high output cam produces on average 13 ft-lb more torque than the delayed closure cam. This is because the delayed closure cam expels some of the air-fuel mixture back into the intake. Both the cam configurations produced an increasing amount of torque as speed and load increased. Both are much more dependent on load though.

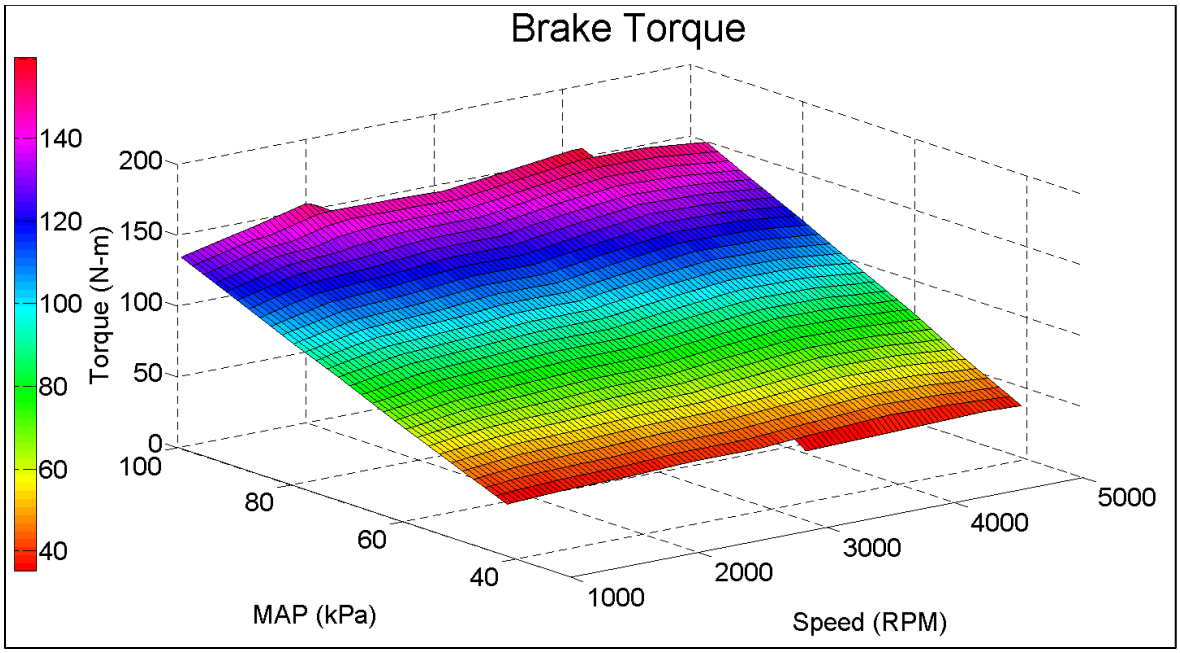


Figure 25: Coarse map surface brake torque with high output cam, long runner

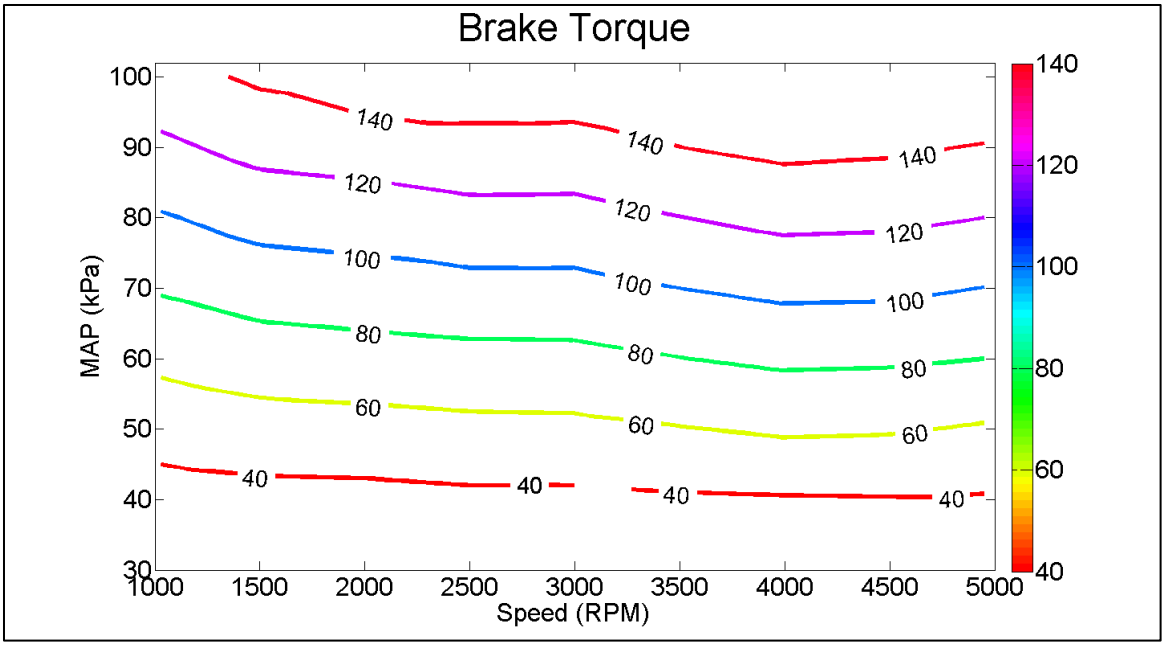


Figure 26: Coarse map contour brake torque with high output cam, long runner

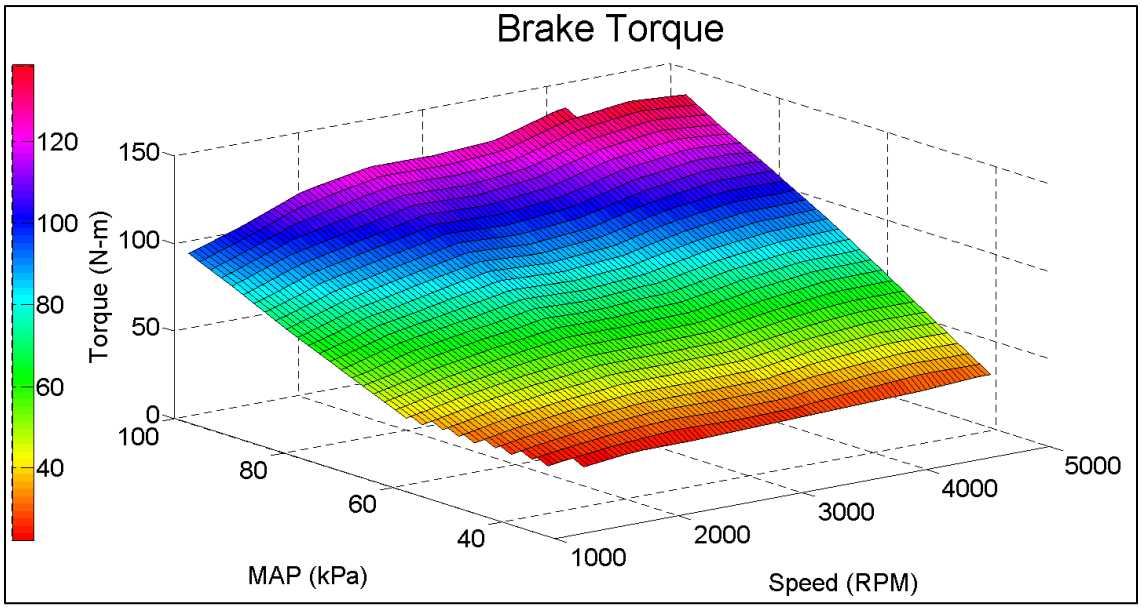


Figure 27: Coarse map surface brake torque with delayed closure cam, long runner

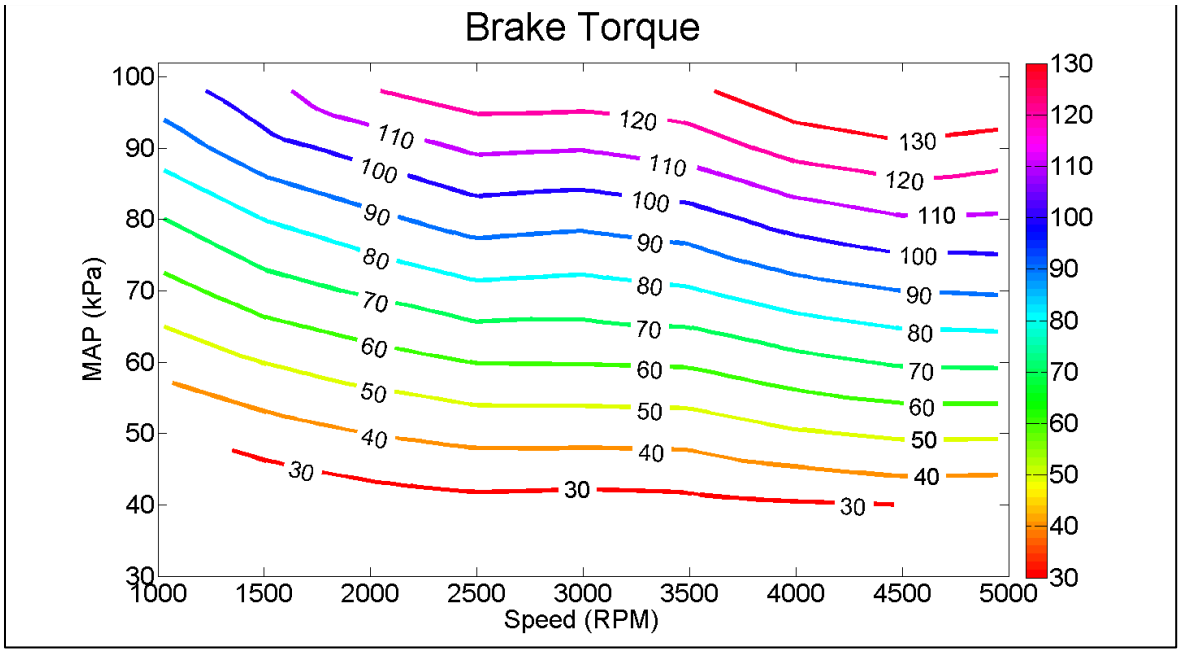


Figure 28: Coarse map contour brake torque with delayed closure cam, long runner

Figure 30 and Figure 31 summarize the percent difference between the high output and delayed closure cams with the long intake runner. To summarize the findings Figure 29 shows the result of subtracting the high output and delayed closure cam torque maps. There is a substantial increase in torque when using the high output cam.

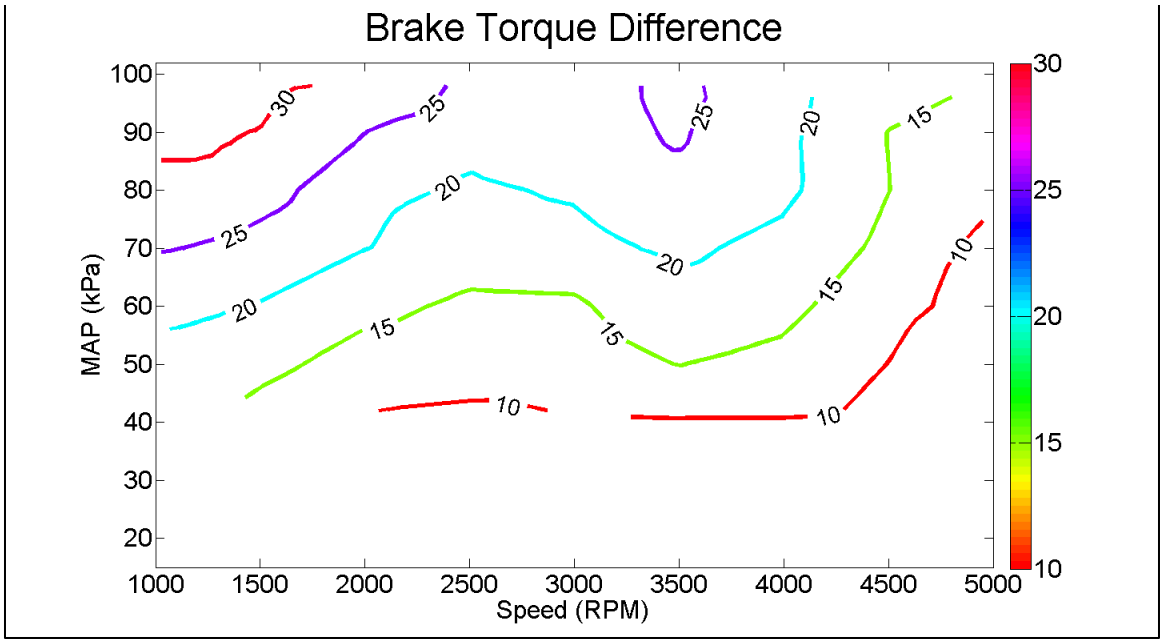


Figure 29: Brake torque (N-m) difference for high output vs. delayed closure cam

Figure 30 shows that the high output cam has a greater efficiency at a majority of the coarse map operating points.

Figure 31 displays that except for one case the high output cam produces more torque than the delayed closure cam. This was expected.

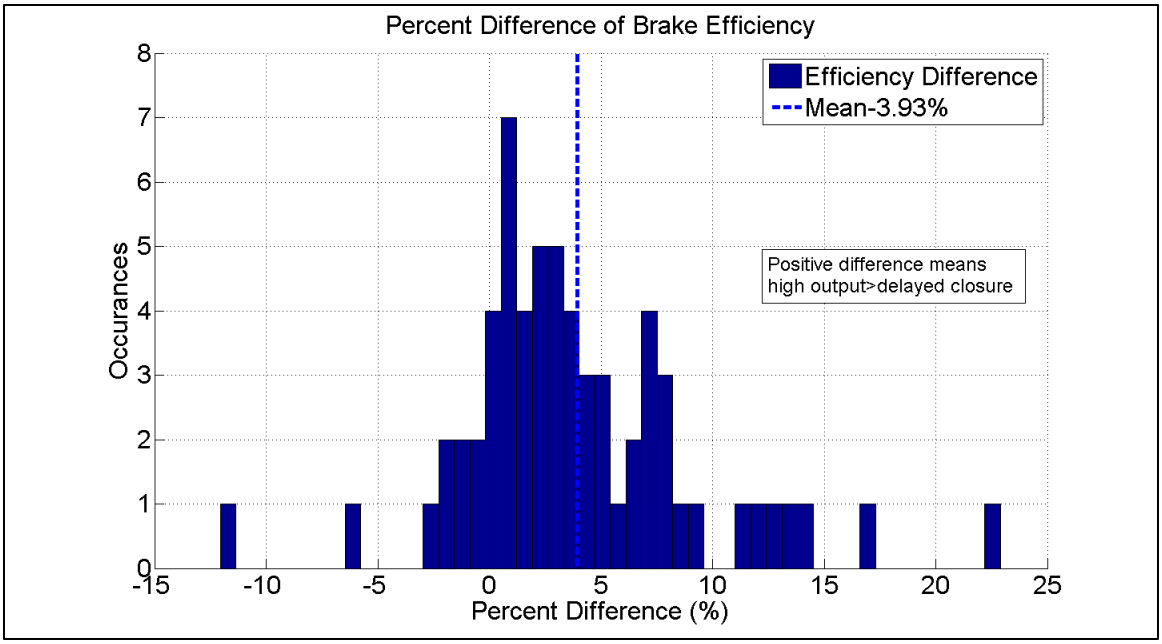


Figure 30: Percent difference of brake efficiency between the high output and delayed closure cam

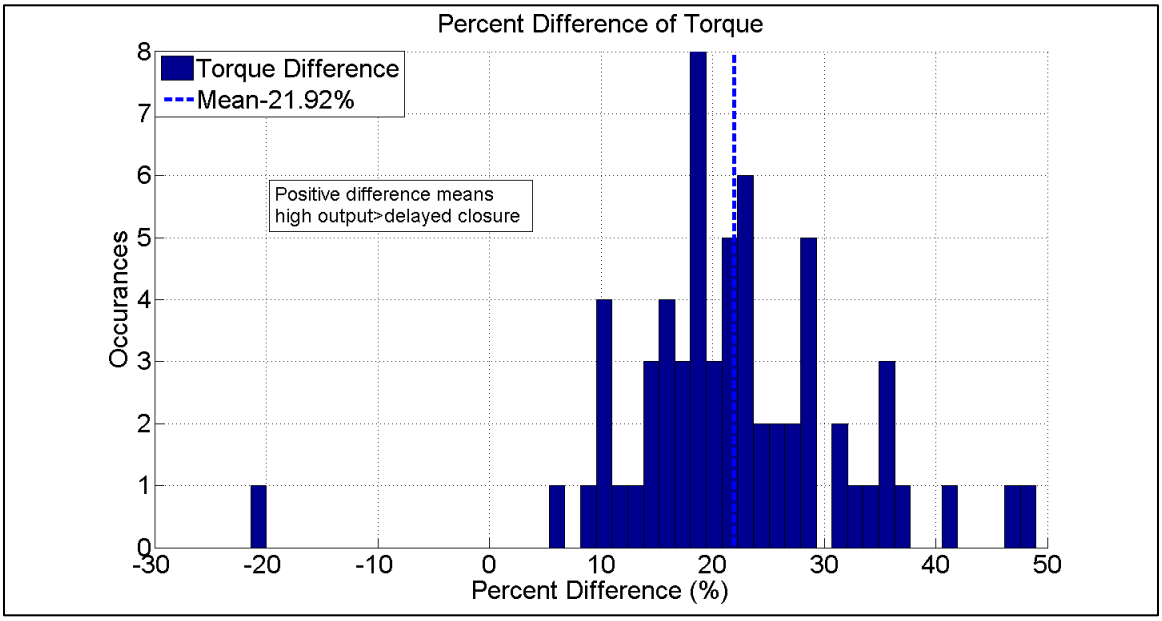


Figure 31: Percent difference of torque between the high output and delayed closure cam

All the previous analysis would seem to indicate no reason for using the delayed closure cam, despite documentation that it improved efficiency (Nakajima, Goto, & Matsunaga, 2007). Figure 32 displays why the delayed closure cam would be used. When analyzing the difference between the cams with engine torque the delayed closure cam has a higher efficiency in almost all operating regions. This is due to a reduction in pumping losses. The delayed closure cam requires a higher manifold pressure to achieve the same torque as the high output cam because some of the charge is displaced back into the intake manifold. Notice that the figure only encompasses the region of the two cams maps that share the same torque value.

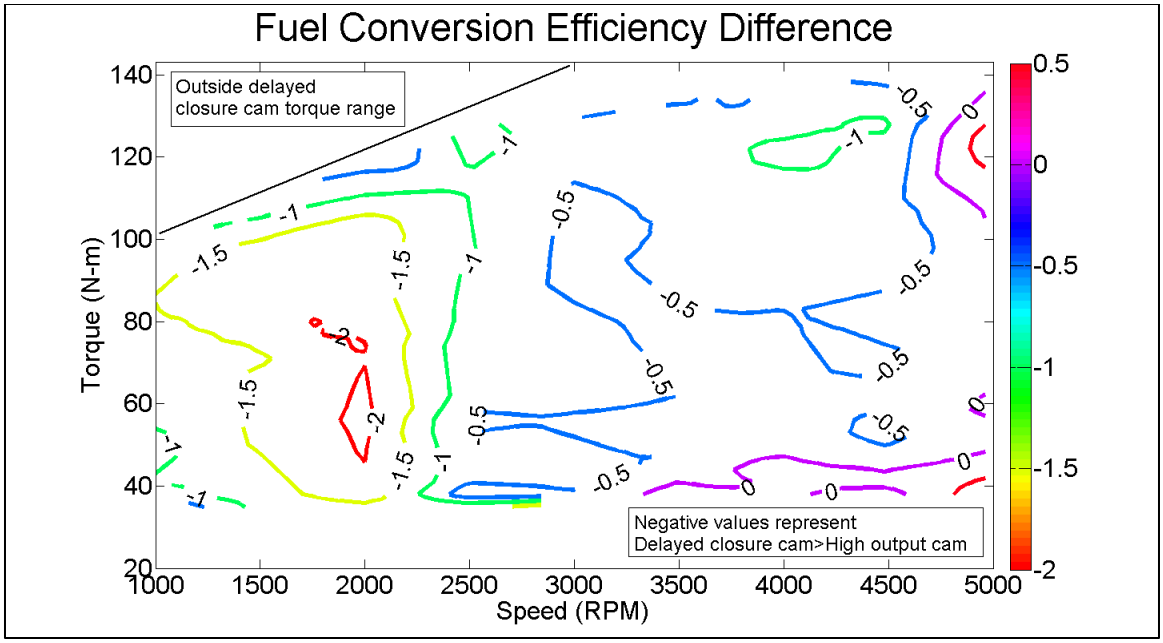


Figure 32: Subtraction of efficiency high output and delayed closure cam maps vs. torque

This figure is especially applicable to use in the EcoCAR vehicle, since the supervisory controller will sent torque requests to the engine. Although the delayed

closure cam can increase the engines efficiency, the main effect is reduction of pumping losses. The pumping losses are nearly eliminated during high manifold pressure conditions. During the second year of the EcoCAR competition the vehicle will operate in series mode with the front electric motor. This means that the engine can operate at the most efficient conditions since it is not directly driving the wheels. The most efficient operation as seen in the previous graphs is at high manifold pressures where pumping losses are reduced. This makes the delayed closure cam less of an advantage, since its primary effectiveness is in reducing the pumping losses. This is the reason that the high output cam was chosen. In year three when the vehicle operates in all operating modes including parallel, the delayed closure cam should be used.

## 4.2 **Fine Mapping**

Once the coarse mapping process was completed a fine design of experiment was created as seen in Table 6. The chosen intervals for speed and manifold pressure are a compromise. Spark timing and volumetric efficiency maps are both input as a calibration into the engine control code as a table. Since the engine will be operating at points at which a tabulated value is not available the engine controller interpolates. It is very important to create a small enough increment between values so that the interpolation does a good job of predicting the correct value. This is linked to how smooth the spark surface is. If increments for spark timing are too large a loss of efficiency and torque could result as well as knock could occur at the interpolated points. Volumetric efficiency is more severe. Since the volumetric efficiency maps are used to predict the mass flow of air, interpolation errors could result in large increases in emissions due to incorrect air to

fuel ratios. Volumetric efficiency increase and decrease over a small operating range due to tuning effects which create peaks and valleys. However, if the intervals are too mall calibration time can increase immensely. Shrinking both the engine speed and manifold pressure intervals in half would result in four times as many data points to calibrate. Therefore the chosen intervals are a compromise.

Table 6: Design of experiment-Fine

| **Stage** | |
|---|---|
| 1 | Engine speed set: 200 rpm intervals, 1000 RPM to 5000 RPM |
| 2 | Manifold pressure (MAP): 10 kPa intervals, 20 kPa to wide open throttle |

The fine mapping was performed in 200 RPM intervals of engine speed and 10 kPa intervals of manifold pressure as seen in Table 6. Engine speed and load were set using the same process as the coarse mapping. Once a speed and load was set a spark sweep was performed.

The fine increment testing followed the exact same procedure except the coarse map was used as a starting point for determining MBT spark timing. A 10 degree retard was applied to the closest coarse map point to start the spark sweep. This ensured that as spark was advanced toward MBT a rise in torque could be recorded. As was the case with almost all points the MBT point was very flat. Generally the peak was at least 5 degree wide, with no drop in torque. MBT cannot always be achieved. Particularly at high manifold pressures engine knock was a limit on the amount of spark advance that could

be applied. Due to the flatness of the MBT curve this necessary spark retard did not always yield significant torque reductions. However, at WOT spark retard was large enough to affect torque output. Once knocking occurred during the spark sweep a certain degree of spark retard was needed. Depending on the severity of the knock, spark was retarded accordingly. Spark was generally retarded until knock stopped and then several degrees of retard were applied past the point where knocking stopped. An extra cushion is important when used in a vehicle. Generally 2-3 degrees of cushion were applied to the spark retard after the knocking subsided. The second year of the EcoCAR competition will take place in Yuma, Arizona. The large increase in air temperature from the lab environment to the desert will increase the likelihood of knock. Since a knock sensor will not be used in this point of the competition, less aggressive spark timing is needed. Peak in-cylinder pressure was another limiting factor. A maximum pressure of 60 bar was set in order to allow for safe engine operation. Using the in-cylinder pressure transducers spark was retarded in real-time to keep peak pressures below 60 bar.

The results of the spark timing map can be viewed in Table 7 and Figure 33. Figure 5 has a smaller mesh size than the actual data points in order to provide a smoother curve. Linear interpolation was used, which is how the engine controller will determine spark timing for intermediate points.

As was initially thought, spark advance for MBT increased as speed increased. This is due to the shrinking crank angle degree domain in which combustion can occur as speed is increased. Spark timing was retarded once engine MAP was increased.

Table 7: MBT spark timing map

| Engine Speed (RPM) | Manifold Air Pressure (MAP) (kPa) | | | | | | | | |
|---|---|---|---|---|---|---|---|---|---|
| | 20 | 30 | 40 | 50 | 60 | 70 | 80 | 90 | WOT |
| 1000 | 20 | 15 | 15 | 15 | 15 | 15 | 15 | 10 | 8 |
| 1200 | 20 | 19 | 19 | 19 | 15 | 15 | 15 | 13 | 10 |
| 1400 | 20 | 20 | 20 | 20 | 20 | 20 | 16 | 16 | 14 |
| 1600 | 20 | 20 | 20 | 20 | 20 | 20 | 18 | 16 | 15 |
| 1800 | 25 | 25 | 23 | 20 | 20 | 20 | 20 | 17 | 15 |
| 2000 | 25 | 25 | 25 | 25 | 25 | 21 | 21 | 18 | 15 |
| 2200 | 25 | 25 | 25 | 25 | 25 | 23 | 23 | 20 | 17 |
| 2400 | 35 | 30 | 25 | 25 | 25 | 25 | 25 | 22 | 19 |
| 2600 | 35 | 30 | 30 | 30 | 25 | 25 | 23 | 21 | 17 |
| 2800 | 40 | 30 | 30 | 30 | 30 | 27 | 23 | 21 | 18 |
| 3000 | 40 | 30 | 30 | 30 | 30 | 25 | 25 | 21 | 18 |
| 3200 | 40 | 30 | 30 | 30 | 25 | 25 | 22 | 20 | 18 |
| 3400 | 40 | 30 | 30 | 30 | 25 | 25 | 21 | 19 | 17 |
| 3600 | 35 | 30 | 30 | 30 | 25 | 25 | 23 | 19 | 17 |
| 3800 | 40 | 30 | 30 | 30 | 28 | 23 | 22 | 19 | 17 |
| 4000 | 40 | 30 | 30 | 25 | 25 | 23 | 20 | 17 | 15 |
| 4200 | 40 | 30 | 30 | 30 | 25 | 23 | 21 | 19 | 16 |
| 4400 | 40 | 30 | 30 | 30 | 25 | 25 | 21 | 18 | 16 |
| 4600 | 40 | 30 | 30 | 25 | 25 | 23 | 21 | 19 | 17 |
| 4800 | 40 | 30 | 30 | 28 | 25 | 23 | 22 | 19 | 17 |
| 5000 | 40 | 30 | 30 | 28 | 25 | 23 | 22 | 19 | 17 |

As speed was increased the load at which spark retarding was necessary was decreased. By 5000 RPM spark retarding was necessary at 50 kPa, whereas at 1000 RPM spark retarding was not needed until 90 kPa. This is due to two different effects. At low speeds knock was the limiting factor. At higher engine speeds the limiting factor was peak cylinder pressure.

There was some variability in the spark map as seen in Table 7 and Figure 33. One reason is that while knock is very noticeable using the knock listening device, as it fades away the mix of valve noise tends to make it hard to distinguish small sounds. At lower manifold pressures there is also some variability between speeds. Variability in the spark map also occurred when peak pressures exceeded 60 bar. Like knock, the amount of spark retard was variable, with the goal to lower peak pressures below 60 bar. When not knock or peak pressure related it is due to the difficulty in differentiating between small torque changes with spark. This is due to the relatively flat MBT point and also due to the varying small amounts of varying torque cycle to cycle. The variability between speeds is not a negative, just a product of the mapping process. In the future spark could potentially be retarded based on emissions, since higher spark advances produce higher combustion temperatures, but at this point in the map the only goal was to optimize MBT and therefore efficiency.

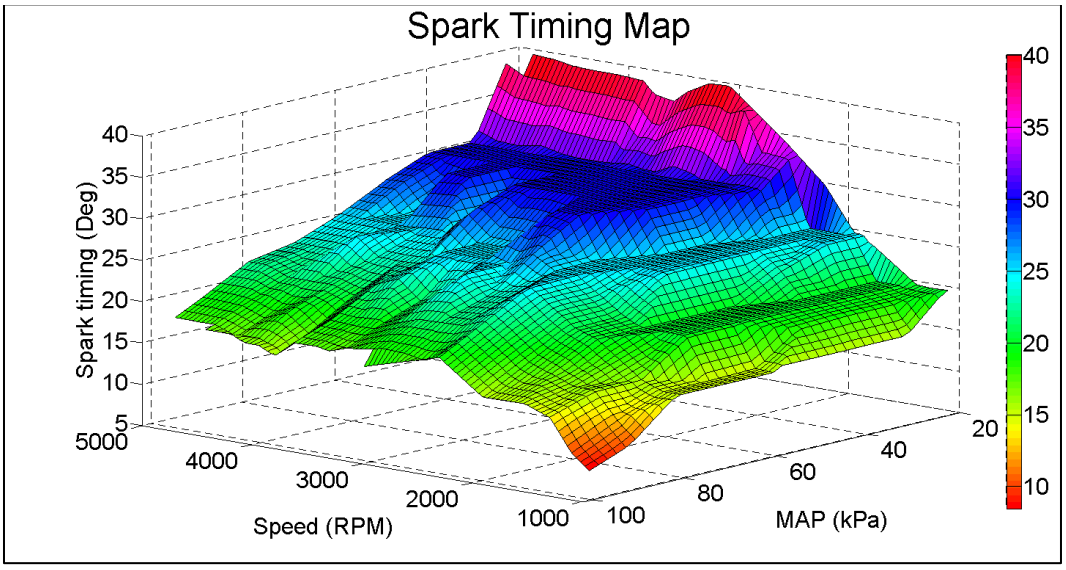


Figure 33: Fine map Spark timing map

Another noticeable trait of the spark timing map is at low loads, specifically 20 kPa. In order for completeness a MAP pressure of 20 kPa was included in the map. However this load point will not be used during vehicle operations. A large spark advance was necessary in most cases to make any torque, generally making less than 5 lb ft.

As a result of the spark timing map MBT was produced as shown in Figure 34 and Figure 35. There is almost no change in torque through the speed range. Torque also increases very linearly throughout the manifold pressure range.

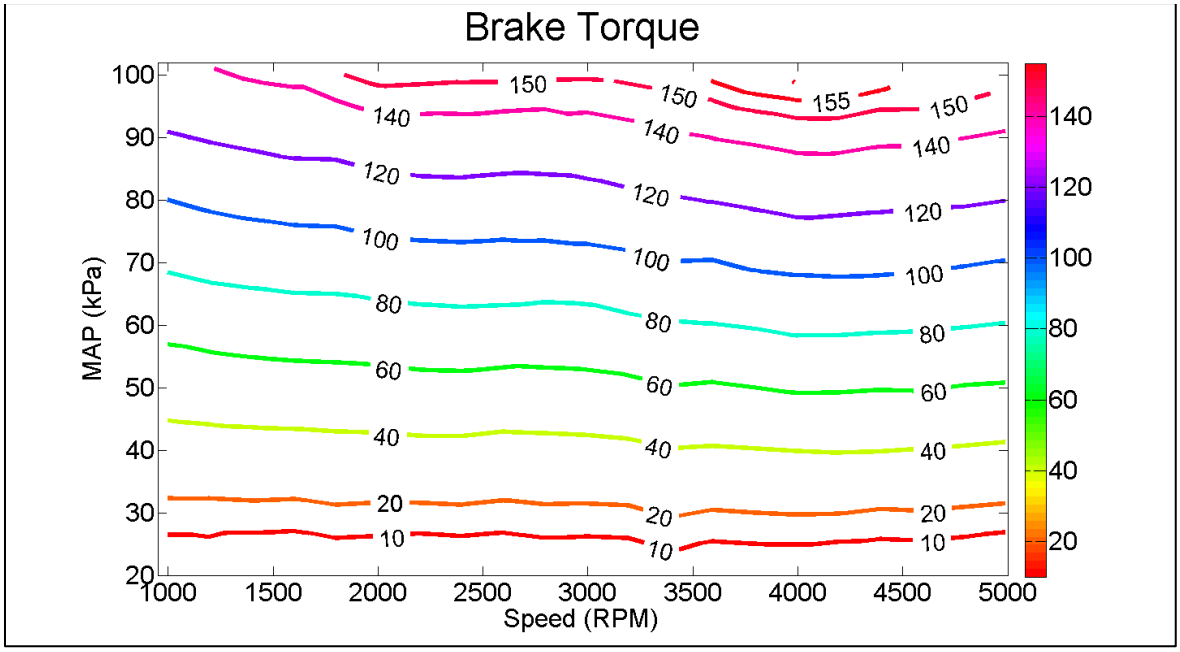


Figure 34: Fine map brake torque contour

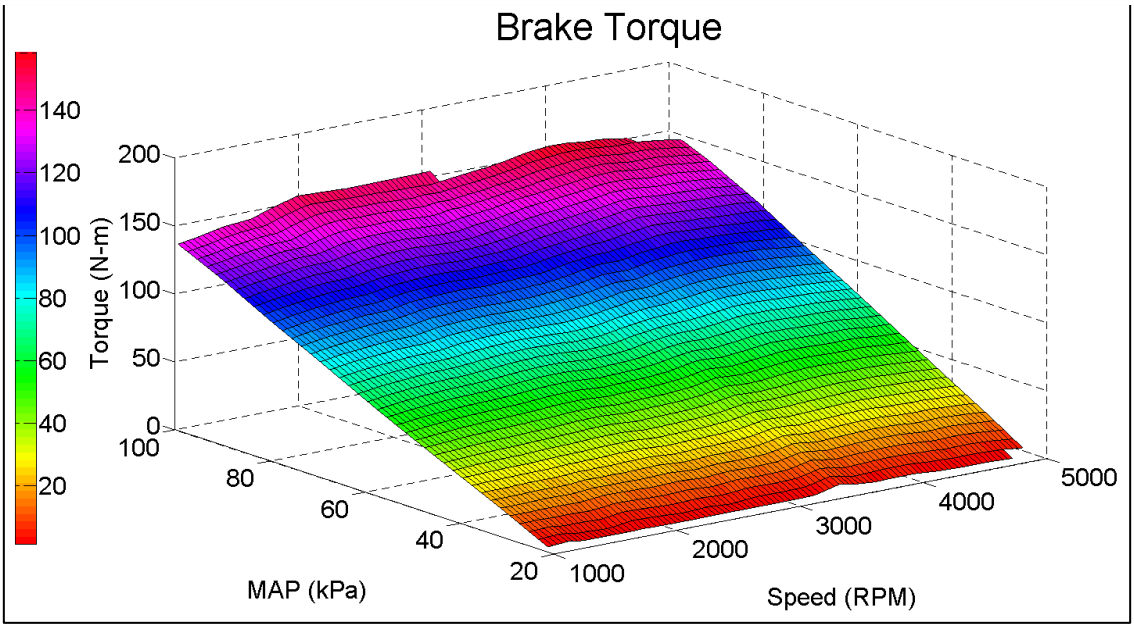


Figure 35: Fine map brake torque surface

Brake torque is also very important for the supervisory control of the vehicle. The supervisory controller requests torque outputs from various components. In order to be able to do this the engine controller must know how to obtain the torque requested. This will be done based on a desired manifold pressure (MAP).

An interesting result of the brake torque data is a comparison of the original CNG engine to the newly converted E85 engine. Figure 36 shows the brake torque at wide open throttle, which can be compared to the original torque plot in Figure 6 on page 14. The shape of the curve is very similar, with many of the peaks and valleys in nearly the same engine speed locations. The magnitude of the torque between the CNG engine and the new E85 engine however is different. The E85 engine has between 10 and 15 N-m

higher torque than the original CNG engine. The E85 however has approximately 5-10 N-m less torque than the gasoline engine, which can be seen in Figure 7 on page 15.

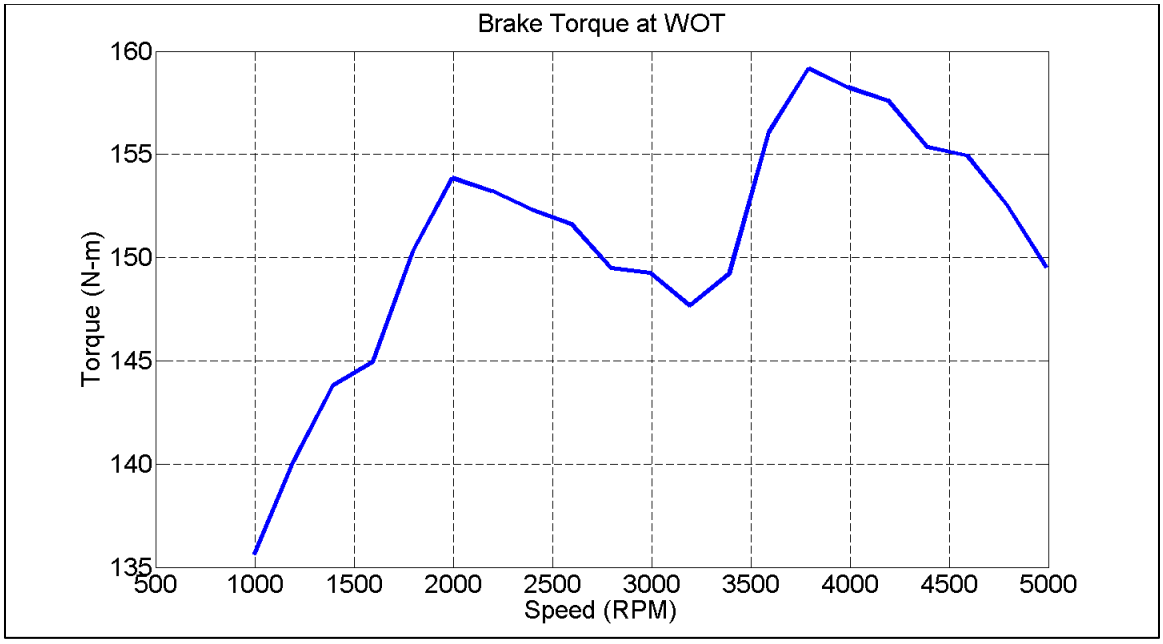


Figure 36: Brake torque and wide open throttle (WOT)

Spark timing can significantly change the exhaust temperature. This can be very important for emissions as high temperatures promote oxidation within the exhaust stream.

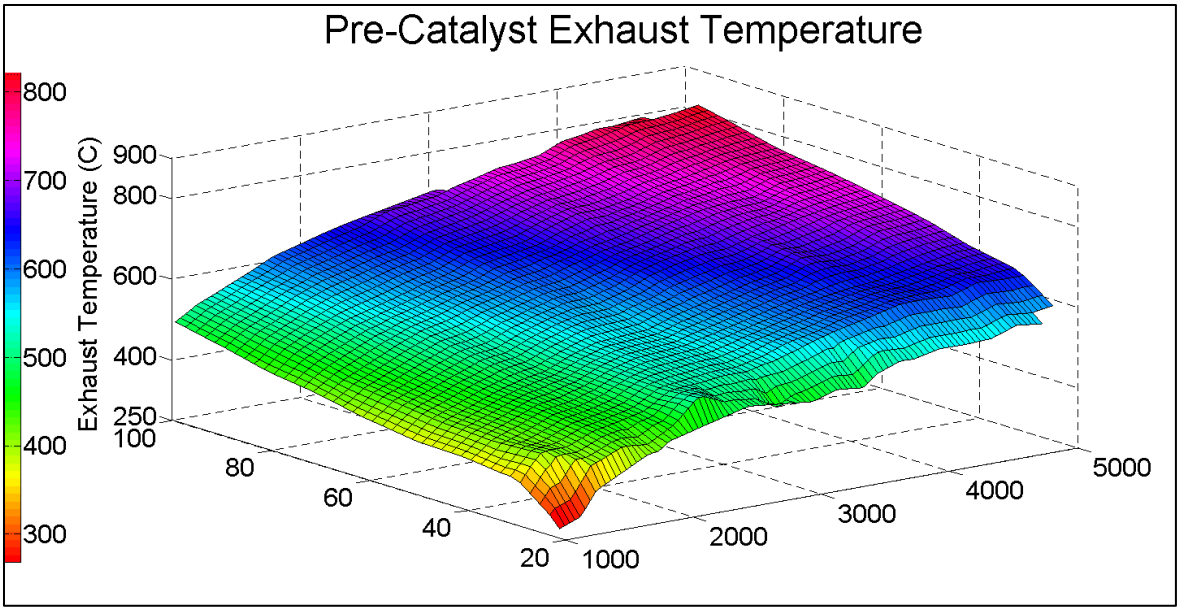


Figure 37: Pre-Catalyst Exhaust Temperature

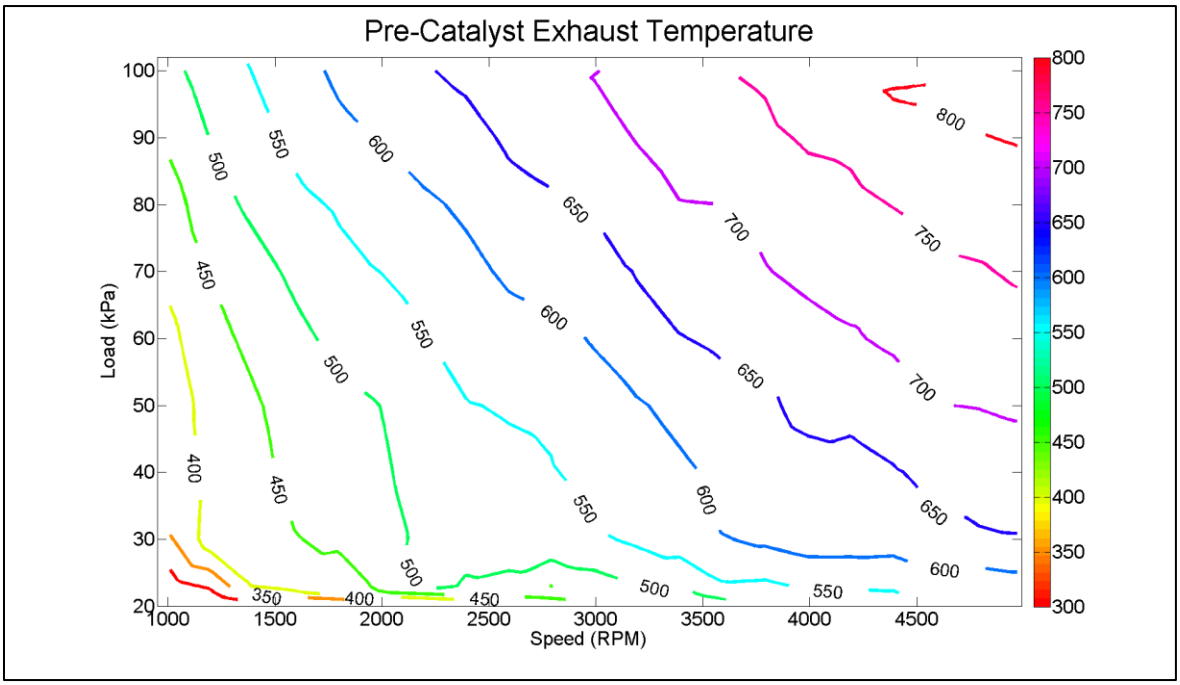


Figure 38: Pre-catalyst exhaust temperature contour

After completion of the spark timing map is was implemented into the engine controller. It was inserted as a table referenced versus speed and MAP. The implementation into the control code can be viewed in Figure 62 and Figure 63 in the appendix. The spark timing map was verified across a wide range of points. The main verification needed was that knock would not occur. Since engine testing will resume with other projects the map will continuously be verified across many points.

As mentioned earlier once spark timing for a given engine speed and load was set 30 seconds of data was recorded. This steady data included the necessary variables to calculate volumetric efficiency. The choice of which sensors to use to calculate volumetric efficiency is important. Volumetric efficiency can be referenced to a number of locations. This location is determined by where the air density is recorded. Since volumetric efficiency will be used in feed forward air predictions, the only choice for where to reference volumetric efficiency is the sensors that will be used for this calculation. The location of the MAP sensor is just after the throttle and the air temperature sensor is located with the MAF sensor in the air cleaner box. Engine speed was recorded using the dynamometer speed sensor. In order to calculate volumetric efficiency a mass air flow is needed. It is assumed that when the engine is operating at steady state the sensors are recording the true value. For more accuracy the laminar flow element is used for MAF.

Once all 189 data points were recorded data processing was performed. A Matlab script was written in order to process the data. Data files were in a binary file format. In order to process this file format a .dat to.mat file converter Matlab program was used.

Once the files were in a useable format the Matlab script was used to average the data and calculate other functions such as brake efficiency and volumetric efficiency.

The results of the volumetric efficiency calculations are shown in Figure 39 and Figure 40. A finer mesh was used than the original experimental spacing.

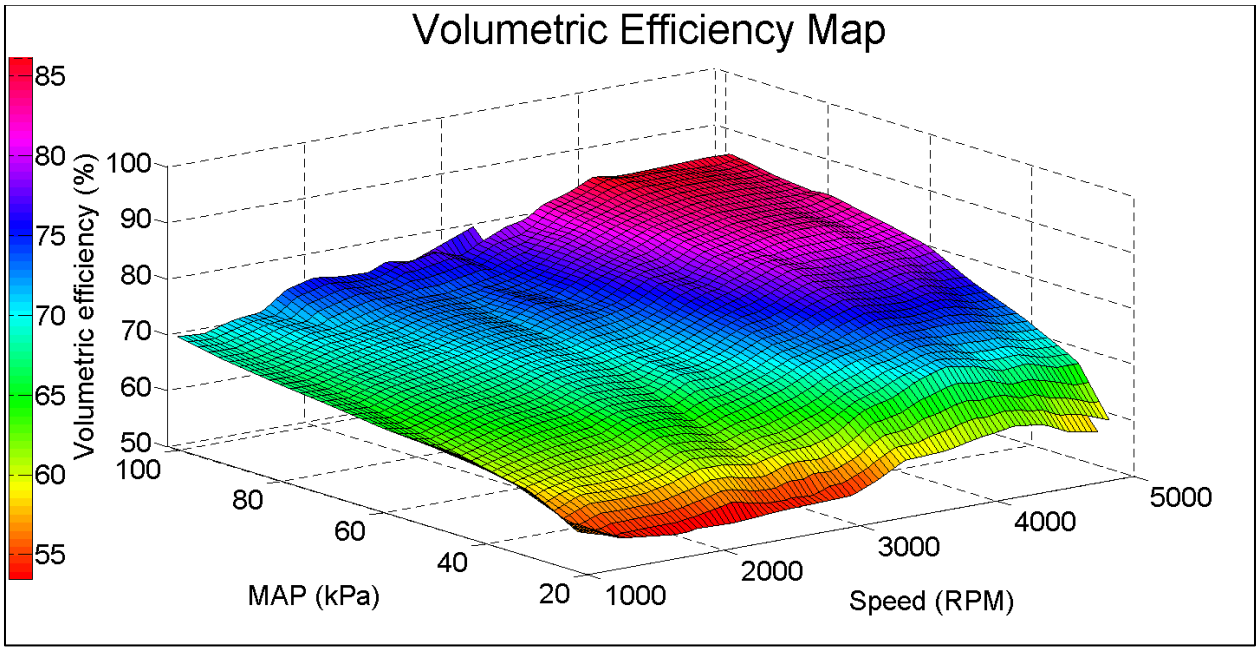


Figure 39: Volumetric efficiency map

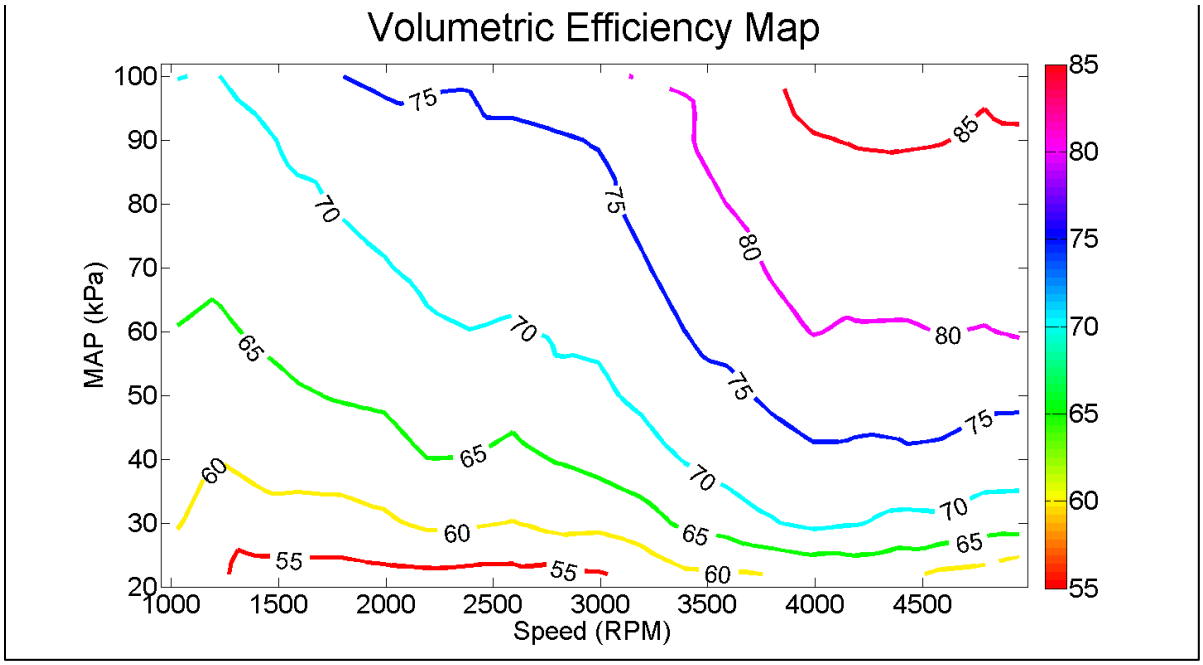


Figure 40: Volumetric efficiency map contour

There are two general trends that are present in the volumetric efficiency map. The first is that as load is increased volumetric efficiency increases. This is due to the increased manifold pressure which allows for more air to enter the cylinder. The second trend is that as engine speed is increased volumetric efficiency increases as well. This is to be expected as the optimal point for high volumetric efficiency is when maximum torque is needed. At high speeds and loads maximum torque is demanded and thus a high volumetric efficiency was designed at these points. At engine speeds of 4000 to 5000 RPM the volumetric efficiency flattens off, so that a change in speed does not result in an increase in volumetric efficiency. From engine speeds of 4500 RPM to 5000 RPM volumetric efficiency declines to some degree. These trends at engine speeds 4000 to

5000 RPM is consistent with the literature review (Figure 6) as torque drops off at these points.

## 4.3 Volumetric Efficiency Validation

It is important to validate the results of the volumetric efficiency map. One source of error is derived from the fact that the map that is used by the engine controller is regularly spaced based on engine speed and load. This spacing was not exactly achieved during testing. In order to resolve the problem of an irregularly spaced map from engine testing, a linear interpolation was performed to the regularly spaced map. In order to determine the validity of this interpolation, the original data points from the testing were calculated using the new map. From this a new volumetric efficiency value was obtained and compared to the original volumetric value from testing. The error from the conversion is seen in Figure 41. It was determined that the magnitude of error was acceptable.

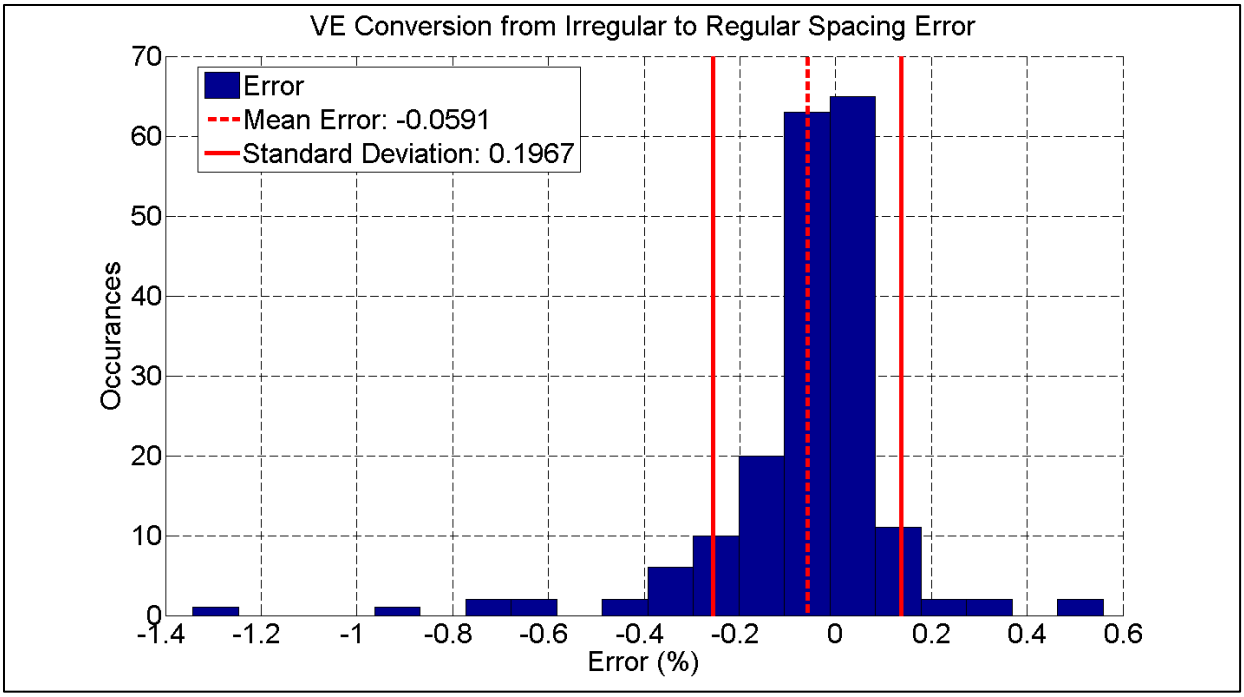


Figure 41: Volumetric efficiency conversion from irregular to regular spacing map error

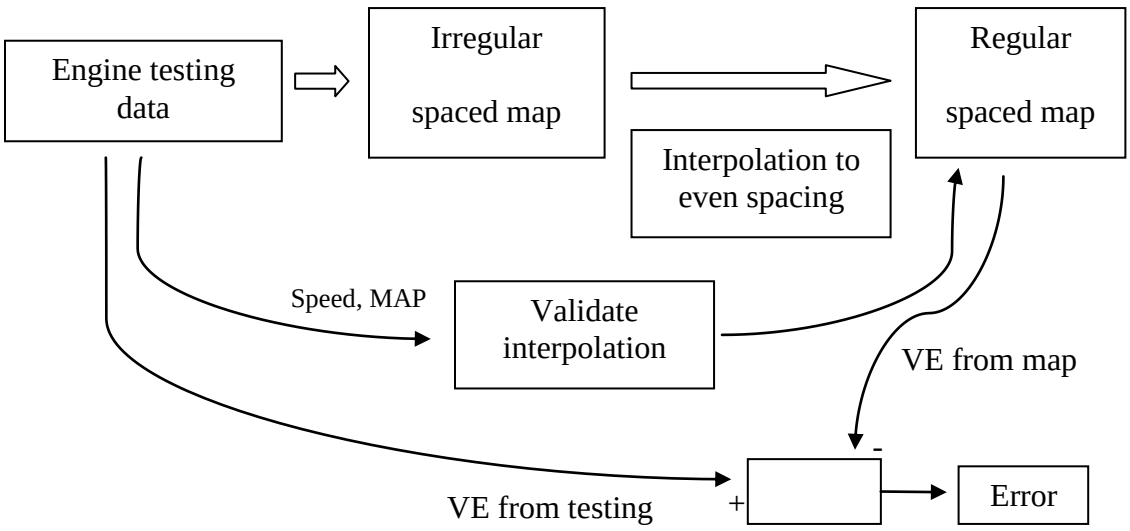

Table 8: Regularly spaced volumetric efficiency map

| | | Load (kPa) | | | | | | | | |
|---|---|---|---|---|---|---|---|---|---|---|
| | | 20 | 30 | 40 | 50 | 60 | 70 | 80 | 90 | 100 |
| Engine Speed (RPM) | 1000 | 56.23 | 61.19 | 63.15 | 64.31 | 64.98 | 66.15 | 67.15 | 68.39 | 70.13 |
| | 1200 | 55.57 | 56.36 | 59.97 | 62.00 | 64.12 | 65.85 | 67.12 | 68.26 | 69.83 |
| | 1400 | 52.14 | 58.20 | 61.06 | 63.36 | 65.58 | 67.43 | 68.39 | 69.32 | 71.17 |
| | 1600 | 52.39 | 58.07 | 61.91 | 64.63 | 66.75 | 68.25 | 69.39 | 70.85 | 71.75 |
| | 1800 | 52.31 | 58.23 | 62.22 | 65.37 | 67.02 | 68.89 | 70.34 | 71.21 | 75.02 |
| | 2000 | 52.81 | 59.31 | 62.87 | 65.87 | 67.99 | 69.82 | 70.68 | 72.59 | 76.21 |
| | 2200 | 53.61 | 60.83 | 64.99 | 67.52 | 69.48 | 70.88 | 72.18 | 73.47 | 75.56 |
| | 2400 | 51.96 | 60.68 | 64.82 | 67.48 | 69.95 | 71.51 | 72.70 | 73.72 | 75.46 |
| | 2600 | 51.99 | 59.91 | 63.65 | 66.96 | 69.62 | 71.33 | 72.13 | 73.69 | 76.84 |
| | 2800 | 50.47 | 61.12 | 65.28 | 69.40 | 70.44 | 72.77 | 74.36 | 74.48 | 78.23 |
| | 3000 | 52.94 | 61.32 | 66.59 | 69.33 | 70.76 | 73.37 | 73.97 | 75.31 | 76.56 |
| | 3200 | 55.12 | 62.94 | 68.11 | 70.96 | 72.84 | 74.58 | 76.44 | 76.85 | 79.33 |
| | 3400 | 57.61 | 66.05 | 70.34 | 73.18 | 75.06 | 77.39 | 78.43 | 79.66 | 79.45 |
| | 3600 | 57.50 | 67.30 | 72.01 | 73.80 | 76.63 | 77.75 | 80.14 | 81.82 | 83.02 |
| | 3800 | 57.81 | 69.71 | 72.67 | 76.03 | 78.42 | 80.48 | 82.20 | 83.43 | 84.48 |
| | 4000 | 58.71 | 71.14 | 74.07 | 77.53 | 80.13 | 81.36 | 82.97 | 84.77 | 86.92 |
| | 4200 | 59.82 | 70.33 | 74.05 | 76.77 | 79.54 | 82.27 | 83.81 | 85.16 | 86.05 |
| | 4400 | 59.35 | 68.65 | 74.19 | 76.62 | 79.46 | 82.56 | 83.68 | 85.24 | 86.09 |
| | 4600 | 56.62 | 68.99 | 73.78 | 77.43 | 80.11 | 82.51 | 83.51 | 85.08 | 85.59 |
| | 4800 | 56.05 | 67.48 | 72.36 | 75.98 | 79.79 | 81.35 | 83.19 | 84.50 | 85.46 |
| | 5000 | 55.07 | 65.78 | 71.61 | 75.32 | 79.03 | 80.94 | 82.93 | 83.58 | 84.22 |

The regularly spaced volumetric efficiency map (Table 8) was inserted into the controller code. This volumetric efficiency map is a calibration parameter, which allows for a simple insertion of the map using INCA. The SIMULINK engine controller code is located in the appendix in Figure 60 and Figure 61.

The second step in validating the volumetric efficiency map was to validate the engine controller hardware. Once the volumetric efficiency map was loaded using INCA a coarse mapping process was completed in order to validate the engine controller was using the correct volumetric efficiency values when given a engine speed and load. The

coarse mapping process consisted of engine speed from 1000 RPM to 5000 RPM in 400 RPM increments. Load ranged from 20 kPa to 100 kPa in 10 kPa increments. This test was performed without running the engine. Both the engine speed and load were overridden using INCA so that the engine controller would find a value of volumetric efficiency to use. This value that the engine controller found was then compared to the correct value from the map for a set engine speed and load using Matlab. It was found that there was zero error. This validated that the engine controller's hardware was correctly calculating volumetric efficiency.

The third step in validating the volumetric efficiency map was to perform a coarse mapping process. This mapping process consisted of engine speeds from 1000 RPM to 5000 RPM in 400 RPM increments. Load ranged from 20 kPa to WOT in 10 kPa increments. 30 seconds of steady state data was recorded for each condition. Once this process was completed the data was analyzed using Matlab in order to determine the error. Error was quantified by comparing the mass air flow recorded from the LFE to the calculated mass air flow using the volumetric efficiency map. Results can be seen in Figure 42. Error of $\pm$4% was considered to be acceptable for a feed forward air prediction based on volumetric efficiency when compared to a LFE. The volumetric efficiency map was within the acceptable error. One standard deviation from the mean was +0.8%, -2.98%. Error can be attributed to engine controller interpolations and deviations in conditions from when the original volumetric efficiency map was created.

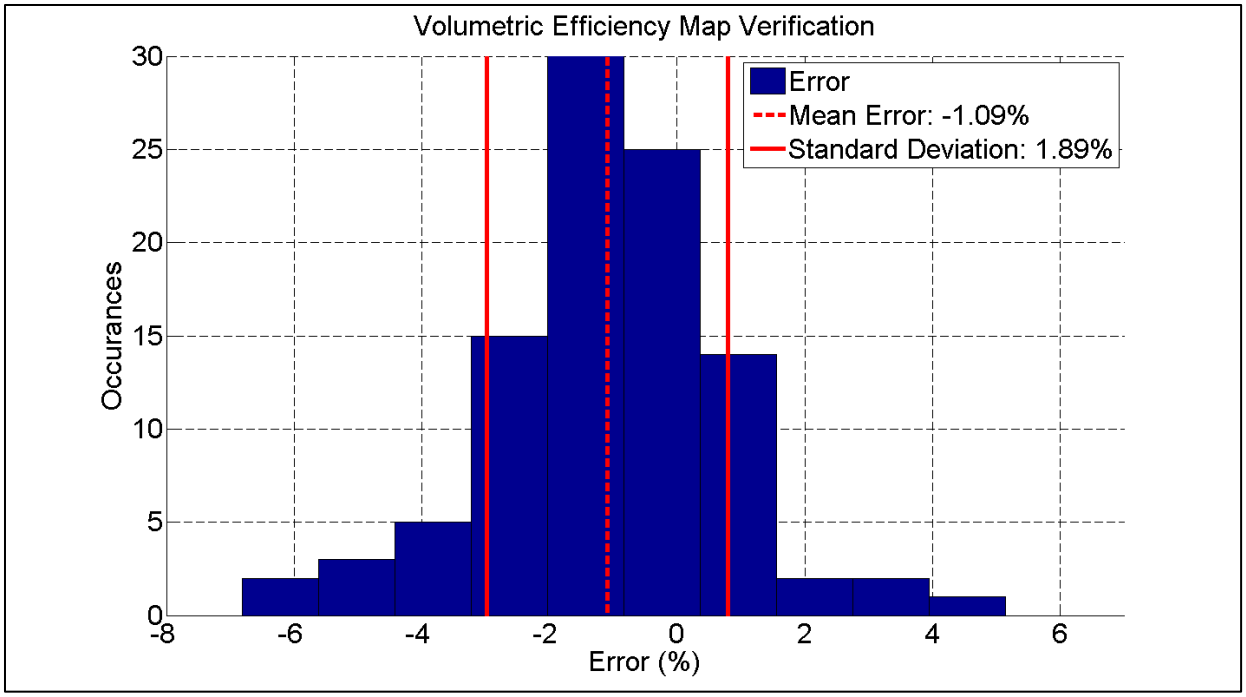


Figure 42: Volumetric Efficiency Map Validation using coarse mapping steady-state error

In order to demonstrate the usefulness of the volumetric efficiency map as a means of a feed forward air prediction several different test cases were performed. These included load transients. A filling-and-emptying map would do a much better job at predicting the dynamics of the manifold, but a volumetric efficiency map has proved to be an useful intermediate step. Volumetric efficiency will be used in the filling-and-emptying map, which means that it is important beyond using it as solely a feed forward prediction of air flow.

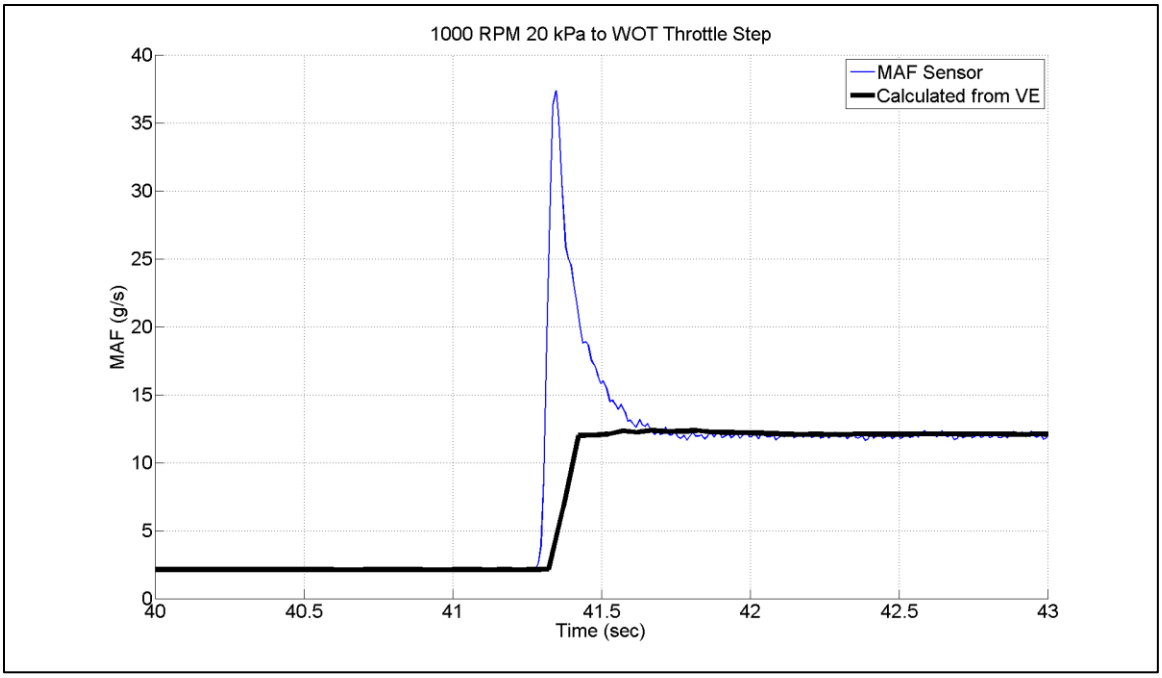


Figure 43: 20 kPa to WOT throttle step at 1000 RPM

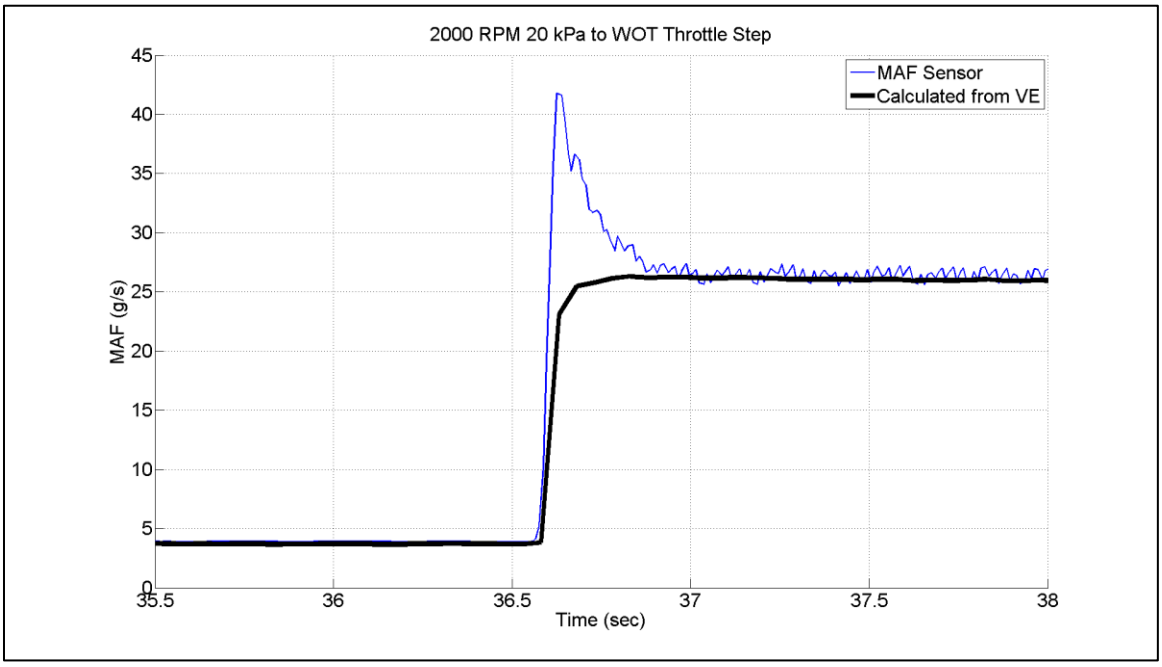


Figure 44: 20 kPa to WOT throttle step at 2000 RPM

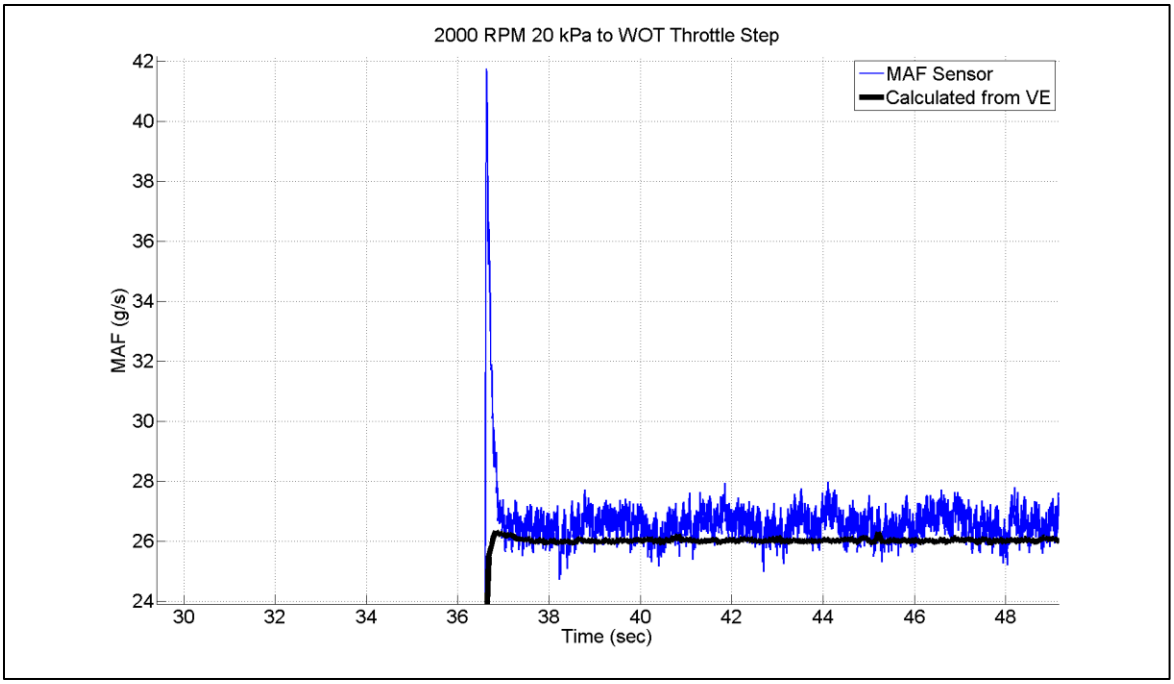


Figure 45: 20 kPa to WOT throttle step at 1000 RPM zoomed in

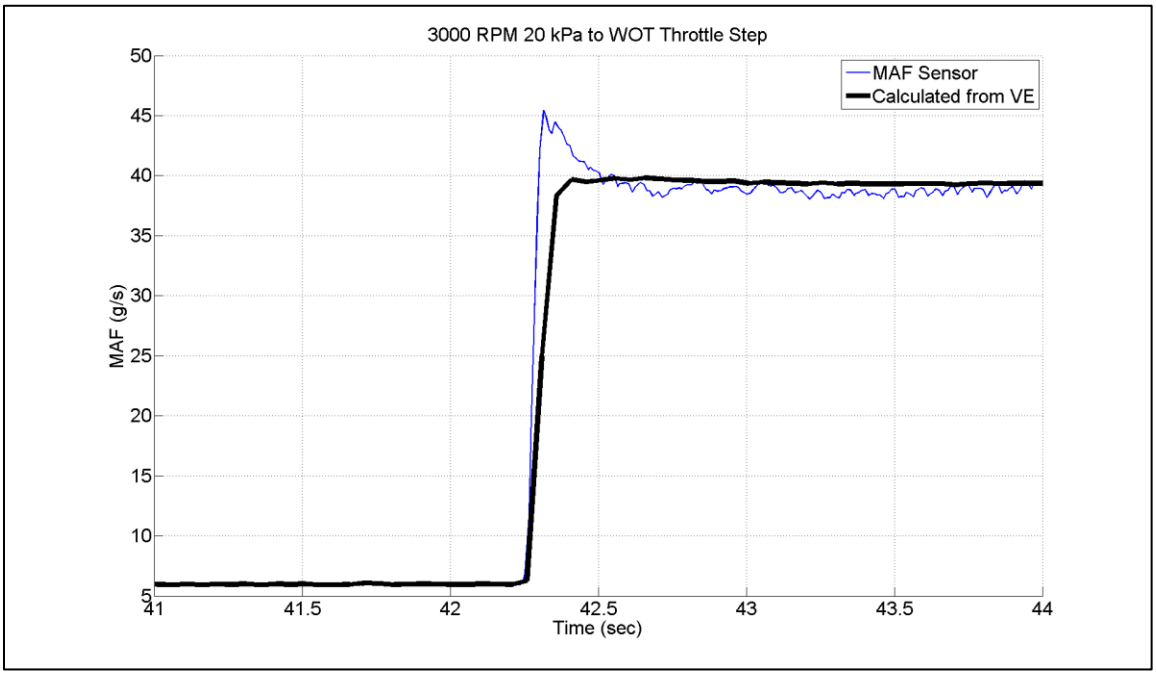


Figure 46: 20 kPa to WOT throttle step at 3000 RPM

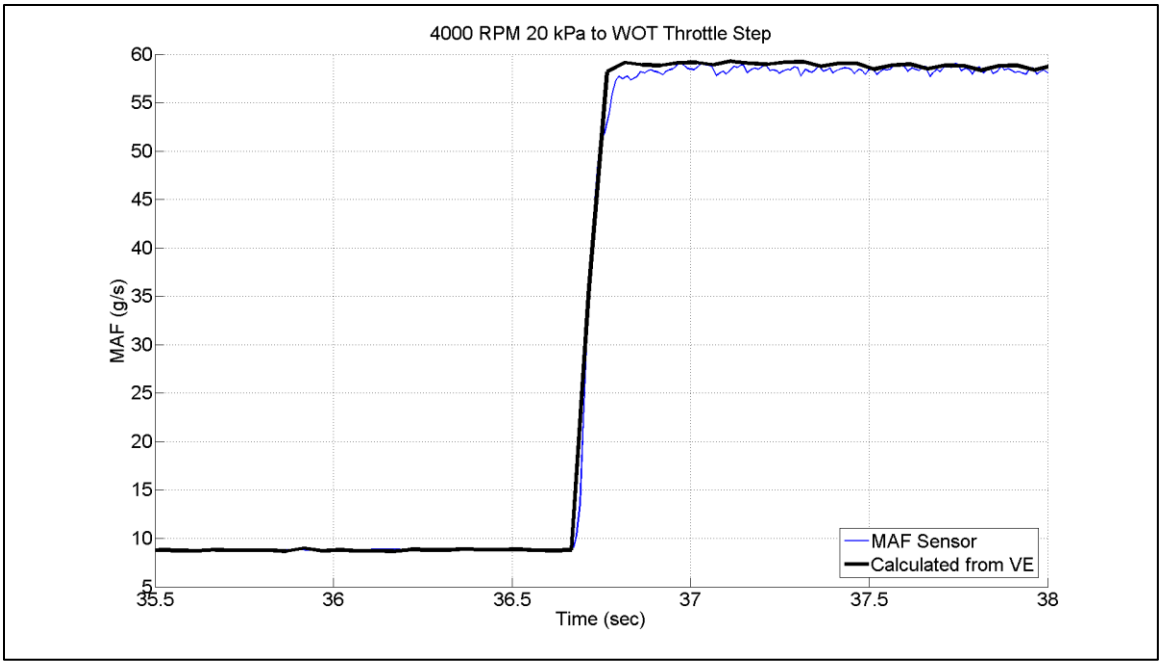


Figure 47: 20 kPa to WOT throttle step at 4000 RPM

As can be seen from Figure 43 to Figure 47 the MAF sensor has large errors when throttle steps occur. This is especially noticeable at low engine speeds. These large overshoots are due to a sudden rush of air past the sensor. This creates inaccurate readings which would cause very poor emissions due to the extra fuel that would be injected to compensate for the inaccurate air measurement. By using volumetric efficiency as a feed forward air estimation the large overshoot of mass air flow is eliminated. This produces better transient emissions than using the MAF sensor for the air measurement.

## 4.4 Cold Start Volumetric Efficiency Corrections

One unanticipated error point is during engine warm up. It was found that when the engine was "cold" there was a significant error between actual volumetric efficiency and the volumetric efficiency from the volumetric efficiency map as seen in Figure 48. The two volumetric efficiencies never converge partly because the thermostat opens and changes the coolant temperature around 650 seconds. The second reason as mentioned earlier in Figure 42, steady state error is present in using volumetric efficiency.

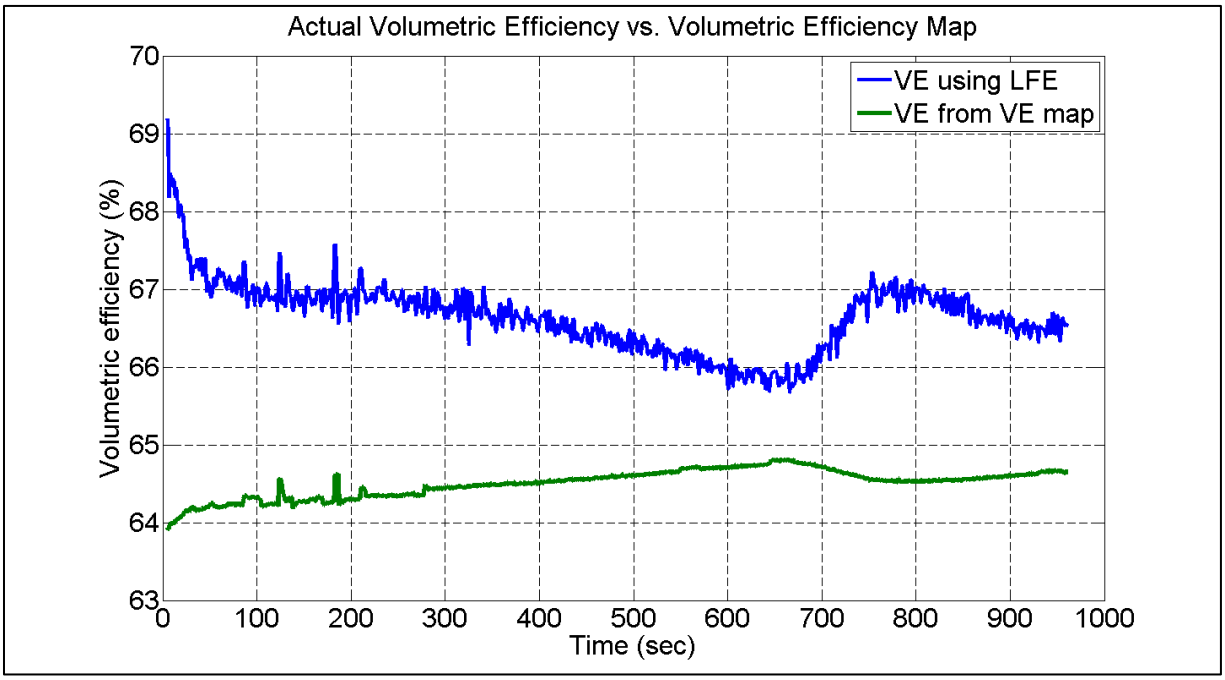


Figure 48: Engine cold start actual VE vs. VE from VE map error at 1400 RPM 50 kPa

In order to correct for this error a multiplier factor will be applied to the volumetric efficiency map. The correction needed to be as simplistic as possible. Each variable added to the correction adds a calibration parameter, which increases calibration

time and effort. Therefore a simplistic two variable linear correction factor was chosen. Although the error is time based, a time based correction factor is not ideal. Warm up times can vary significantly due to climate changes. Therefore the correction factor was decided to use coolant temperature. Coolant temperature is the main cause of the volumetric efficiency error. This is because the coolant runs through passages in the throttle. This heats up the air entering the cylinders. Since the volumetric efficiency map was obtained during warm steady state conditions, the deviation from this state creates errors. It can be seen how much the volumetric efficiency changes with coolant temperature from Figure 49. When the thermostat opens around 97 ℃ and drops rapidly in temperature volumetric efficiency also drops. Around 760 seconds the coolant temperature begins to rise and at this point the volumetric efficiency also rises. Based on this it seems acceptable to use coolant temperature as a means for correcting for the cold start errors in volumetric efficiency.

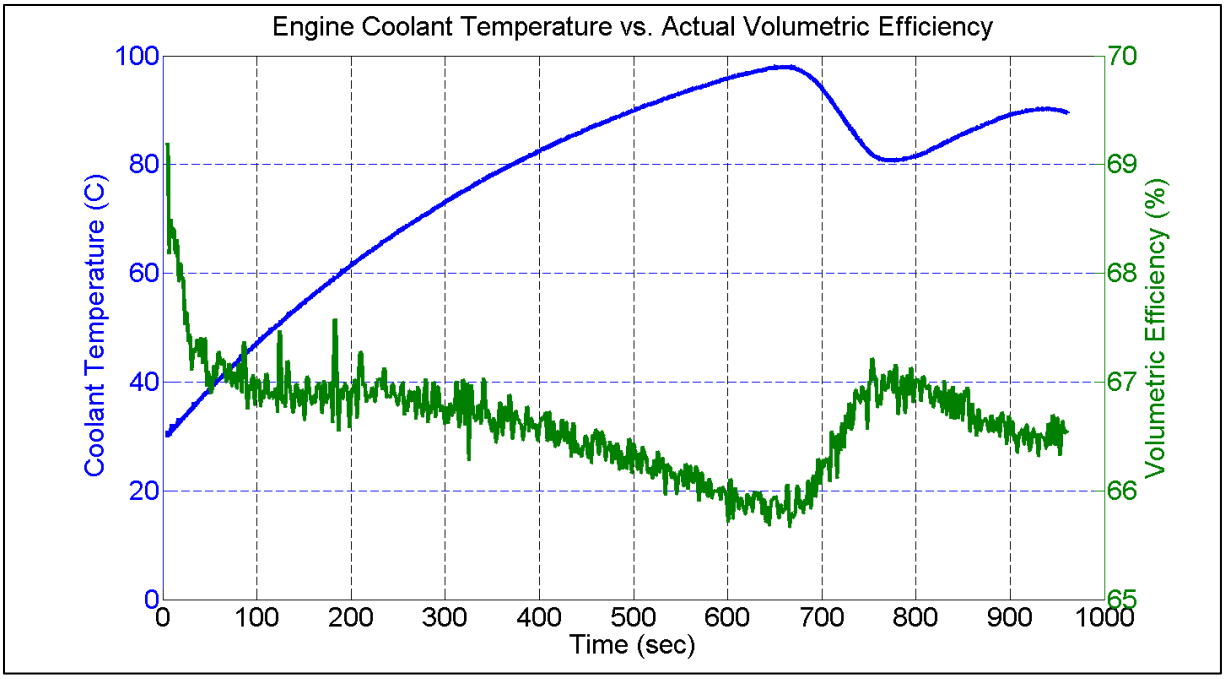


Figure 49: Engine coolant temperature vs. volumetric efficiency calculated for 1400 RPM 50 kPa

As seen in Figure 50 the error decreases linearly. This means that the multiplier factor can also be linear.

$$Correction = \alpha T_{coolant}\ [°C] + \beta \tag{4}$$

Equation (4) shows the multiplier factor that will be used in the cold start MAF calculation correction. $\alpha$ and $\beta$ are both calibration variables. In order to determine these variables error was plotted against coolant temperature, which can be seen in Figure 50. Based on this a linear curve fit using Matlab was performed. This represents the desired

correction factor. Therefore $\alpha$ and $\beta$ were selected to fit this desired line. The curve fit to the error is shown in Figure 50.

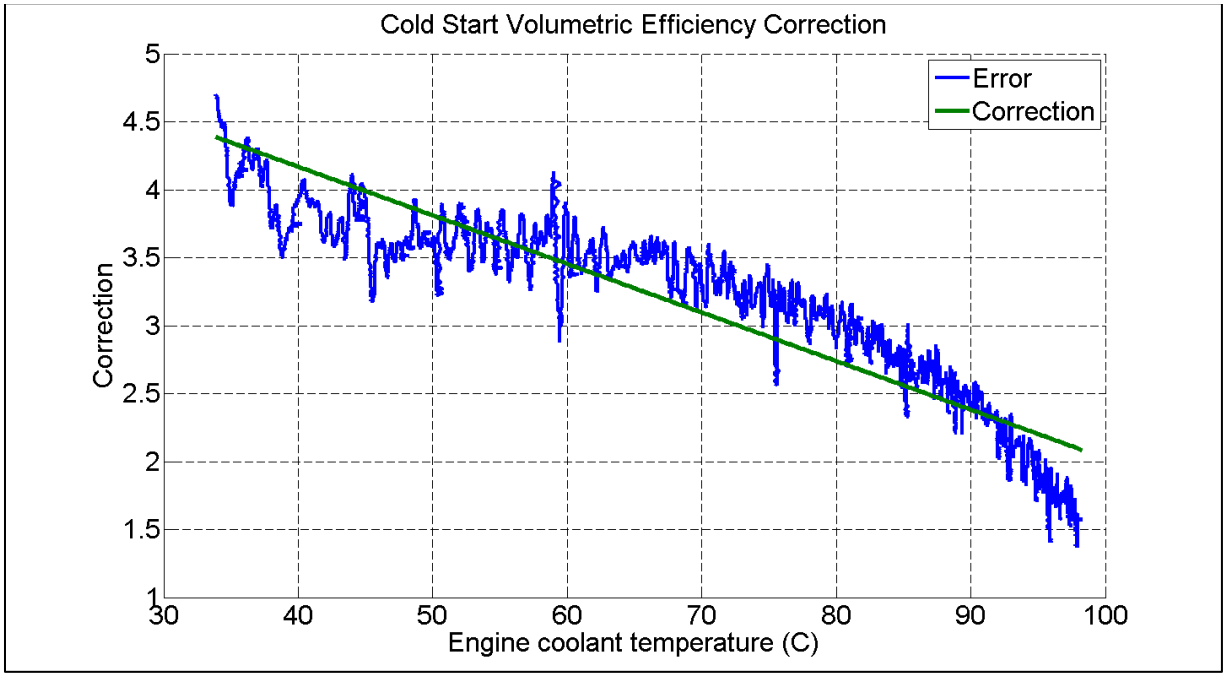


Figure 50: Cold start error, desired correction and actual correction

The Correction line in Figure 50 is then converted into a multiplier factor as seen in Equation (5). The final correction multiplier to calculated MAF is located in Equation (6).

$$\frac{\text{Error Fit Correction line formula}}{100} + 1 \tag{5}$$

$$Correction = -0.00036T_{coolant}\ [℃] + 1.056 \tag{6}$$

Based on this correction the new comparison between the volumetric efficiency map and volumetric efficiency calculated from the LFE is seen in

Figure 51.

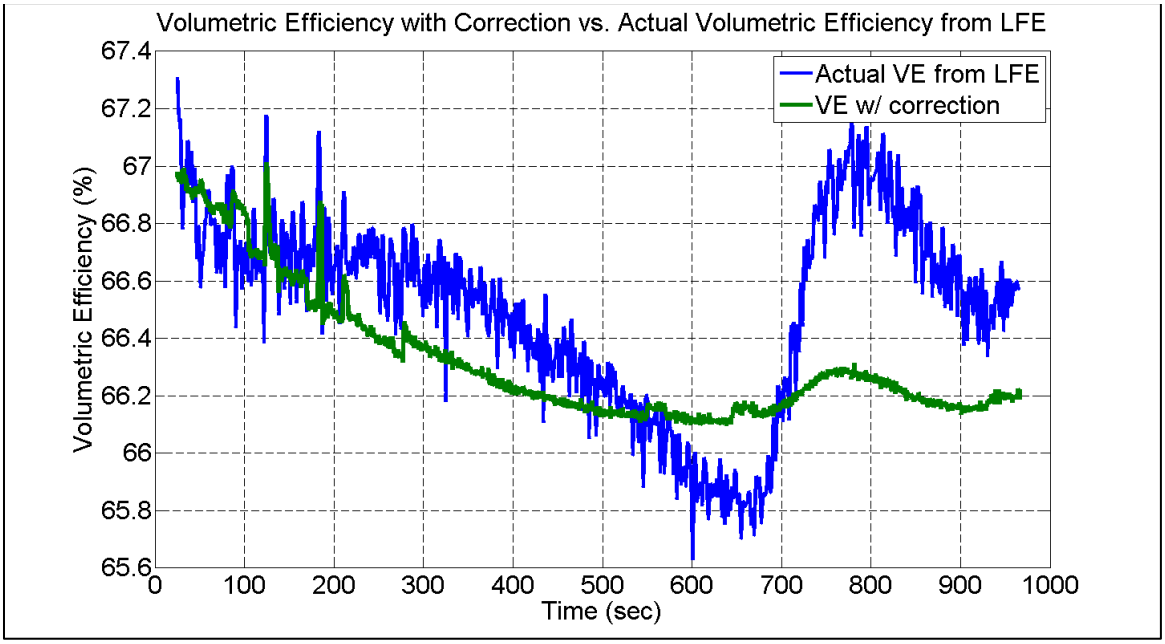


Figure 51: Engine cold start actual VE vs. VE with correction at 1400 RPM 50 kPa

The correction allows for a significant reduction in volumetric efficiency error during cold starts. The difference in error between corrected and not corrected can be seen in Figure 52. This will allow for a much better feed forward air prediction and should allow for improved emissions over not using the correction.

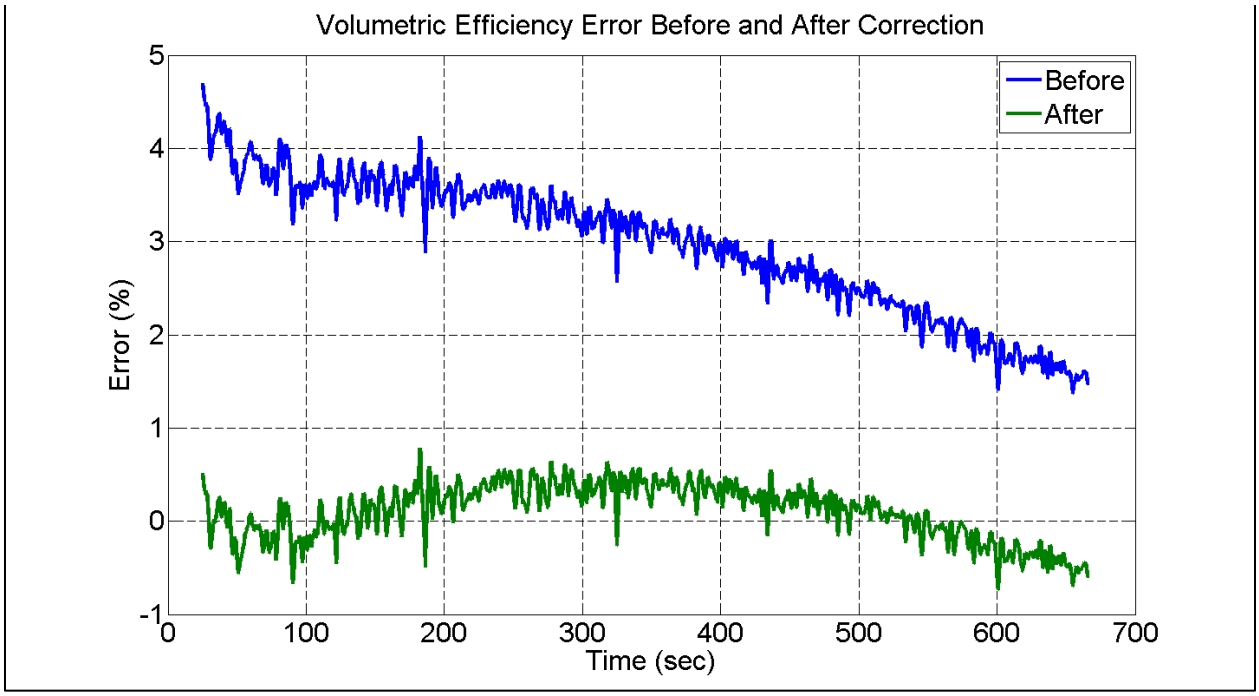


Figure 52: Error before and after the coolant temperature correction to volumetric efficiency is applied

Another concern similar to the cold start volumetric efficiency calculation error is variations in coolant temperature during regular driving. Figure 53 displays that there is a broad range of temperatures over the test matrix. It is expected that a similar distribution could occur during regular steady state driving cycles because the thermostat is very similar between the cooling tower used and the one that is used in the vehicle.

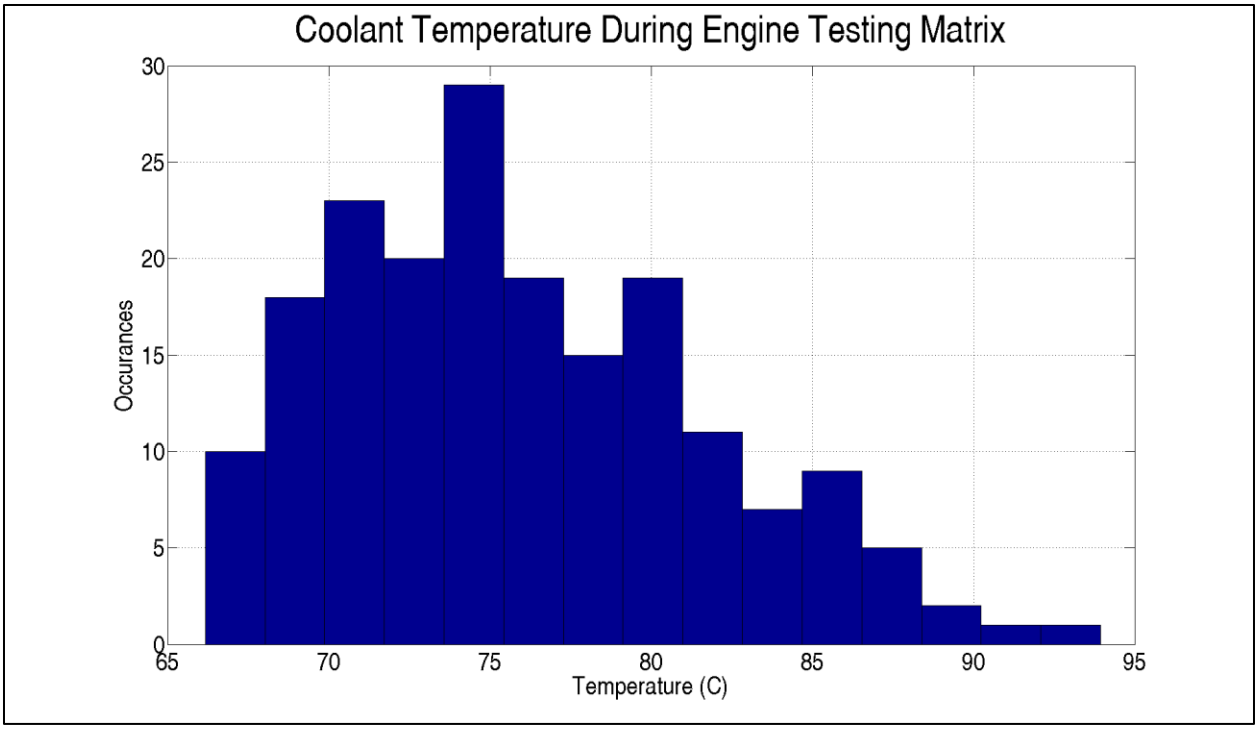


Figure 53: Average coolant temperature variation during test matrix

In the future, a possibility is that the temperature correction, which initially was used for cold starts, could be used during all engine operation to correct for changes in coolant temperature.

## 4.5 Efficiency and Torque Request Maps

A large part of the validation of the EcoCAR engine design is brake fuel conversion efficiency. The use of a high compression engine in conjunction with E85 was designed in order to achieve high engine efficiency values. The spark timing map is very important in the brake efficiency of the engine. The brake efficiency plots can be seen in Figure 54 and Figure 55. Brake efficiency varyes almost completely with engine

manifold pressure. Engine speed does not have a large effect of the brake efficiency values. Brake efficiency increases with increasing engine manifold pressure because as the throttle is opened pumping losses are reduces, leading to higher efficiencies. Another important aspect to the brake efficiency plots is the location of the peak efficiency. In Figure 55 it is very noticable that there is a region around an engine speed of 1500 RPM to about 2700 RPM and a load of 90 kPa to 100 kPa. This region will be a focus of operation in order to achieve the highest efficiency possible. The peak efficiency located at an engine speed of 2200 RPM and a load of 100 kPa was 40.74%.

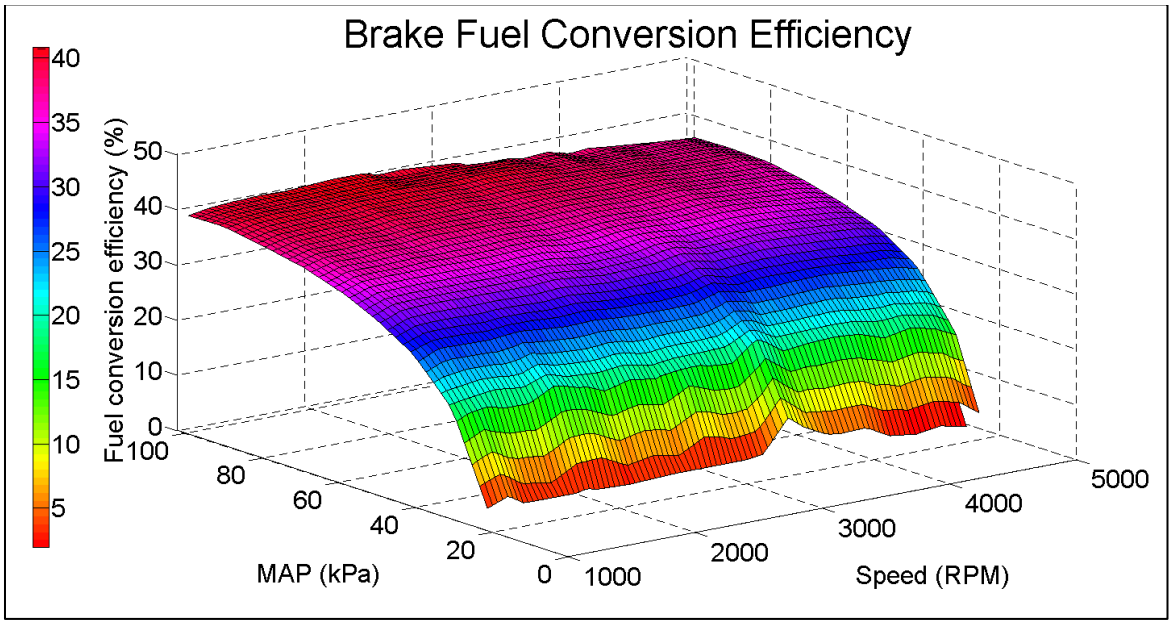


Figure 54: Brake fuel conversion efficiency

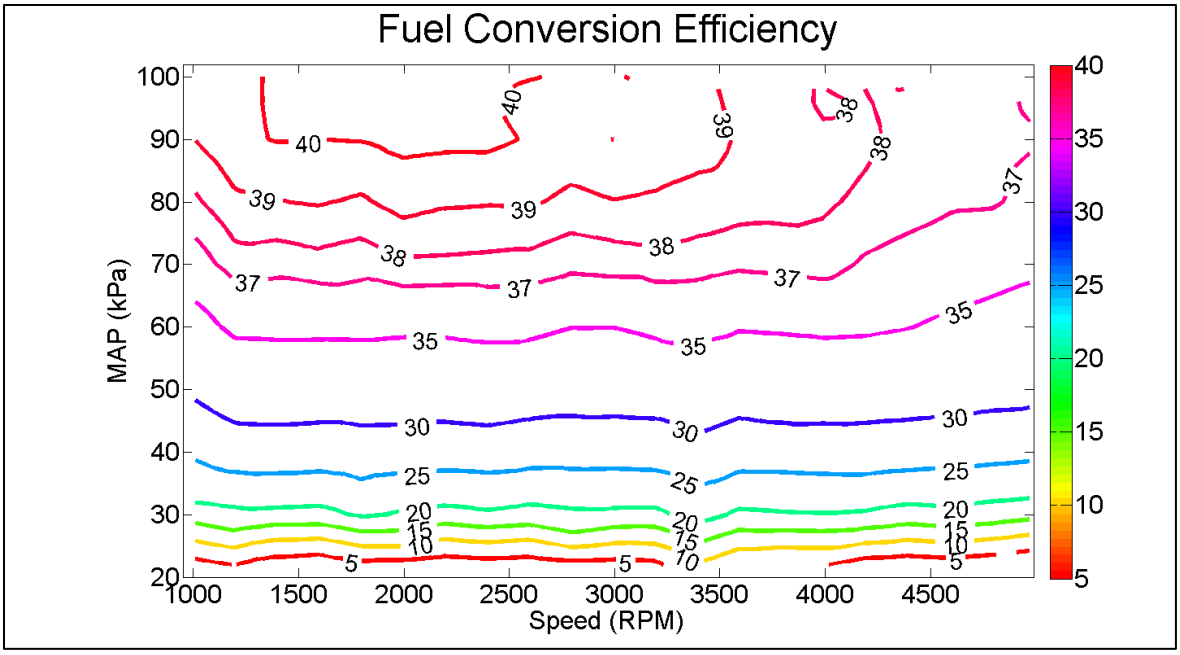


Figure 55: Brake fuel conversion efficiency contour

Using these efficiency maps an overall efficiency map was created for the combination of the front Remy electric machine and the Honda engine when operating in series. This combined efficiency map is shown in Figure 58. The surrounding black line that encloses the efficiency map is the limits of the electric machine. This means that the full torque output of the engine cannot be used at all conditions. The engine limited the maximum torque at lower speeds and the electric machine at higher speeds. The dashed line represents the optimal path of operation, in which the highest efficiencies will result at each torque output. The efficiency maps of the Remy and the Honda engine can be seen in Figure 56 and Figure 57.

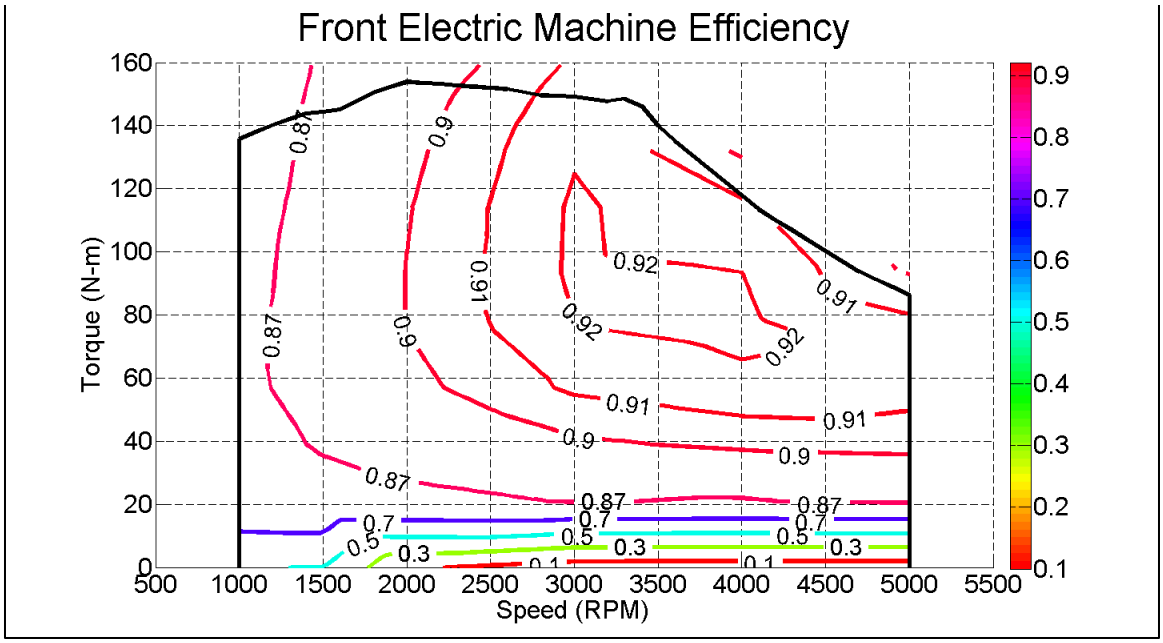


Figure 56: Front electric machine efficiency

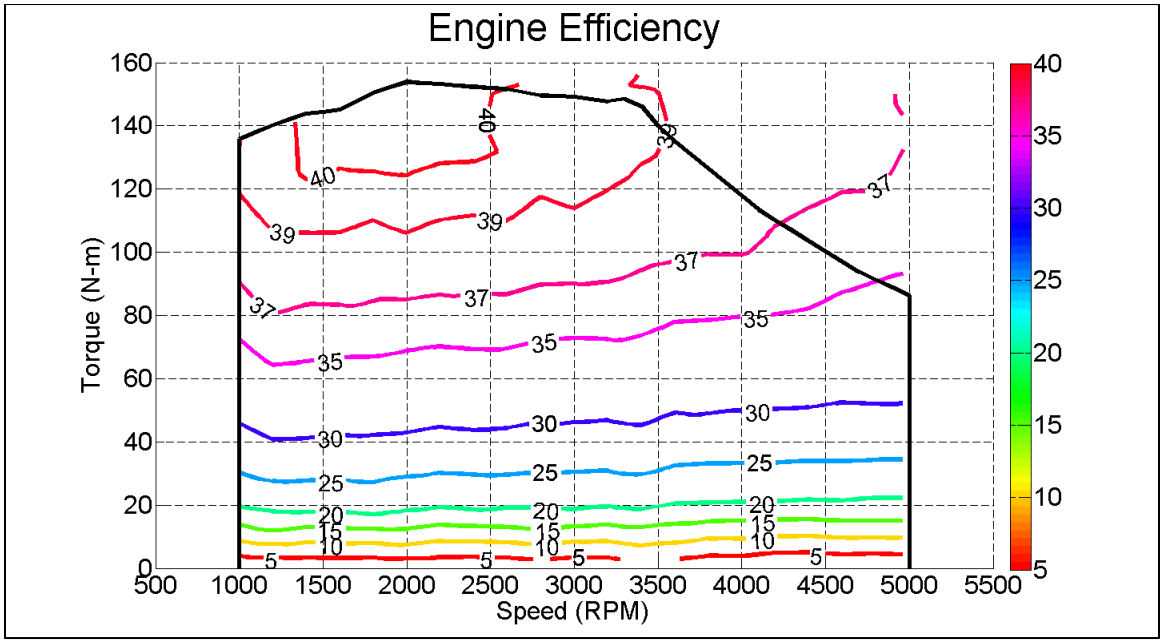


Figure 57: Engine efficiency

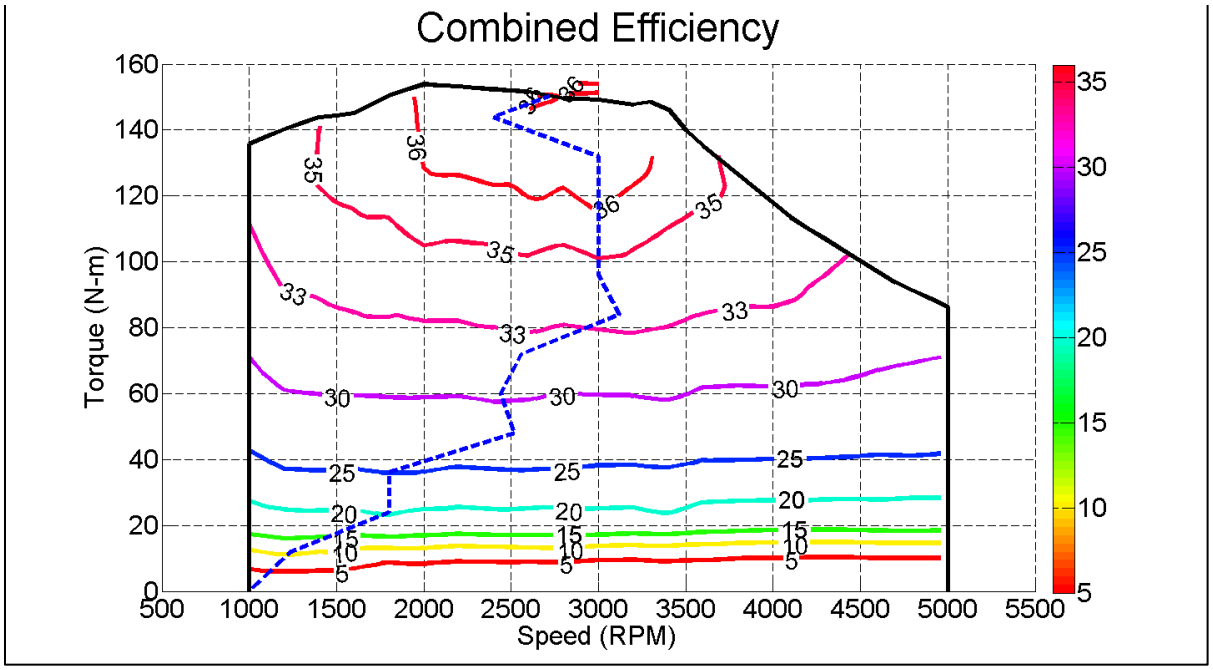


Figure 58: Combined front electric motor and Honda engine efficiency map

In order for the two electric machines and engine to work together in the vehicle a supervisory controller is used. This supervisory controller requests torque from the electric motors and from the engine. Once the torque request has been made by the supervisory controller the engine ECU must interpret this request and produce the desired torque output. To do this three different maps were created in order to achieve the requested torque. These can be seen in Table 9, Table 10 and Table 11. Not all desired points in the maps are obtainable. If the torque is not obtainable at a given speed the maximum air per cylinder from engine testing is used. If an air per cylinder request could not be made at a given speed 100 kPa was used in its place.

Figure 59 shows how the supervisory control interacts with the engine. The supervisory controller requests a torque and a speed. The speed request is sent to the front electric motor. Based on the electric machines speed output and the requested torque the engine controller attempts to achieve a desired MAP which will allow the engine to output the requested torque. The throttle angle is used as a feed forward prediction of the throttle angle which produces the desired MAP. The feedback control loop is then used to achieve the desired MAP.

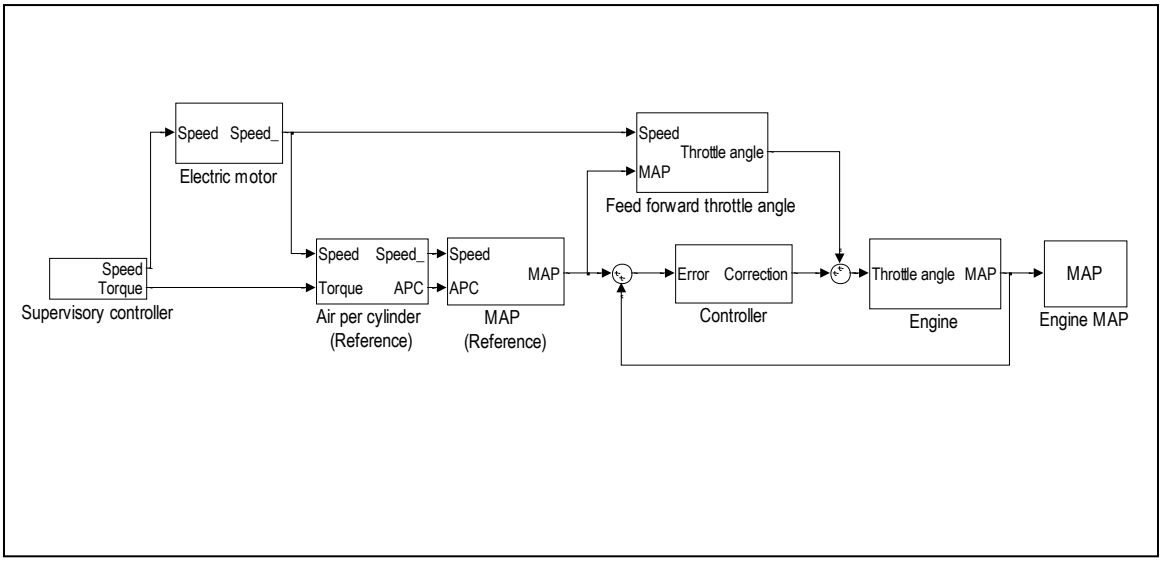


Figure 59: Simple torque based control for series mode

Table 9: Torque request map

| | | Torque request map with Air Per Cylinder [g/cylinder/cycle] | | | | | | | | |
|---|---|---|---|---|---|---|---|---|---|---|
| | | Torque Request (ft-lb) | | | | | | | | |
| | | 0 | 15 | 30 | 45 | 60 | 75 | 90 | 105 | 120 |
| Engine Speed (RPM) | 1000 | 0.12 | 0.21 | 0.30 | 0.39 | 0.48 | 0.57 | 0.66 | 0.74 | 0.74 |
| | 1200 | 0.11 | 0.20 | 0.29 | 0.37 | 0.46 | 0.56 | 0.65 | 0.75 | 0.75 |
| | 1400 | 0.12 | 0.20 | 0.29 | 0.38 | 0.47 | 0.56 | 0.65 | 0.75 | 0.76 |
| | 1600 | 0.12 | 0.20 | 0.29 | 0.38 | 0.47 | 0.56 | 0.65 | 0.75 | 0.76 |
| | 1800 | 0.11 | 0.19 | 0.29 | 0.38 | 0.47 | 0.56 | 0.65 | 0.75 | 0.79 |
| | 2000 | 0.12 | 0.20 | 0.29 | 0.38 | 0.47 | 0.56 | 0.65 | 0.75 | 0.81 |
| | 2200 | 0.13 | 0.21 | 0.30 | 0.38 | 0.47 | 0.56 | 0.65 | 0.74 | 0.80 |
| | 2400 | 0.12 | 0.20 | 0.29 | 0.38 | 0.47 | 0.56 | 0.65 | 0.75 | 0.79 |
| | 2600 | 0.12 | 0.20 | 0.29 | 0.38 | 0.47 | 0.56 | 0.65 | 0.76 | 0.81 |
| | 2800 | 0.11 | 0.20 | 0.30 | 0.39 | 0.48 | 0.57 | 0.66 | 0.76 | 0.80 |
| | 3000 | 0.12 | 0.21 | 0.30 | 0.39 | 0.48 | 0.57 | 0.65 | 0.76 | 0.88 |
| | 3200 | 0.12 | 0.21 | 0.30 | 0.39 | 0.48 | 0.57 | 0.66 | 0.76 | 0.89 |
| | 3400 | 0.10 | 0.20 | 0.30 | 0.39 | 0.48 | 0.57 | 0.67 | 0.76 | 0.87 |
| | 3600 | 0.12 | 0.22 | 0.31 | 0.40 | 0.49 | 0.58 | 0.67 | 0.78 | 0.90 |
| | 3800 | 0.12 | 0.22 | 0.31 | 0.40 | 0.49 | 0.58 | 0.67 | 0.78 | 0.89 |
| | 4000 | 0.12 | 0.22 | 0.31 | 0.40 | 0.49 | 0.58 | 0.68 | 0.79 | 0.92 |
| | 4200 | 0.13 | 0.22 | 0.31 | 0.40 | 0.49 | 0.59 | 0.69 | 0.79 | 0.91 |
| | 4400 | 0.13 | 0.22 | 0.31 | 0.40 | 0.49 | 0.59 | 0.69 | 0.80 | 0.92 |
| | 4600 | 0.13 | 0.22 | 0.31 | 0.41 | 0.50 | 0.60 | 0.70 | 0.80 | 0.91 |
| | 4800 | 0.13 | 0.22 | 0.31 | 0.41 | 0.50 | 0.60 | 0.70 | 0.81 | 0.92 |
| | 5000 | 0.13 | 0.22 | 0.31 | 0.41 | 0.51 | 0.60 | 0.70 | 0.82 | 0.94 |

Table 10: Air per cylinder request map

| | | Air Per Cylinder Request map with MAP (kPa) | | | | | | | | |
|---|---|---|---|---|---|---|---|---|---|---|
| | | Air Per Cylinder Request (g/cylinder/cycle) | | | | | | | | |
| | | 0.1 | 0.195 | 0.29 | 0.385 | 0.48 | 0.575 | 0.67 | 0.765 | 0.86 |
| Engine Speed (RPM) | 1000 | 18.07 | 30.62 | 43.86 | 57.13 | 69.05 | 80.63 | 92.22 | 100.00 | 100.00 |
| | 1200 | 17.54 | 30.40 | 42.63 | 54.86 | 67.09 | 79.31 | 91.54 | 100.00 | 100.00 |
| | 1400 | 19.05 | 31.81 | 44.36 | 56.23 | 68.11 | 79.99 | 91.62 | 100.60 | 100.00 |
| | 1600 | 19.02 | 31.09 | 42.82 | 54.55 | 66.28 | 78.00 | 89.73 | 100.98 | 100.00 |
| | 1800 | 18.92 | 30.49 | 41.64 | 52.79 | 63.94 | 75.09 | 86.25 | 97.40 | 100.00 |
| | 2000 | 18.84 | 30.21 | 41.08 | 51.95 | 62.82 | 73.69 | 84.55 | 95.42 | 100.00 |
| | 2200 | 18.73 | 30.30 | 41.95 | 53.50 | 64.64 | 75.78 | 86.92 | 96.85 | 100.00 |
| | 2400 | 19.18 | 30.47 | 42.13 | 53.30 | 64.47 | 75.65 | 86.40 | 96.85 | 100.00 |
| | 2600 | 19.25 | 30.33 | 41.03 | 51.74 | 62.44 | 73.15 | 83.85 | 94.56 | 100.00 |
| | 2800 | 19.86 | 30.97 | 42.23 | 52.78 | 63.34 | 73.90 | 84.46 | 95.01 | 100.00 |
| | 3000 | 19.03 | 30.02 | 40.93 | 51.83 | 62.74 | 73.65 | 84.56 | 95.47 | 100.00 |
| | 3200 | 18.46 | 29.41 | 40.30 | 51.20 | 62.09 | 72.99 | 84.07 | 94.36 | 100.00 |
| | 3400 | 17.86 | 28.70 | 39.66 | 50.39 | 61.03 | 71.67 | 82.30 | 92.94 | 100.00 |
| | 3600 | 18.32 | 28.43 | 38.65 | 48.93 | 59.22 | 69.50 | 79.78 | 90.03 | 99.81 |
| | 3800 | 18.17 | 28.17 | 38.32 | 48.46 | 58.61 | 68.76 | 78.90 | 88.59 | 98.56 |
| | 4000 | 18.03 | 27.75 | 37.59 | 47.44 | 57.29 | 67.14 | 76.98 | 86.05 | 95.21 |
| | 4200 | 17.64 | 27.42 | 37.20 | 46.97 | 56.75 | 66.53 | 76.31 | 86.08 | 95.88 |
| | 4400 | 17.62 | 27.66 | 37.77 | 47.86 | 57.91 | 67.30 | 76.62 | 86.26 | 95.85 |
| | 4600 | 18.47 | 28.16 | 38.01 | 47.86 | 57.66 | 67.37 | 77.06 | 86.73 | 96.30 |
| | 4800 | 18.50 | 28.27 | 38.03 | 47.78 | 57.54 | 67.30 | 77.05 | 86.81 | 96.64 |
| | 5000 | 18.93 | 28.77 | 38.93 | 49.04 | 58.38 | 68.15 | 77.58 | 87.29 | 97.40 |

Table 11: MAP request map

| | | MAP Request map with Throttle angle (%) | | | | | | | | |
|---|---|---|---|---|---|---|---|---|---|---|
| | | Torque request map (Throttle angle) | | | | | | | | |
| | | 20 | 30 | 40 | 50 | 60 | 70 | 80 | 90 | 100 |
| Engine Speed (RPM) | 1000 | 0.79 | 2.10 | 3.35 | 4.44 | 5.55 | 6.92 | 8.96 | 12.62 | 95.87 |
| | 1200 | 1.09 | 3.12 | 4.74 | 5.96 | 7.33 | 9.01 | 11.29 | 17.06 | 90.12 |
| | 1400 | 1.73 | 3.57 | 5.08 | 6.47 | 7.82 | 9.57 | 11.94 | 15.69 | 90.65 |
| | 1600 | 1.99 | 4.09 | 5.76 | 7.25 | 8.83 | 10.70 | 13.15 | 19.23 | 92.68 |
| | 1800 | 2.63 | 4.75 | 6.58 | 8.23 | 9.85 | 11.93 | 14.56 | 21.86 | 95.34 |
| | 2000 | 3.14 | 5.58 | 7.60 | 9.42 | 11.42 | 13.81 | 16.79 | 34.79 | 99.90 |
| | 2200 | 3.26 | 5.75 | 7.83 | 9.59 | 11.58 | 13.88 | 16.78 | 24.72 | 99.74 |
| | 2400 | 3.41 | 6.14 | 8.27 | 10.20 | 12.32 | 14.71 | 17.73 | 22.69 | 99.99 |
| | 2600 | 3.66 | 6.46 | 8.68 | 10.80 | 13.06 | 15.52 | 18.29 | 25.00 | 99.98 |
| | 2800 | 4.10 | 7.24 | 9.76 | 12.11 | 14.45 | 16.69 | 15.42 | 22.84 | 99.98 |
| | 3000 | 2.38 | 5.48 | 8.02 | 10.28 | 12.73 | 15.60 | 18.94 | 29.72 | 100.00 |
| | 3200 | 4.41 | 7.51 | 10.12 | 12.53 | 14.96 | 17.70 | 21.44 | 31.17 | 100.00 |
| | 3400 | 4.81 | 8.03 | 10.71 | 13.25 | 15.76 | 18.63 | 22.51 | 36.42 | 100.00 |
| | 3600 | 2.83 | 6.81 | 9.57 | 12.00 | 14.74 | 17.34 | 20.94 | 34.10 | 100.00 |
| | 3800 | 3.62 | 7.50 | 10.19 | 13.02 | 15.70 | 18.44 | 22.30 | 31.77 | 100.00 |
| | 4000 | 4.03 | 8.16 | 11.11 | 14.09 | 16.96 | 19.78 | 26.21 | 37.38 | 100.00 |
| | 4200 | 7.05 | 10.85 | 14.01 | 16.71 | 19.47 | 22.53 | 27.12 | 38.15 | 100.00 |
| | 4400 | 4.99 | 9.28 | 12.97 | 15.76 | 20.86 | 24.27 | 29.42 | 43.25 | 100.00 |
| | 4600 | 6.24 | 10.76 | 14.32 | 14.33 | 17.36 | 21.10 | 26.62 | 40.82 | 100.00 |
| | 4800 | 5.79 | 6.88 | 10.64 | 13.98 | 17.25 | 21.49 | 27.37 | 37.59 | 100.00 |
| | 5000 | 3.41 | 7.08 | 10.19 | 15.05 | 18.24 | 21.99 | 27.95 | 39.92 | 100.00 |

# Chapter 5 : Future Work and Conclusions

To conclude the cold start volumetric efficiency corrections, the correction factor formula must be implemented in the ECU. Additional engine testing will be needed in order to verify that it will work as planned. Tests should also be run in order to determine the suitability of the correction factor for normal engine operations in order to correct for the coolant temperature fluctuations.

The volumetric efficiency map should also be used in conjunction with a filling and emptying model to better model the intake manifold dynamics, producing better air-fuel control as opposed to a purely volumetric efficiency based control. This will be necessary for operating the vehicle in parallel mode with the electric machines.

The delayed closure cam configuration should also be examined for year 3 of the EcoCAR competition. Higher part-load efficiency would result and would be particularly useful during highway driving. A fine mapping process would need to be performed using the delayed closure cam if it is to be used as a engine operating mode.

In conclusion, a volumetric efficiency and spark timing map have been created for the EcoCAR challenge hybrid vehicle competition in order to improve transient emissions and optimize fuel economy. Each map was created using 189 data points obtained during dynamometer engine testing. A wiring harness was designed, built

and tested in order utilize the new Woodward engine controller. Cold start volumetric efficiency error was also analyzed and a correction multiplier was created in order to reduce this error. Engine efficiency and a combined efficiency with the front electric machine in series mode were found, as well as an optimal path of operation. Finally torque request maps were created from the engine testing data which allow for the interaction between the vehicles supervisory controller and the engine.

My future plans include attending graduate school at The Ohio State University to obtain my Masters Degree in Mechanical Engineering. A Masters Degree will allow me to continue to develop my understanding of complex internal combustion engines. I will be working on a diesel controls project with Cummins and should further develop my understanding of engine controls.

# Chapter 6 Bibliography

Heywood, J. B. (1988). *Internal Combustion Engine Fundamentals.* Mcgraw-Hill Inc.

Infineon. (2008, 06 24). *PROFET Data Sheet BTS555.* Retrieved 07 2009, from Infineon Technologies: www.Infineon.com

Lumsden, G., Browett, C., Taylor, J., & Kennedy, G. (2004). Mapping Complex Engines. *SAE International*.

Martin, F. G. (1992). *The 6.270 Robot Builder's Guide.*

Moran, M. J., & Shapiro, H. N. (2004). *Fundamentals of Engineering Thermodynamics.* John Wiley and Sons.

Nakajima, S., Goto, H., & Matsunaga, T. (2007). Development of CNG Engine with Variable Valve Timing Electronic Control. *SAE International*.

Okazaki, S., Kato, N., Kako, J., & Ohata, A. (2009). Development of a New Model Based Air-Fuel Ratio Control System. *SAE International*.

Roussopoulos, K. (1990). Technique for Determining Comparative Volumetric Efficiency. *SAE International*.

Smith, L., Osborne, R., & Fickenscher, T. (1999). Convient Engine Breathing-Steady Speed Volumetric Efficiency and Its Validity Under Transient Engine Operation. *SAE International*.

Suzuki, K., Nemoto, M., & Machida, K. (2006). Model-Based Calibration Process for Producing Optmial Spark Advance in a Gasoline Engine Equipped with a Variable Valve Train. *SAE International*.

# Appendix A: SIMULINK engine control map

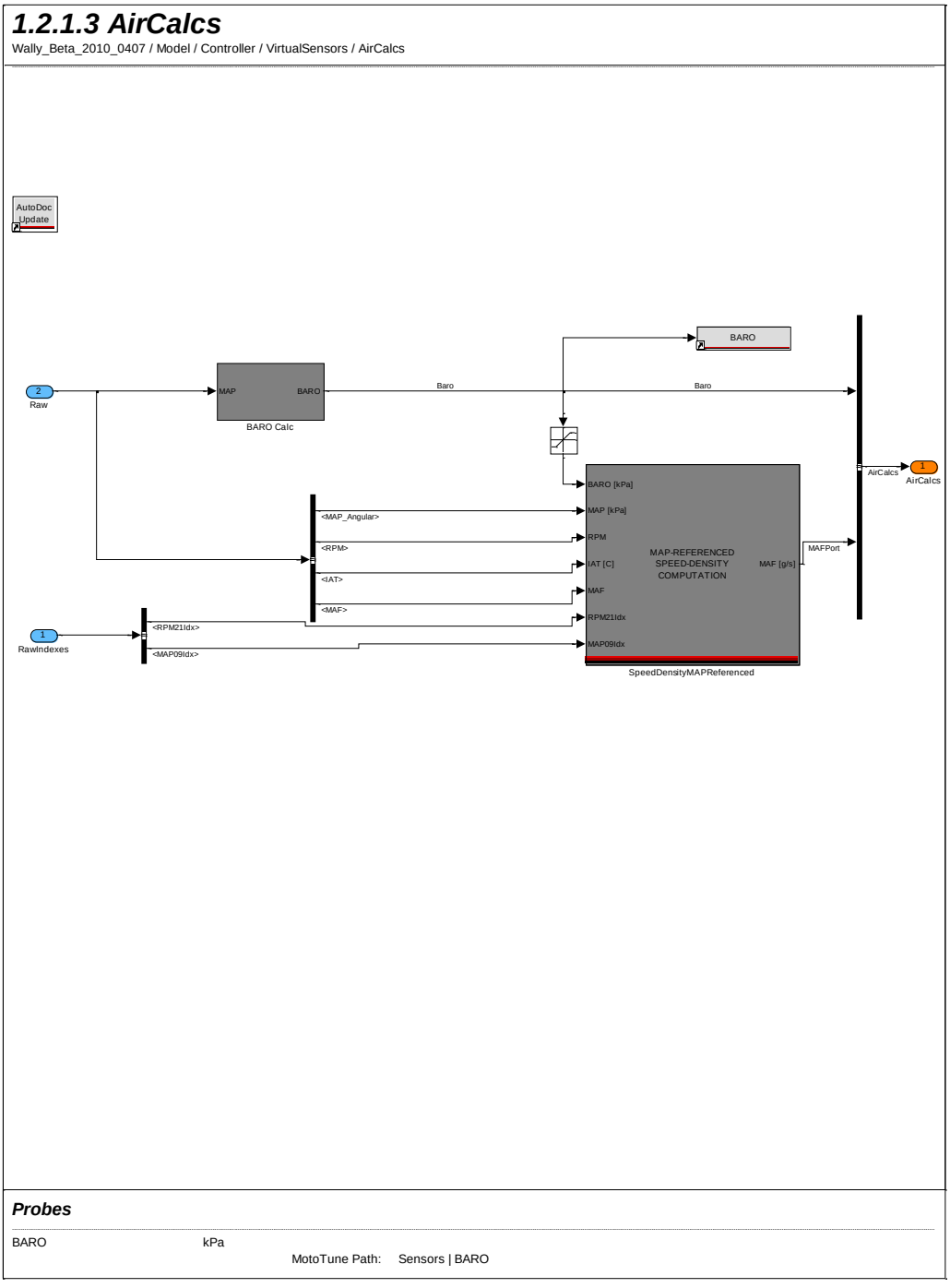


Figure 60: MAP-referenced Speed Density computation SIMULINK map

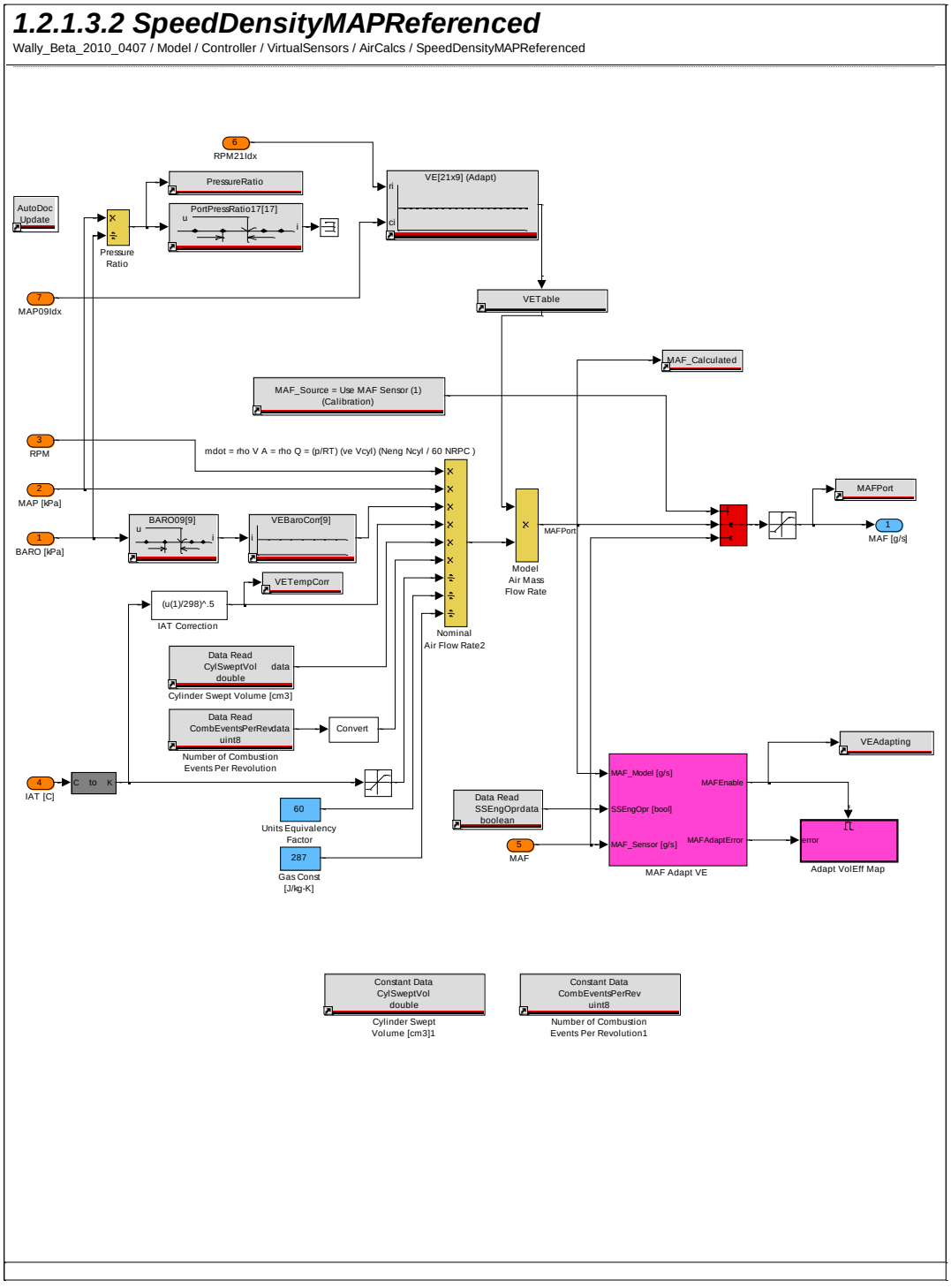


Figure 61: MAP-referenced Speed Density computation SIMULINK map block

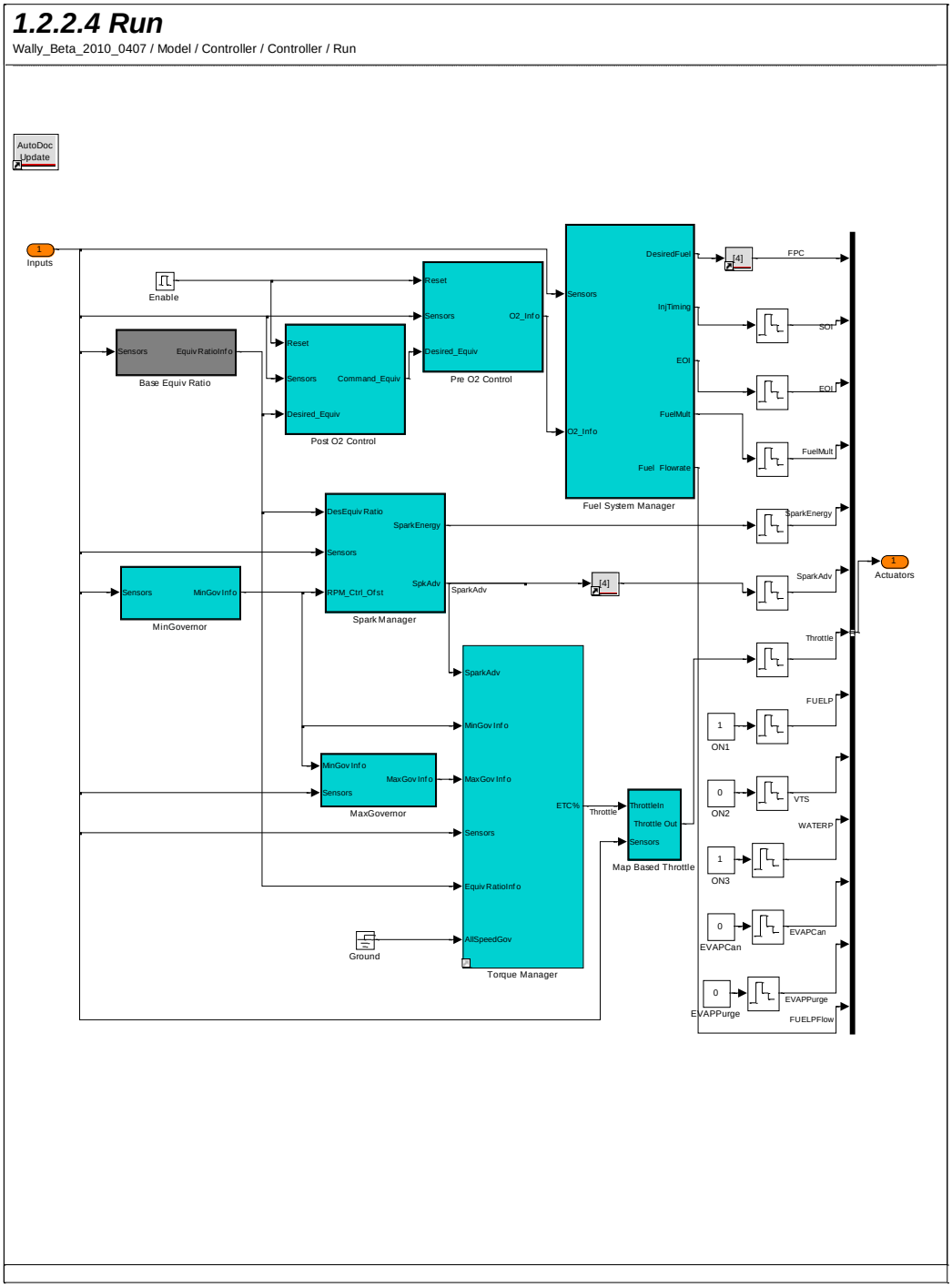


Figure 62: Spark manager SIMULINK map

## 1.2.2.4.4 Spark Manager

Wally_Beta_2010_0407 / Model / Controller / Controller / Run / Spark Manager

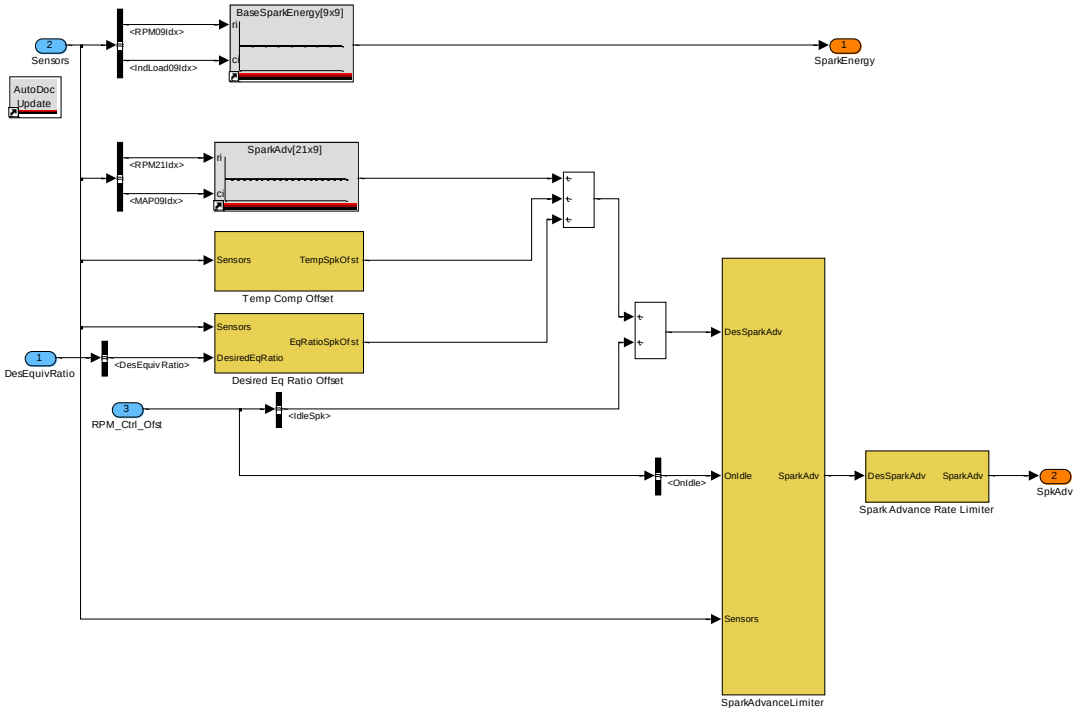


### Calibrations

| | | |
|---|---|---|
| BaseSparkEnergyMap | mJ | Spark energy - Run state<br>MotoTune Path: Engine Control \| Run \| Spark |
| SparkAdvMap | degBTDC | Base spark advance map.<br>MotoTune Path: Engine Control \| Run \| Spark |

Figure 63: Spark manager SIMULINK map block

# Appendix B: wiring harness design

Table 12: Woodward engine controller wiring connections part 1

| Woodward 36321 p. 10 ~ CONNECTOR PINOUTS | | | | Engine Wiring Harness | | | |
|---|---|---|---|---|---|---|---|
| **Pin #** | **ControlCore** | **Function** | **Notes** | **Terminal #** | **Name** | **Description** | **Signal** |
| **ECM** | **Resource Name** | | | | | | |
| J1-A1 | SPD1 | Auxilliary Speed Input | VR or HALL Effect | Not used | | | |
| J1-A2 | CNK_VR- | Return for CRANK VR sensor | | N/A | CKP sensor ground | Return for CKP sensor. Do not connect Engine wiring harness ground wire. | |
| J1-A3 | ISO_9141_K | Serial Data Link | ISO 9141 Compliant | Not used | | | |
| J1-A4 | ISO- 9141 - L | | | Not used | | | |
| J1-A5 | AN15M | Variable Resistance Input | 1K Pull Up | B39 | IMTM (INTAKE MANIFOLD Tuning valve monitor) | Detects IMT valve position | 0-5V |
| J1-A6 | AN6M | Pressure Input | 51K Pull Down | N/A | PF2 (FUEL RAIL PRESSURE SENSOR) | Detects fuel pressure sensor signal | 0.5-4.5V |
| J1-A7 | AN17M | Variable Resistance Input | 1KPullUp | B23 | ECT1 (ECT sensor 1) | Engine coolant temp | 0-5V |
| J1-A8 | AN3M | Pressure Input | 220K Pull Down | Not used | | | |
| J1-A9 | DG4 | Discrete Switch, Frequency | 1K Pull Up | N/A | Ethanol Concentration Signal (E85 S) | Detects percentage of Ethanol in fuel | Pulse width+frequency |
| J1-A10 | AN13M | Potentiometer Input | 2.2K Pull Up | Not used | | | |
| J1-A11 | XDRP_B | Transducer Power B (5V) | 300 mA Transducer Power | C13 | VCC1 (SENSOR VOLTAGE) | Sensor reference voltage to 24P Junction Connector (MAP sensor) | 5V |
| | | | | C12 | VCC3 (SENSOR VOLTAGE) | Provides sensor reference voltage to TPS | With ignition on (II): 5V |
| J1-A12 | SPD2 | Auxilliary Speed Input | VR or HALL Effect | Not used | | | |
| J1-A13 | CNK | Crank Position Signal | vR or HALL Effect | C32 | CKP (CRANKSHAFT POSITION (CKP) SENSOR) | Detects CKP sensor signal | |
| J1-A14 | AN1M | Pressure Input | 220K Pull Down | C20 | TPSA (THROTTLE Position Sensor A) | Detects TP sensor A signal | fully open: 4.1 V fully closed: about 1.6 V |
| J1-A15 | AN12M | Pressure Input | 51K Pull Down | Not used | | | |
| J1-A16 | AN10M | Pressure Input | 51 K Pull Down | Not used | | | |
| J1-A17 | AN8M | Pressure Input | 51K Pull Down | B30 | VG+ (MASS AIR FLOW SENSOR +SIDE) | Detects MAF sensor signal | At idle: 1.1-1.6 V (Between VG+ terminal and VG- terminal) |
| J1-A18 | AN2M | Pressure Input | 220K Pull Down | C21 | TPSB (THROTTLE Position Sensor B) | Detects TP sensor B signal | fully open: 4.2 V fully closed: about 1.7 V |
| J1-A19 | DG3 | Discrete Switch, Frequency | 1K Pull Up | Not used | | | |
| J1-A20 | CAM | Cam Position Signal | VR or HALL Effect | C31 | CMP (CAMSHAFT POSITION (CMP) SENSOR) | Detects CMP sensor signal | |
| J1-A21 | AN7M | Pressure Input | 51K Pull Down | N/A | Exhaust gas reciculation (EGR) valve position sensor (EGR PS) | Detects EGR valve position sensor signal | 0-5 V |
| J1-A22 | TACH | Tachometer Output | 4.75K Pull Up | Not used | | | |
| J1-A23 | LS03 | PWM with current feedback | 4A continuous, 3A PWM | N/A | EVAP canister shut valve ground | Controls EVAP canister shut valve | |
| J1-A24 | XDRG | Transducer Ground A | Return for Transducers | N/A | EGR position sensor ground (EGR PG) | Originally connected to SG2 on gas engine | |
| | | | | N/A | Exhaust RTD 1 | Ground for RTD 1 | |
| | | | | N/A | Exhaust RTD 2 | Ground for RTD 2 | |
| | | | | N/A | Exhaust RTD 3 | Ground for RTD 3 | |
| | | | | B32 | VG- (MASS AIR FLOW SENSOR -SIDE) | Ground for MAF sensor | |
| J1-A25 | AN9M | Pressure Input | 51 K Pull Down | N/A | PFO (FUEL TANK PRESSURE (FTP) SENSOR) | Fuel tank pressure | |
| J1-A26 | AN11M | Pressure Input | 51K Pull Down | Not used | | | |
| J1-A27 | AN16M | Variable Resistance Input | 1K Pull Up | N/A | Fuel Level Sender (FLS) | Signal for fuel tank level | |
| J1-A28 | AN14M | Variable Resistance Input | 1K Pull Up | B31 | IAT (intake air temperature sensor) | IAT sensor | 0-4V |
| J1-A29 | AN4M | Pressure Input | 51K Pull Down | C11 | MAP Sensor | Detects MAP sensor signal | With ignition on (II): about 3.0 V At idle: about 1.0 V (depending on engine speed) |
| J1-A30 | AN5M | Pressure Input | 51K Pull Down | C22 | POILCS (ENGINE OIL PRESSURE (EOP) SENSOR) | Detects EOP sensor signal | with ignition ON (II): about 0.7 V with ignition switch in START (III) position: 0.9 V (momentarily) |
| J1-A31 | CAM_VR- | Return for CAM VR sensor | | N/A | CMP sensor ground | Return for CMP sensor (Disconnect original ground to block) | |
| J1-A32 | SPD- | Return for SPD VR sensors | | Not used | | | |

Table 13: Woodward engine controller wiring connections part 2

| | | | | | | | |
|---|---|---|---|---|---|---|---|
| J1-B1 | LSU1_VM | Lambda Sensing Unit | See datasheet for Bosch LSU4.xand CJ125. | N/A | UEGO sensor 1 VM | UEGOs sensor | |
| J1-B2 | KEY_SW | ECM Wake | Wake Up Module | F on the smartcraft hub | ECM Wake | Turned on using supervisory system in car. Turned on by switch in Dyno. | Connected to Smartcraft hub. See Visio drawing for better description. |
| J1-B3 | AN31M | Analog Inputs Suitable for Low Cost EGO | | Not used | | | |
| J1-B4 | AN32M | | | Not used | | | |
| J1-B5 | AN33M | Variable Resistance Inputs | See section 6 for module configuration options. | Not used | | | |
| J1-B6 | AN34M | Variable Resistance Inputs | See section 6 for module configuration options. | Not used | | | |
| J1-B7 | DG1 | Discrete Switch, Frequency, IRQ | 1K Pull Up | Not used | | | |
| J1-B8 | BATT | Battery Connection | Needs battery voltage at all times | N/A | Supplied from Fuse | See Fuses or Visio drawing | |
| J1-B9 | CAN1+ | Serial Communications | Terminating Resistance Required | Not used | | | |
| J1-B10 | CAN1- | | | Not used | | | |
| J1-B11 | XDRP_A | Transducer Power A (5V) | 300mA Source for Transducers | N/A | EGR position sensor power (EGR PSP) | | 5V |
| | | | | N/A | Fuel Rail pressure power (PF2 P) | Sensor reference voltage for fuel rail pressure sensor | 5V |
| | | | | N/A | FTP sensor power | Sensor reference voltage for fuel tank pressure sensor | With ignition switch ON (II): about 5.0 V |
| | | | | B18 | VCC2 (Sensor voltage) | Sensor reference voltage to 24P Junction Connector (EOP, IMT position) | With ignition switch on: 5.0V |
| J1-B12 | LSU2_UN | Lambda Sensing Unit2 | See datasheet for Bosch LSU4.xand CJ125. | Not used | | | |
| J1-B13 | LSU2_VM | | | Not used | | | |
| J1-B14 | LSU1_IP | Lambda Sensing Unit1 | | N/A | UEGO sensor 1 IP | UEGO sensor | |
| J1-B15 | LSU1_IA | | | N/A | UEGO sensor 1 IA | | |
| J1-B16 | LSU2_IA | Lambda Sensing Unit2 | | Not used | | | |
| J1-B17 | LSU2_IP | | | Not used | | | |
| J1-B18 | MPRD | Main Power Relay Driver | Wire to Coil of Main Power Relay. 1.5A low side driver intended to drive relay coil that supplies DRVP | N/A | MRLY (PGM-FI MAIN RELAY) | Drives PGM-FI main relay | With ignition switch ON (II): about 0 V With ignition switch OFF: battery voltage |
| J1-B19 | LS02/LSUH2 | PWM Output/ LSU Heater | 10A continuous, 3A PWM | Not used | | | |
| J1-B20 | LS01/LSUH1 | | | N/A | UEGO power control 1 | Control for UEGO power control | 4.24 A max |
| J1-B21 | LSU1_UN | Lambda Sensing Unit1 | See datasheet for Bosch LSU4.xand CJ125. | N/A | UEGO sensor 1 UN | UEGO sensor | |
| J1-B22 | SCL+ | RS485 HI | | Not used | | | |
| J1-B23 | SCL- | RS485 LO | | Not used | | | |
| J1-B24 | XDRG | Transducer Ground B | Return for Transducers | C30 | Post-cat EGO sensor ground | Ground for post-cat EGO sensor | |
| | | | | 7 of Coolant pump high-side switch | Current Feedback ground | Feedback ground; Post resistor | |
| | | | | C14 | SG1 (SENSOR GROUND) | Ground for MAP sensor | |
| | | | | N/A | FTP sensor ground | Ground for FTP sensor | Less than 1.0V at all times |
| | | | | N/A | Fuel Level Sender ground (FL G) | Ground for fuel level sender | |
| | | | | C39 | SG3 (SENSOR GROUND) | Ground for TPS | |
| | | | | B33 | SG2 (SENSOR GROUND) | Ground for IAT, EOP and IMT, ECT 1 | |
| | | | | N/A | Fuel rail pressure sensor (PF2 G) | Ground for Fuel rail pressure sensor | Less than 1.0V at all times |
| | | | | N/A | ECT sensor 2 ground | Ground for ECT sensor 2 | Less than 1.0V at all times |
| | | | | N/A | Ethanol Concentration Signal (E85 G) | Ground for Ethanol concentration sensor | |

Table 14: Woodward engine controller wiring connections part 3

| | | | | | | | |
|---|---|---|---|---|---|---|---|
| J1-C1 | AN24M | Variable Resistance Input | 1K Pull Up | N/A | Exhaust RTD 1 | Not apart of engine wiring harness | |
| J1-C2 | AN21M | Variable Resistance Input | 1K Pull Up | N/A | Exhaust RTD 2 | | |
| J1-C3 | AN25M | Variable Resistance Input | 1K Pull Up | N/A | Exhaust RTD 3 | | |
| J1-C4 | AN22M | Variable Resistance Input | 1K Pull Up | N/A | Cooling Pump Feedback | Feedback from Variable Current cooling pump high-side switch | 0-5V |
| J1-C5 | AN23M | Variable Resistance Input | 1KPull Up | N/A | Radiator Fan Feedback | Feedback from Variable Current Radiator Fan high-side switch | 0-5V |
| J1-C6 | AN29M | High Impedance Input | 5.1 M Pull Up, 1M Pull Down | C29 | Post-cat EGO sensor | | 0-5 V |
| J1-C7 | AN28M | Potentiometer Input | 2.2K Pull Up | Not used | | | |
| J1-C8 | AN30M | High Impedance Input | 5.1 M Pull Up | Not used | | | |
| J1-C9 | AN20M | Variable Resistance Input | 1K Pull Up | N/A | ECT2 (ENGINE COOLANT TEMPERATURE (ECT)SENSOR 2) | Detects ECT sensor 2 signal | With ignition switch ON (II): about 0.1-4.8 V (depending on engine coolant temperature) |
| J1-C10 | AN18M | Variable Resistance Input | 1K Pull Up | Not used | | | |
| J1-C11 | AN19M | Variable Resistance Input | 1K Pull Up | Not used | | | |
| J1-C12 | AN26M | Potentiometer Input | 2.2K Pull Up | Not used | | | |
| J1-C13 | DG7 | Discrete Switch, Frequency, IRQ | 1K Pull Up | Not used | | | |
| J1-C14 | DG8 | | | Not used | | | |
| J1-C15 | AN27M | Potentiometer Input | 2.2K Pull Up | Not used | | | |
| J1-C16 | DG2 | Discrete Switch, Frequency, IRQ | 1K Pull Up | B7 | OPSW (OIL PRESSURE Switch) | Detects low oil pressure | With ignition switch on: 0V With engine running: Battery voltage. Will read 0 if low pressure; 1 if normal pressure |
| J1-C17 | CAN2+ | Serial Communications | Terminating Resistance Required | Not used | | | |
| J1-C18 | CAN2- | | | Not used | | | |
| J1-C19 | EK1P | Knock Sensor Positive | Compatible with the Motorola PROSAK IC | N/A | KS+ | Knock sensor positive | |
| J1-C20 | EK1N | Knock Sensor Negative | | N/A | KS- | Knock sensor negative | |
| J1-C21 | EK2P | Knock Sensor Positive | | Not used | | | |
| J1-C22 | EK2N | Knock Sensor Negative | | Not used | | | |
| J1-C23 | DG5 | Discrete Input | 1K Pull Up | Not used | | | |
| J1-C24 | DG6 | Discrete Input | | Not used | | | |

Table 15: Woodward engine controller wiring connections part 4

| | | | | | | | |
|---|---|---|---|---|---|---|---|
| J2-A1 | INJ01 | Injector 1 Driver | 3A/1A peak/hold | C102-6 | INJCNTL1 (No.1 INJECTOR CONTROL) | Drives No.1 injector | Duty controlled |
| J2-A2 | INJ07 | Injector 7 Driver | 7A/3A or 3A/1A peak/hold | Not used | | | |
| J2-A3 | INJ02 | Injector 2 Driver | 3A/1A peak/hold | C102-5 | INJCNTl2 (No.2 INJECTOR CONTROL) | Drives No: 2 injector | Duty controlled |
| J2-A4 | INJ08 | Injector 8 Driver | 7A/3A or 3A/1A peak/hold | Not used | | | |
| J2-A5 | INJ06 | Injector 6 Driver | 3A/1A peak/hold | Not used | | | |
| J2-A6 | INJ04 | Injector 4 Driver | 7A/3A or 3A/1A peak/hold | C102-3 | INJCNTl2 (No.4 INJECTOR CONTROL) | Drives No.4 injector | Duty controlled |
| J2-A7 | INJ03 | Injector 3 Driver | 3A/1A peak/hold | C102-4 | INJCNTl2 (No.3 INJECTOR CONTROL) | Drives No.3 injector | Duty controlled |
| J2-A8 | INJ05 | Injector 5 Driver x | 7A/3A or 3A/1A peak/hold | | | | |
| J2-A9 | H1+ | H-Bridge Output | High Current (5A) | B37 | IMT+ (INTAKE MANIFOLD Tuning actuator + side) | Drives IMT actuator | Battery voltage |
| J2-A10 | EST5 | Electronic Spark Timing | TTL | Not used | | | |
| J2-A11 | EST6 | | | Not used | | | |
| J2-A12 | EST1 | | | C15 | IGPIS1 (No.1 IGNITION COIL PULSE) | Drives No.1 ignition coil | with ignition on(II): about 0 V with engine running: pulses |
| J2-A13 | EST2 | | | C16 | IGPIS1 (No.2 IGNITION COIL PULSE) | Drives No.2 ignition coil | with ignition on(II): about 0 V with engine running: pulses |
| J2-A14 | EST3 | | | C17 | IGPIS1 (No.3 IGNITION COIL PULSE) | Drives No.3 ignition coil | with ignition on(II): about 0 V with engine running: pulses |
| J2-A15 | DVRG | Driver Ground | Connect to Battery Ground | B36 | PG1 (POWER GROUND) | Ground circuit for PCM | |
| J2-A16 | DVRG | | | B1 | PG2(POWER GROUND) | Ground circuit for PCM | |
| J2-A17 | H1- | H-Bridge Output | High Current (5A) | B38 | IMT- (INTAKE MANIFOLD Tuning actuator - side) | Ground for IMT actuator | 4.5 V (between IMT+ terminal and IMT- terminal) |
| J2-A18 | DRVP | Driver Power (VBATT) | Power to H-Bridges and Loads | N/A | MRLY terminal | Connection to main relay terminal | |
| J2-A19 | DRVP | | | N/A | MRLY terminal | Connection to main relay terminal | |
| J2-A20 | EST4 | Electronic Spark Timing | TTL | C18 | IGPIS1 (No.4 IGNITION COIL PULSE) | Drives No.4 ignition coil | with ignition on(II): about 0 V with engine running: pulses |
| J2-A21 | EST7 | | | Not used | | | |
| J2-A22 | EST_RTN | Low Current Return | | Not used | | | |
| J2-A23 | EST8 | Electronic Spark Timing | TTL | N/A | Exhaust gas recirculation (EGR) valve (EGR ) | Drives EGR valve | Duty controlled |
| J2-A24 | DVRG | Driver Ground | Connect to Battery Ground | C2 | PGMETCS (POWER GROUND ETCS) | Ground circuit for PCM | |

Table 16: Woodward engine controller wiring connections part 5

| | | | | | | | |
|---|---|---|---|---|---|---|---|
| J2-B1 | INJ12 | Injector 12 Driver | 7A/3A or 3A/1A peak/hold | Not used | | | |
| J2-B2 | INJ10 | Injector 10 Driver | 3A/1A peak/hold | Not used | | | |
| J2-B3 | INJ09 | Injector 9 Driver | 7A/3A or 3A/1 A peak/hold | Not used | | | |
| J2-B4 | INJ11 | Injector 11 Driver | 3A/1A peak/hold | Not used | | | |
| J2-B5 | EST14/LAMP2 | Electronic Spark Timing/ Low Side Lamp Driver | High Current (1A) | N/A | Fuel Pump | High-side driver for Fuel Pump | |
| J2-B6 | EST13/LAMP1 | | | N/A | Variable current water pump | High-side variable current water pump | Duty controlled |
| J2-B7 | EST15LAMP3 | | | N/A | Variable current cooling fan | High-side variable cooling fan control | Duty controlled |
| J2-B8 | EST16/LAMP4 | | | Not used | | | |
| J2-B9 | DVRG | Driver Ground | Connect to Battery Ground | C102-13 | Ground wire for Injector control module | Injector control module does not exist, only their wires were used | |
| J2-B10 | EST12 | Electronic Spark Timing | TTL | Not used | | | |
| J2-B11 | EST11 | | | Not used | | | |
| J2-B12 | LS05 | PWM Output | 4A continuous, 3A PWM | N/A | Ignition Coil relay | | With ignition switch ON (II): about 0 V With ignition switch OFF: battery voltage |
| J2-B13 | EST10 | Electronic Spark Timing | TTL | Not used | | | |
| J2-B14 | EST9 | | | Not used | | | |
| J2-B15 | LS06 | PWM Output | 4A continuous, 3A PWM | C9 | Post-CAT EGO heater | Controls power to the EGO sensor heater | |
| J2-B16 | H3+ | H-Bridge Output | High Current (10A) | C4 | ETCSM+ (THROTTLE ACTUATOR +SIDE) | Drives throttle actuator | |
| J2-B17 | LS07 | PWM Output | 4A continuous, 3A PWM | N/A | Fuel system relay | Drives fuel pump and EVAP | With engine off: battery voltage With engine on: about 0 V |
| J2-B18 | LS09 | | | N/A | EVAP canister purge valve ground (PCS) | EVAP canister purge valve control | |
| J2-B19 | LS08 | | | N/A | Cooling relay | Drives relay for radiator fan and electric water pump smart high-side switches | With engine off: battery voltage With engine on: about 0 V |
| J2-B20 | LS010 | | | N/A | Sensor Power Relay | Powers O2, CMP and CKP sensors | With engine off: battery voltage With engine on: about 0 V |
| J2-B21 | LS04 | PWM Output with current feedback | 4A continuous, 3A PWM | Not used | | | |
| J2-B22 | H2+ | H-Bridge Output | High Current (5A) | B34 | VTS (ROCKER ARM Oil CONTROL SOLENOID) | Drives rocker arm oil control solenoid | |
| J2-B23 | H2- | | | Not used | | | |
| J2-B24 | H3- | | High Current (10A) | C3 | ETCSM (THROTTLE ACTUATOR -SIDE) | Negative side for throttle actuator | |

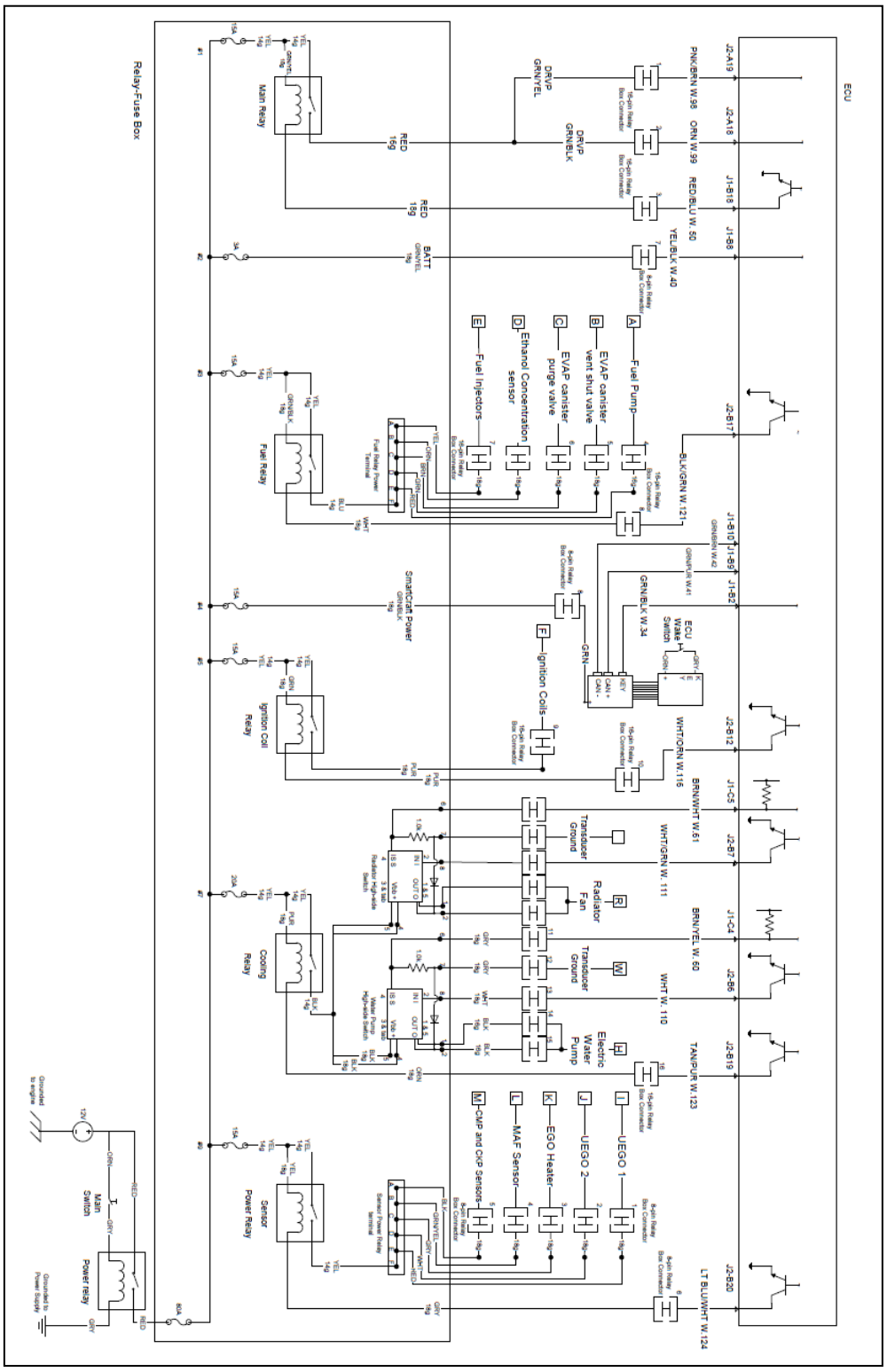


Figure 64: Wiring harness diagram part 1

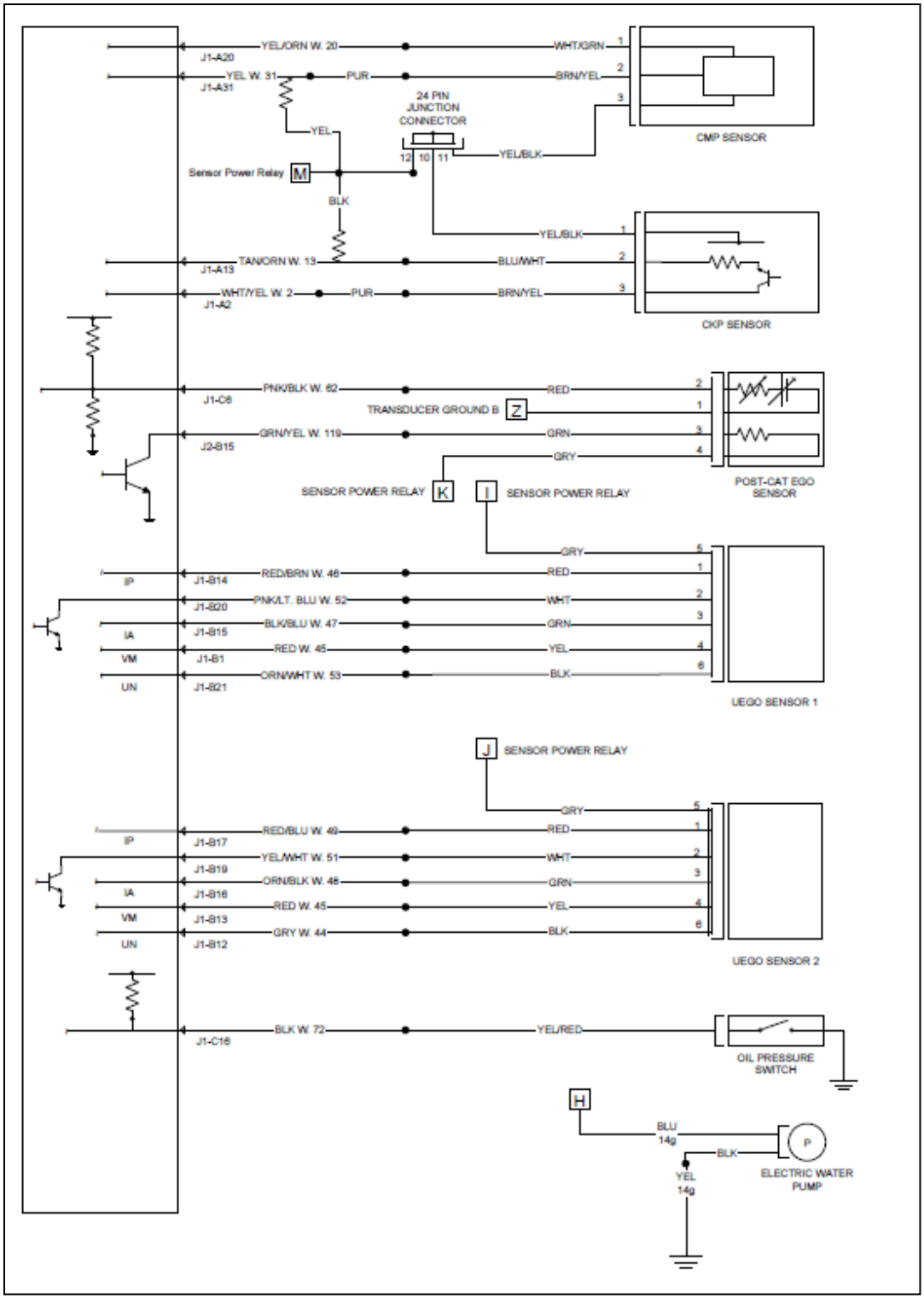


Figure 65: Wiring harness diagram part 2

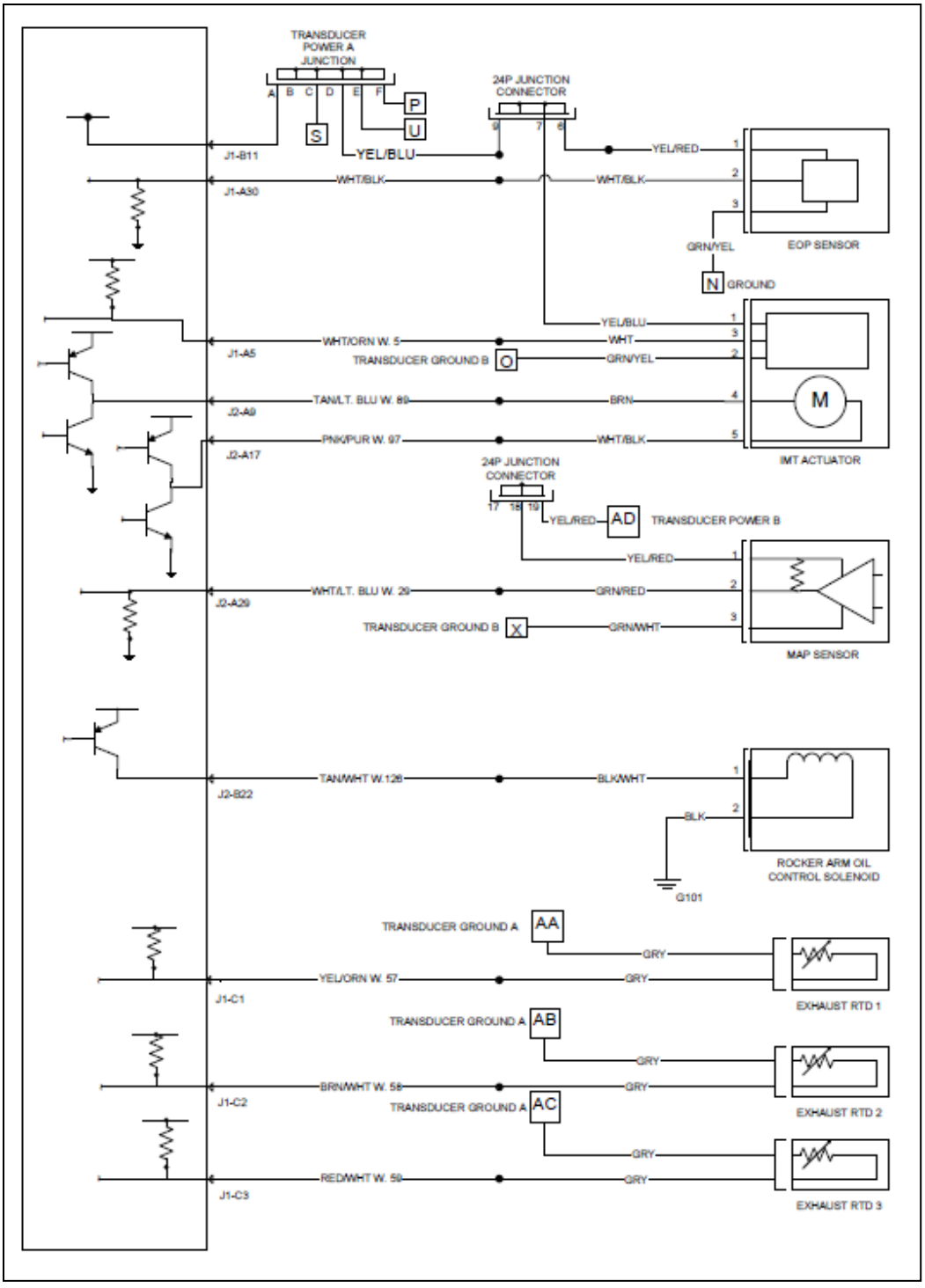


Figure 66: Wiring harness diagram part 3

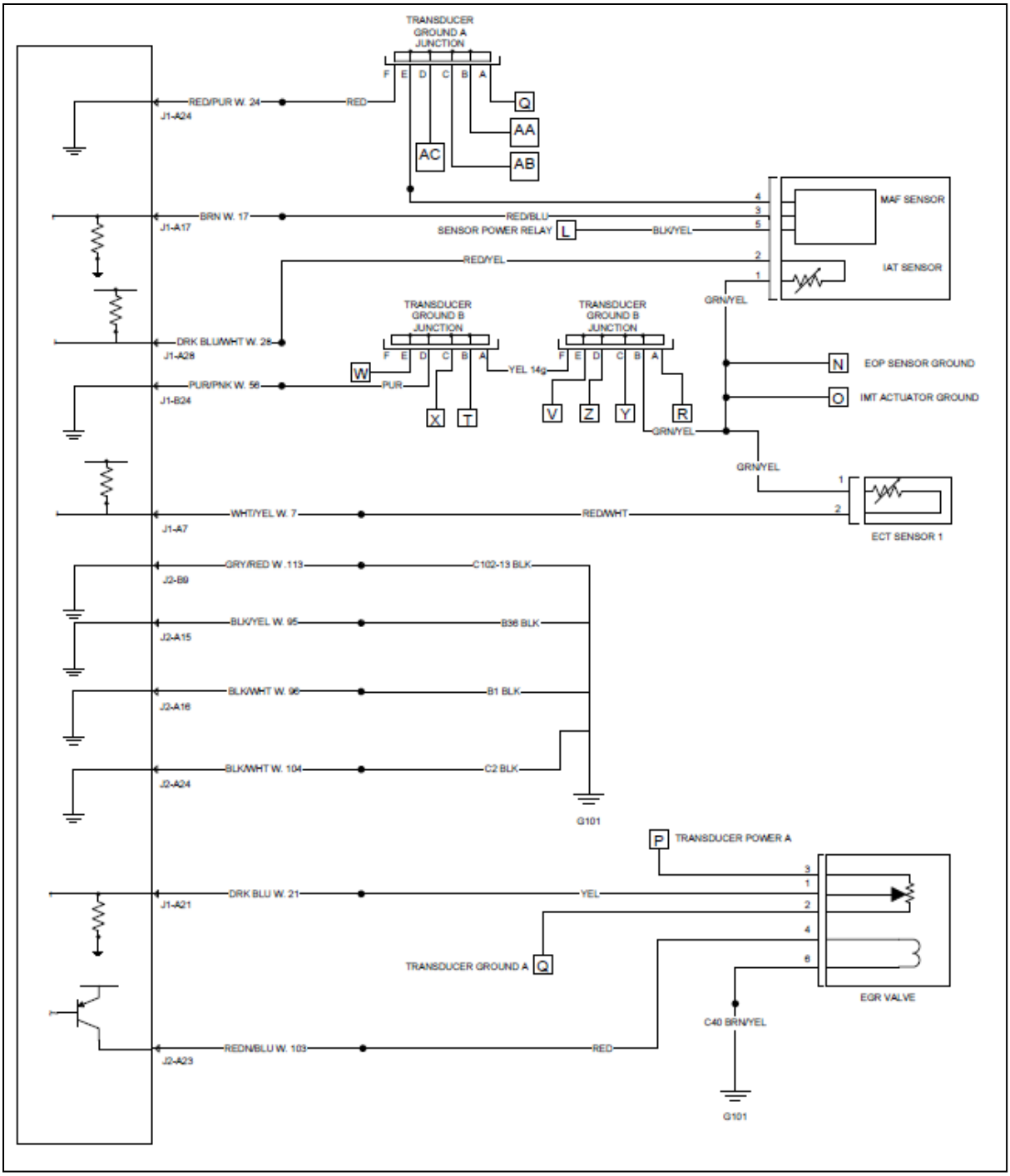


Figure 67: Wiring harness diagram part 4

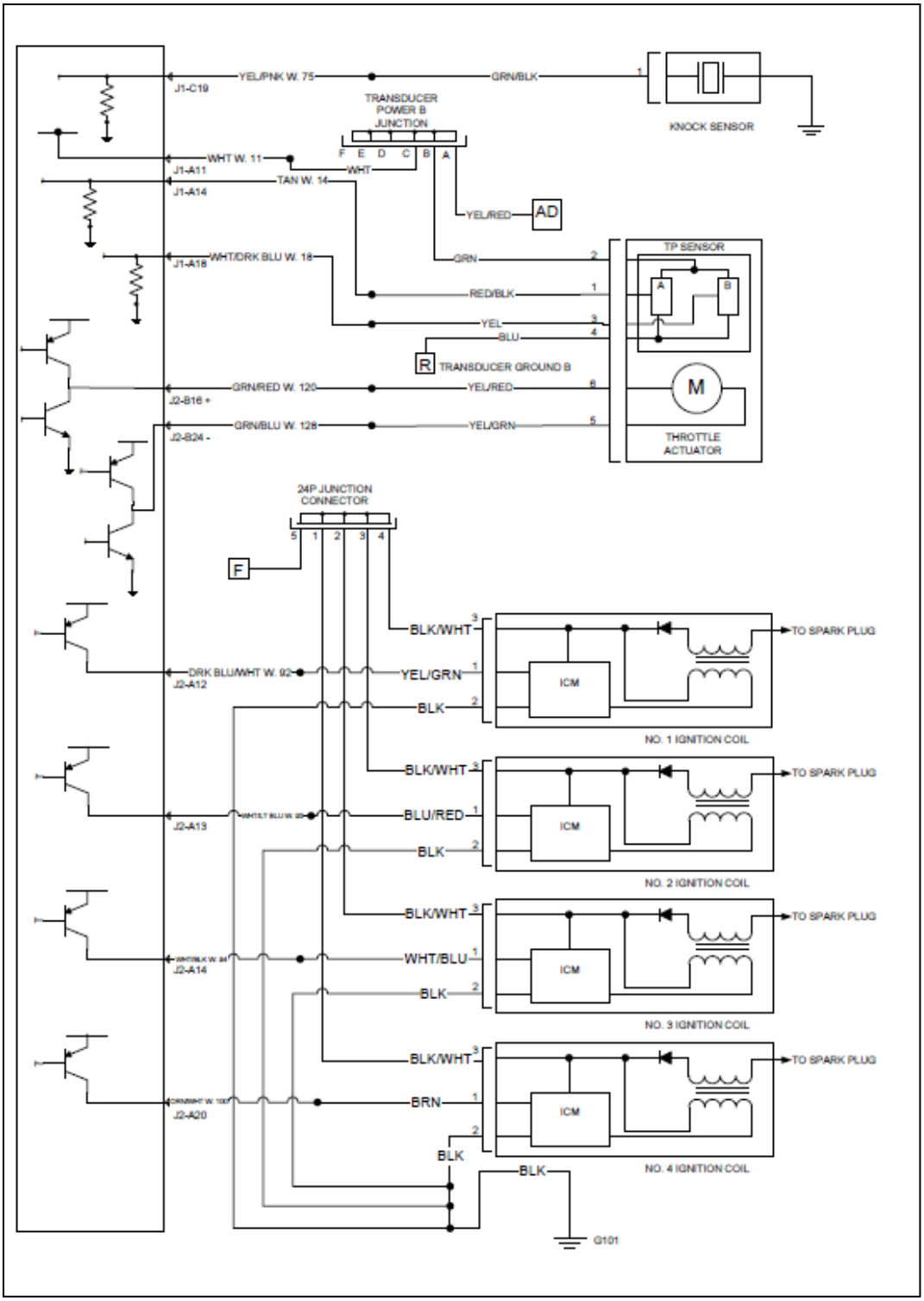


Figure 68: Wiring harness diagram part 5

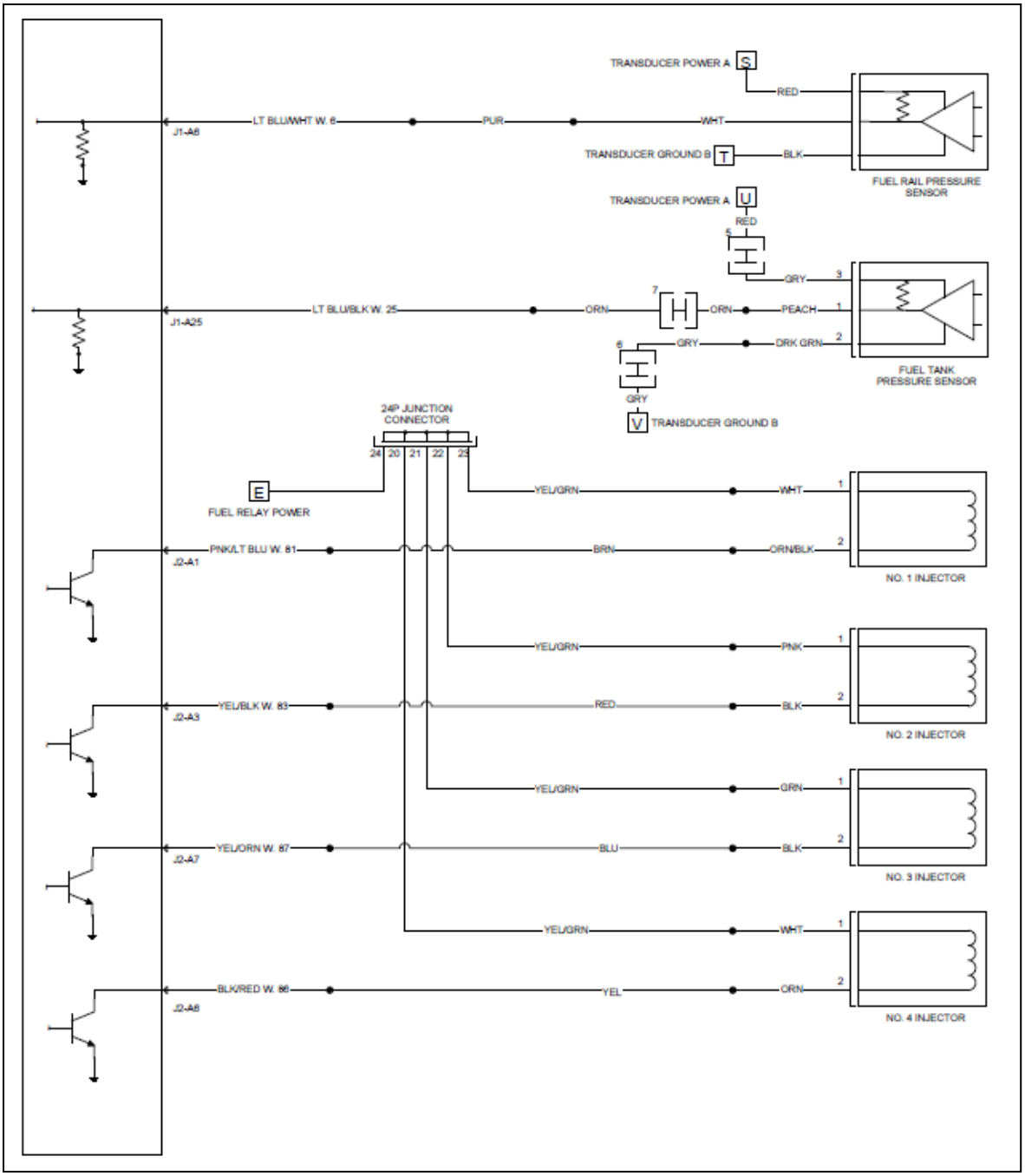


Figure 69: Wiring harness diagram part 6

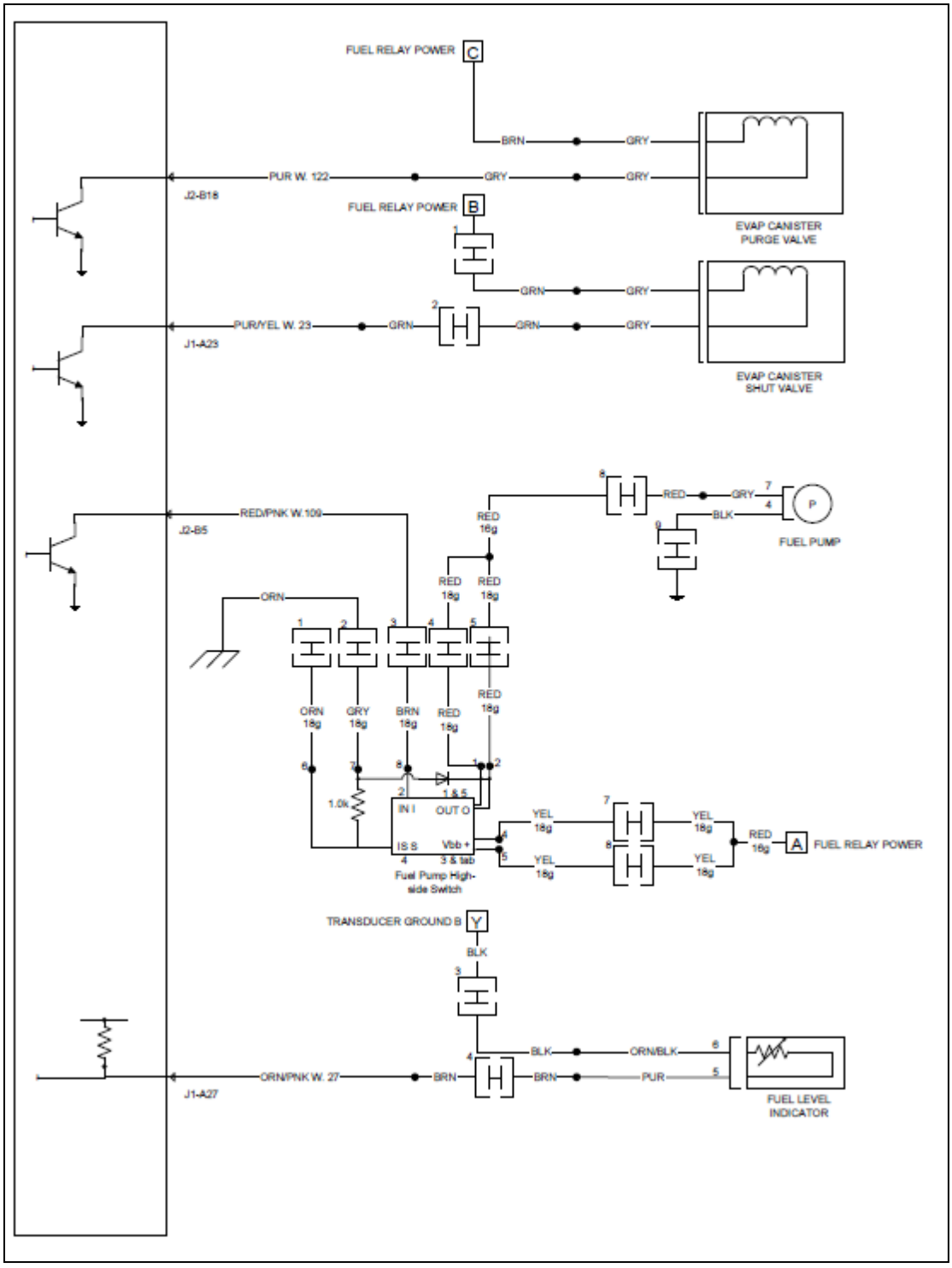


Figure 70: Wiring harness diagram part 7